EFFECTS OF METHANOL ON SPECIES CONCENTRATIONS IN n-HEPTANE FLAMES

A Thesis Submitted to
the Graduate School of Engineering and Sciences of
İzmir Institute of Technology
in Partial Fulfillment of the Requirements for the Degree of

MASTER OF SCIENCE

in Chemical Engineering
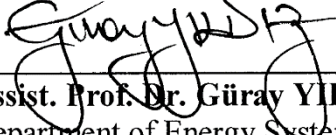
by
Abdalwahab Rashed M. ALAZREG

November 2019
İZMİR

We approve the thesis of **Abdalwahab Rashed M. ALAZREG**
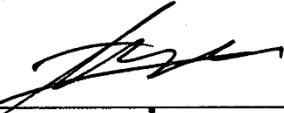
Examining Committee Members:

_____
Prof. Dr. Fikret İNAL
Department of Chemical Engineering, İzmir Institute of Technology

_____
Assist. Prof. Dr. Güray YILDIZ
Department of Energy Systems Engineering, İzmir Institute of Technology
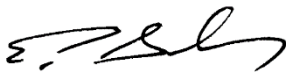

_____
Assist. Prof. Dr. Başar ÇAĞLAR
Department of Energy Systems Engineering, Yaşar University

13 November 2019

_____
Prof. Dr. Fikret İNAL
Supervisor, Department of Chemical
Engineering, İzmir Institute of Technology

_____   _____
Prof. Dr. Erol ŞEKER   **Prof. Dr. Mehtap EANES**
Head of the Department of Chemical   Dean of the Graduate School of
Engineering   Engineering and Science

ACKNOWLEDGMENTS

ABSTRACT

EFFECTS OF METHANOL ON SPECIES CONCENTRATIONS IN n-HEPTANE FLAMES

Fuel oxygenate additives have been used as an alternative method to reduce the combustion emissions. The effects of methanol addition on n-heptane oxidation were investigated for one-dimensional, atmospheric pressure, laminar, premixed, fuel-rich flame at an equivalence ratio of 2.10. The Detailed Chemical Kinetic Modeling approach has been used to obtain information about the combustion characteristics of n-heptane and n-heptane/methanol flames. A detailed chemical kinetic mechanism was generated by merging two mechanisms of n-heptane (with the formation of polycyclic aromatic hydrocarbons (PAHs)) and methanol. The Master Mechanism consists of 4480 reactions and 945 species. Model validation was carried out using the experimental data available in the literature for different combustion systems. The Master Mechanism was investigated for the combustion of n-heptane and n-heptane/methanol flames using reaction sensitivity, rate of production, and reaction pathway analyses. The mole fraction profiles of low-molecular-weight stable species, single ring aromatics, and PAHs have been predicted by the model. Good agreements between the modeling and experimental results of species mole fractions for both flames have been achieved. The mole fractions of low-molecular-weight species, aromatics, and PAHs were reduced as the methanol was added to n-heptane flame. Acetylene, propargyl radical, and vinylacetylene have been found as important species for the formation of the first aromatic ring and PAH species. Model reduction was also carried out using directed relation graph method. The Reduced Mechanism consists of 1113 reactions and 156 species. The Reduced Mechanism was in a good agreement with the Master Mechanism in terms of the species mole fraction predictions of the n-heptane/methanol flame.

ÖZET

METANOL'ÜN n-HEPTAN ALEVLERİNDE YANMA ÜRÜNLERİ KONSANTRASYONLARI ÜZERİNE ETKİLERİ

Oksijenli yakıt katkı maddeleri, yanma süreçlerinden kaynaklanan emisyonları azaltmak için alternatif bir yöntem olarak kullanılmaktadır. Metanol ilavesinin n-heptan oksidasyonuna etkileri 2.10 eşdeğerilk oranında, bir boyutlu, atmosferik basınç, laminer, önceden karıştırılmış, yakıt bakımından zengin alev için araştırılmıştır. Detaylı Kimyasal Kinetik Modelleme yaklaşımı, n-heptan ve n-heptan/metanol karışımının yanma özellikleri hakkında bilgi edinmek için kullanılmıştır. Detaylı kimyasal kinetik mekanizmada, n-heptan oksidasyonunu (polisiklik aromatik hidrokarbonların (PAH) oluşumu ile birlikte) ve metanol oksidasyonunu içeren literatürdeki iki farklı mekanizma kullanıldı. Geliştirilen Detaylı kimyasal Kinetik Mekanizma, 4480 reaksiyon ve 945 bileşikten oluşmaktadır. Modelin doğrulanması, literatürdeki farklı yanma sistemleri (laminer, önceden karıştırılmış, alev ve hızlı sıkıştırma makinesi) için mevcut deneysel veriler kullanılarak yapılmıştır. Geliştirilen ayrıntılı kimyasal kinetik model, n-heptan ve n-heptan/metanol alevlerinin yanması için reaksiyon hassasiyeti, üretim hızı ve reaksiyon yolu analizleri kullanılarak incelenmiştir. Düşük moleküler ağırlıklı kararlı bileşiklerin, tek halka aromatiklerin ve PAH'ların alev içerisindeki konsantrasyon (mol fraksiyon) profilleri model tarafından tahmin edilmiştir. n-Heptan/Metanol alevi için detaylı mekanizmanın bileşiklerin mol fraksiyonu tahminleri ile deneysel veriler arasında uyum vardır. Hem deneysel hem de modelleme sonuçlarına göre kararlı yapıdaki düşük moleküler ağırlıklı öncül bileşiklerin, aromatikler ve PAH'ların mol fraksiyonları, n-heptan alevine eklenen metanol katkısı ile azaldı. Asetilen, propargil radikali ve vinilasetilen, ilk aromatik halkanın ve PAH bileşiklerinin oluşumu için önemli öncül olarak bulunmuştur. Ayrıca, indirgenmiş mekanizma, yönlendirilmiş ilişki grafiği yöntemi kullanılarak üretildi. Geliştirilen İndirgendirmiş Mekanizma, 1113 reaksiyon ve 156 bileşikten oluşmaktadır. İndirgendirmiş Mekanizma, n-

heptan/metanol alevi sırasında oluşan bileşiklerin mol fraksiyonu tahminleri açısından Detaylı Mekanizma ile iyi bir uyum göstermiştir.

TABLE OF CONTENTS

LIST OF FIGURES

LIST OF TABLES

CHAPTER 1

INTRODUCTION

A combustion reaction is a major class of chemical reactions. The complete combustion usually occurs when a hydrocarbon reacts with oxygen to produce carbon dioxide and water. Simply, combustion can be defined as an exothermic reaction between any combustible material and an oxidizer to form an oxidation product. Combustion has been used for many applications such as industrial and heating. Around 90% of the global energy demand is provided by combustion. However, as combustion of hydrocarbon fuels has increased worldwide, some of the side-products from combustion applications are distinctly identified as a severe source of damage for the human health and the environment. Reducing the emissions from the combustion processes has become a public issue in the recent years by using alternative fuels and low emission technologies (Warnatz, Maas, and Dibble 2006).

Most of the air toxic fractions emitted and/or formed during combustion are organic molecules and carbonaceous structures. These organic compounds can be relatively simple molecules, such as formaldehyde (CH_2O), or increasing in complexity to compounds like 1,3-butadiene, aromatics, polycyclic aromatic hydrocarbons (PAHs), and some sources emit soot. Inorganic emissions of concern include acids, such as sulphuric and hydrochloric acid, sulphur (SO_x) and nitrogen oxides (NO_x), and particulate matter (PM). Emission sources can be classified into four categories; mobile sources, like vehicle emission, stationary sources, like industrial emission, natural sources, like natural wind-blown dust, and area-wide sources, like residential fireplaces. The formation of combustion products depends on several factors such as oxidation chemistry, fuel type, and operating conditions. Therefore, there is a need to investigate and better understand the chemical kinetics of the combustion phenomena.

The global energy consumption by transportation sector (EIA 2019) is shown in Figure 1.1. Although there are other sources of energy used in the transportation sector, still gasoline is the most consumable source of energy (EIA 2019). Gasoline is a mixture of volatile and flammable liquid hydrocarbons derived from crude oil and used as fuel for

internal-combustion engines. The antiknock characteristics of gasoline, its ability to resist knocking, are important features which can be expressed in octane number (ON). n-Heptane (C_7H_{16}) and iso-octane (C_8H_{18}), primary reference fuels (PRF), are used as reference to predict the auto-ignition of gasoline. n-Heptane has an octane number of 0, iso-octane has an octane number of 100, and gasoline has an octane number of 93 – 97. The higher the octane number the more difficult the auto-ignition. n-Heptane can well represent the combustion characteristics of gasoline for combustion modeling. (Warnatz, Maas, and Dibble 2006).
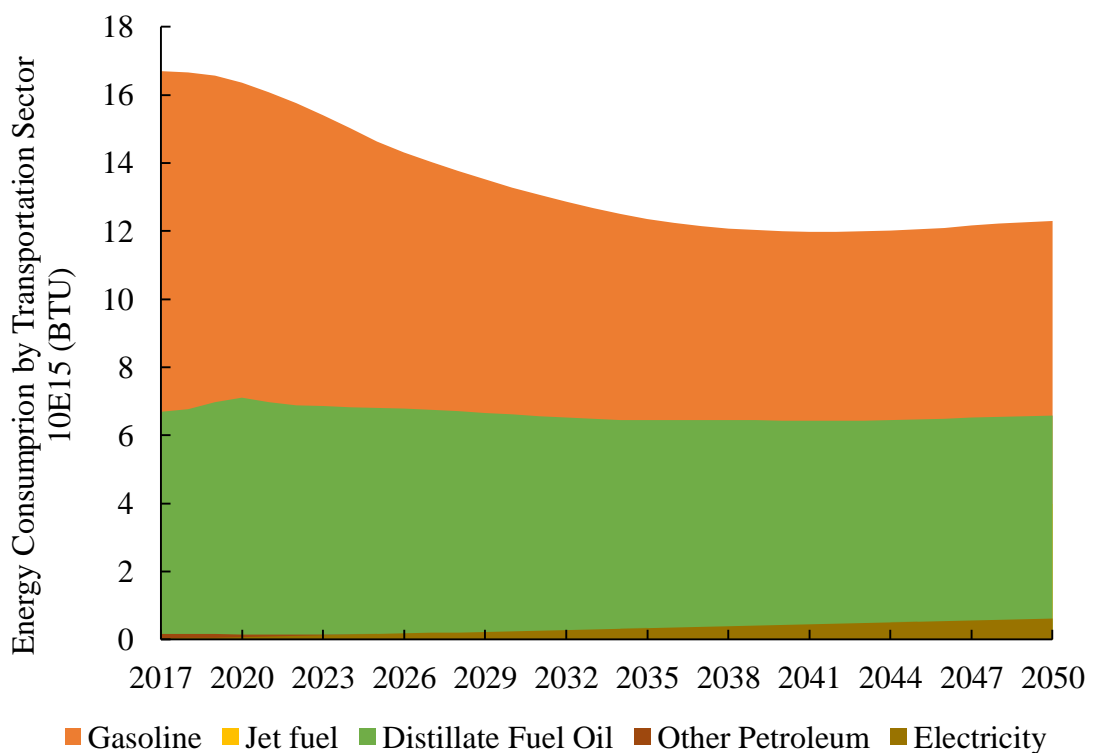
Figure 1.1.   World energy consumption by transportation sector and energy source (EIA 2019)

The incomplete combustion can cause the formation of polycyclic aromatic hydrocarbons species that are defined as organic compounds containing two or more fused aromatic rings in linear, angular, or clustered arrangements. The formation of PAH and soot in combustion processes is a widely recognized public concern due to their toxic properties. They are the largest class of chemical carcinogens known. Their metabolites

show mutagenic and carcinogenic activity toward human and animals (Samanta, Singh, and Jain 2002, Skupinska, Misiewicz, and Kasprzycka-Guttman 2004).

There has been a need to improve the fuel properties by pursuing to reduce the volatile organic compounds and air toxic emissions. Beside the changes in fuel properties, the alternative clean fuels such as alcohols, natural gas and hydrogen play important role in pollutants reduction. These alternative fuels are found to be limited by cost, availability, and vehicles to make use of these fuels. Therefore, fuel additives can be added to the fuel and gain promising reduction in pollutants. One of the most important additives to improve fuel performance is oxygenate (oxygen containing organic compounds). These oxygenates are used for octane replacement for lead in gasoline and reduction of carbon monoxide emissions. The focus for oxygenates was initially on several ethers (Methyl tertiary-butyl ether (MTBE) and Ethyl tertiary-butyl ether (ETBE)) and alcohols (Methanol and Ethanol). The typical properties of different oxygenates are shown in Table 1.1. (Methanol_Institute 2016). These oxygenates have been considered as potentially attractive fuel additives to fossil fuels in order to reduce NO_x and particulate emissions. MTBE was authorized by the United States for use as an anti-knock additive in 1979 (Braids 2001). By the late 1990s, because of its high solubility in water, it was found to leak from underground storage tanks and contaminate the groundwater. Thus, more than 19 states began to ban MTBE for a national ban in the U.S at early 2000s (Energy-Information-Administration 2003). Alcohols are the most widely used nonpetroleum fuel among all the oxygenated alternative fuels. Alcohols have higher heat of vaporization and can supply high amount of oxygen at low concentrations. Particularly, methanol is a clean burning fuel with high octane number, and can be produced from different sources such as natural gas, coal, and biomass (Methanol_Institute 2016). Methanol has been found to be efficient in reducing PAHs and soot emissions since it has high oxygen weight fraction, no C–C bond, and low production cost (Popa et al. 2001, Saravanan et al. 2002, Canakci, Sayin, and Gumus 2008). The addition of these oxygenates can cause reduction in toxic emissions. The reduction in toxic emissions would happen when oxygenates are added, the carbon atoms attach to the oxygen atoms and these carbon atoms would not be able to participate in any other reactions. Additionally, at high temperature oxidation the carbon atoms form carbon dioxide rather than soot (Westbrook, Pitz, and Curran 2006). The addition of oxygenates would convert an active hydroxyl radical, OH, into inactive hydrogen peroxide, H_2O_2, that leads to reduction the system reactivity.

Table 1.1. Typical Properties of Oxygenates (Methanol_Institute 2016)

	Methanol CH$_3$OH	Ethanol CH$_3$CH$_2$OH	MTBE CH$_3$OC(CH$_3$)$_3$
Carbon number	1	2	3
Oxygen content, (wt %)	49.9	34.7	18.15
Molecular Wieght (g/gmole)	32	46	88
Octane, (R+M)/2	116.5	114	110
Reid vapour pressure, RVP (KPa)	32	15.9	8

Computational models or mathematical models are used as computational solutions to study the behaviour of complex systems. Fundamentally, modeling is the description of a process mathematically within a set of equations that illustrate the behaviour of the process. The Detailed Chemical Kinetic Modeling (DCKM) approach is widely used to understand the combustion processes. To carry out a computational model for combustion phenomena (by computer simulation), chemical kinetic knowledge in molecular level is essential. Detailed chemical kinetic mechanisms are useful engineering tools, which allow exploration of the microscopic chemical processes. A package of elementary reactions (chemical kinetic mechanism), thermodynamic properties, and molecular transport data are required to model combustion system in molecular level. These are the three major parts for modeling a system, in some cases (i.e., jet stirred reactor system) the transport properties are not necessary while in systems such as diffusion flames and flow reactors the transport properties are needed. There is a continued interest in developing a better insight of the oxidation of large hydrocarbon fuels over a wide range of operating conditions. This interest is motivated by the need to improve the efficiency and performance of currently operating combustors and reduce the formation of pollutant species in combustion processes. The outcome of the modeling either species mole fractions, temperature, pressure, or ignition delay profiles need to be verified by comparing with experimental measurements.

In this study, the aim is to investigate the effects of methanol addition on n-heptane oxidation using detailed chemical kinetic modeling approach. Chemkin-Pro® (2018) was used as it is the appropriate and dominant software for chemical kinetic modeling, since the input data format of Chemkin is able to describe the reactions, the thermodynamic data and the transport properties of species. A chemical kinetic

4

mechanism of the n-heptane/methanol oxidation was proposed and developed. The proposed model was applied to atmospheric pressure, laminar, premixed, fuel-rich n-heptane and n-heptane/methanol flames at an equivalence ratio of 2.10 with 2.7 percent (weight) of oxygen in n-heptane/methanol mixture. Major, minor, and trace species mole fractions were compared with the experimental measurements. Important reaction steps were identified by the sensitivity analysis. Additionally, rate of production and pathway analyses for important species were carried out to understand the n-heptane and n-heptane/methanol oxidations. Finally, a model reduction for the n-heptane/methanol oxidation was done to simulate the n-heptane/methanol combustion with less computational effort.

CHAPTER 2

LITERATURE SURVEY

2.1. General Information of Hydrocarbon Combustion

The behaviour of the hydrocarbon oxidation changes when the combustion parameters (i.e., temperature, pressure and equivalence ratio) change, due to the dependence of various elementary reactions on these parameters. The combustion products can be different when different initial conditions are applied, even though the initial reactant are the same.

The most important parameter in combustion processes to define the oxidizer and fuel mixture is the equivalence ratio (φ). It can be defined as a ratio of fuel and oxidizer at the actual state over stoichiometric ratios.

$$Equivalence\ Ratio\ \varphi = \frac{\left(\frac{Fuel}{Air}\right)_{actual}}{\left(\frac{Fuel}{Air}\right)_{stoichiometric}} \tag{2.1}$$

Accordingly, it is used to indicate quantitatively whether a fuel-oxidizer mixture is rich, lean or stoichiometric as following:

Rich fuel	$\varphi > 1$
Stoichiometric fuel	$\varphi = 1$
Lean fuel	$\varphi < 1$

In combustion processes there are different flame categories. These categories can be identified based on the way of mixing of the fuel and the oxidizer, and how they are burned. When the fuel and oxidizer are mixed first and burned later, it is called premixed flame. It is non-premixed or diffusional flame when combustion and mixing occur simultaneously. Each of these categories is further subdivided based on whether the fluid flow is laminar or turbulent.
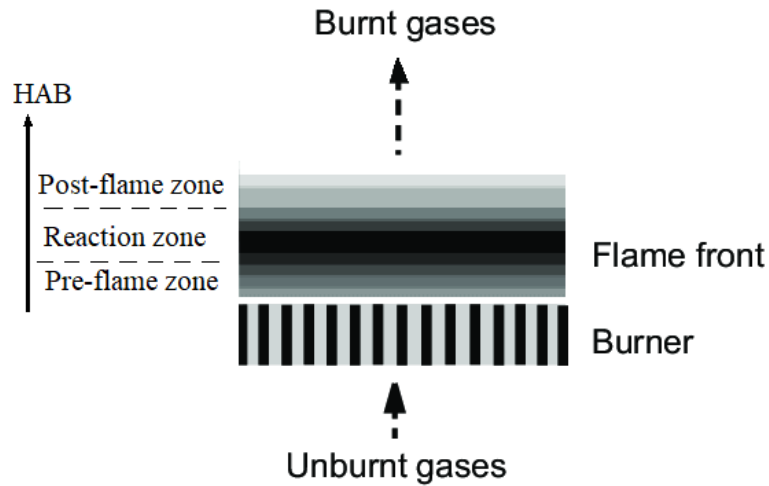
Figure 2.1.   Schematic sketch of a laminar premixed flat flame

Mainly, the premixed laminar flat flames can be classified into three zones, pre-flame zone, reaction zone, and post flame zone. The reaction rates at the pre-fame zone is the lowest comparing with other zones because of its low temperature. At the reaction zone, the temperature and reaction rates become higher. The heat release from reactions and fuel decomposition are mainly in this zone. In post flame zone, the maximum temperature is achieved and it remains constant. Figure 2.1. shows the schematic sketch of a laminar premixed flat flame.

2.2. n-Heptane Oxidation

Because of the importance of n-heptane primary reference fuel for gasoline, the oxidation of n-heptane fuel has been studied extensively in the literature in both experimental and computational works. Several combustion systems are studied to develop and validate a detailed chemical kinetic model of the n-heptane oxidation in the literature.

n-Heptane oxidation has been investigated in a jet-stirred reactor at atmospheric pressure in the temperature range of 950-1200 K at equivalence ratios of 0.2 to 2.0 (Chakir et al. 1992). A chemical kinetic reaction mechanism was developed for major species and aromatics up to C_7. A good agreement between modeling and experimental data of major species mole fractions was achieved. To investigate the reactions with the greatest

influence on the modeling results, sensitivity analysis was carried out. The reaction pathway analysis was done to identify the main paths of formation and consumption of the different intermediate species. It was found that the main reactions lead to n-heptane consumption, in lean mixture oxidation, are:

$$n\text{-}C_7H_{16} + O = 1C_7H_{15} + OH$$

$$n\text{-}C_7H_{16} = PC_4H_9 + n\text{-}C_3H_7$$
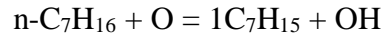
While in rich mixture, n-heptane consumption is mainly by:

$$n\text{-}C_7H_{16} = C_2H_5 + 1\text{-}C_5H_{11}$$

$$n\text{-}C_7H_{16} = PC_4H_9 + n\text{-}C_3H_7$$
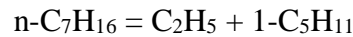
Dagaut, Reuillon, and Cathonnet (1995) have investigated experimentally the oxidation of n-heptane in a high-pressure, perfectly jet-stirred reactor in a temperature range of 550–1150 K, and pressure range of 1–40 atm for a stoichiometric mixture of n-heptane and oxygen highly diluted by nitrogen. Reactants, intermediates, and final products have been investigated. The products formed during the oxidation of n-heptane depended on temperature. It was reported that large amount of intermediate species were produced in a rapid oxidation of n-heptane at temperatures above 750 K. Moreover, an important reactivity has been observed at low temperatures (below 750 K). At low temperature, the oxidation of n-heptane started with O_2 and produced alkyl radical and HO_2. HO_2 radical reacted back with fuel (RH) to produce H_2O_2.

$$RH + O_2 \rightarrow R + HO_2$$

$$HO_2 + RH \rightarrow H_2O_2 + R$$
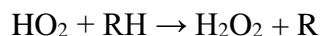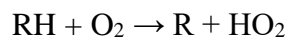
A modeling work was carried out by involving flow reactor, shock tube and rapid compression machine under conditions of 1-42 atm pressure range, temperature range of 550-1700 K, the equivalence ratio from 0.3 to 1.5, and nitrogen-argon dilution of 70-99% (Curran et al. 1998). Species mole fractions data from variable pressure flow reactor and jet stirred reactor have been used for the low temperature part of the mechanism. Experimental results from the literature regarding ignition delay time were used to validate and developed reaction mechanism at low and high temperatures. The proposed mechanism consists of 990 species and 4060 reactions. According to the study, a very good agreement between modeling and experimental results was achieved.

An experimental study of laminar, premixed, fuel-rich n-heptane/O_2/N_2 and iso-octane/O_2/N_2 flames was conducted at equivalence ratio 1.9 and pressure of 6 kPa (Bakali, Delfau, and Vovelle 1998). The species mole fraction profiles have been obtained by GC/MS analyses of samples. A detailed experimental data on the nature and concentration of the intermediate species formed has been obtained. The mole fraction profiles of major products, and C_1-C_7 species have been measured.

The laminar flame speeds of n-heptane/air mixtures at atmospheric pressure have been measured over an extensive range of equivalence ratios at atmospheric pressure (Davis and Law 1998). The experimental measurements were compared to three n-heptane mechanisms and their predictions agreed quite well with the experimental data.

A premixed laminar n-heptane/air flame at atmospheric pressure for a stoichiometric mixture was investigated experimentally and computationally (Ingemarsson, Pedersen, and Olsson 1999). The on-line GC/MS sampling was used to determine species profiles. Key finding of this study was that alkene concentrations were significantly higher than corresponding alkanes. The flame was modeled using n-heptane mechanism and satisfactory agreement were found between the experimental and modeling results.

Inal and Senkan (2002a) have studied experimentally the formation of polycyclic aromatic hydrocarbons (PAHs) in premixed, laminar, fuel-rich n-heptane/oxygen/argon flames at atmospheric pressure with two equivalence ratios of 1.97 and 2.1. The mole fraction profiles of stable major, minor, and trace species up to four aromatic ring PAHs were obtained by the online GC/MS and GC/TCD analyses.

A detailed chemical kinetic mechanism of gasoline surrogate fuel components (n-heptane, iso-octane, and toluene) and mixtures has been proposed (Mehl et al. 2011). The proposed mechanism consists of 6000 reactions and 1550 species. Validation work for ignition delay time has been done against experimental measurements of PRFs, 1-hexene, toluene, and their mixtures in a rapid compression machine and a jet stirred reactor. The results have shown that the model was able to predict the ignition delay time very well at an equivalence ratio of 1, and the pressure and temperature ranges from 3 to 50 atm and 650 to 1200 K, respectively. The information provided by modeling work can be a valuable help for better understanding of the combustion phenomena of fuels in internal combustion engines.

The ignition delay times of stoichiometric n-heptane/air mixtures have been measured at different pressures (15, 20, and 38 bar) and in the temperature range of 726–

1412 K, experimentally in a shock tube (Zhang et al. 2016). In addition, in the same study concentration versus time profiles of species have been measured in a jet-stirred reactor at atmospheric pressure, in the temperature range of 500–1100 K at different equivalence ratios φ =0.25, 2.0, and 4.0. In parallel, a detailed chemical kinetic model has been developed, and it was claimed a good agreement between the model predictions and experimental measurements.

An updated comprehensive kinetic model of gasoline surrogate fuels (iso-octane, n-heptane, and toluene) that consists of formation of PAH species have developed by Park et al. (2017). High number of reactions and species are proposed by this study (i.e., 2021 species and 8688 reactions) for gasoline surrogates. Also, the high-temperature sub-mechanism for premixed laminar and counter-flow diffusional flames was proposed (i.e., 574 species and 3379 reactions). PAHs with pyrene (A_4) and larger were used for the inception of soot particles. The model was validated against different combustion systems for the ignition delay times, premixed, and partially premixed laminar flames. Even though there were slight underestimation by the model for the species mole fractions, the performance of the model was generally good. The results of the pathway analyses showed that the propargyl radicals (C_3H_3) play an important role for the formation of PAHs for n-heptane/iso-octane mixture. However, for n-heptane/iso-octane/toluene mixture, reactions containing benzyl radicals ($C_6H_5CH_2$) had a significant impact in the formation of PAHs.

2.4. The Oxidation of Methanol and n-Heptane/Methanol

A comprehensive detailed chemical kinetic mechanism for the oxidation of methanol has been developed by Held and Dryer (1998). The mechanism was validated against different experimental data sets (i.e., static reactor, flow reactor, shock tube, and laminar flame) at temperature range from 633 to 2050 K, pressure from 0.26 to 20 atm, and equivalence ratio from 0.05 to 2.6. The proposed model was successful for predicting experimental measurements from four different systems over a wide range of temperature, pressure, and equivalence ratio.

In a flow reactor the oxidation of methanol has been studied experimentally at fuel-lean conditions and temperature range of 650–1350 K (Rasmussen et al. 2008). The O_2 concentrations was over a wide range of (1%–16%). A generated chemical kinetic

model of H_2, CO, CH_2O, and CH_3OH oxidation was used to interpret the experimental measurements. It was found that at temperatures below 1100 K the modeling predictions was in a good agreement with experimental results, whereas there were underpredictions at higher temperatures and high oxygen concentration.

The auto-ignition of methanol has been investigated experimentally and computationally over a pressure range of 7-30 bar, a temperature range of 850-1100 K, and an equivalence ratio range of 0.25-2.0 (Kumar and Sung 2011). Using a rapid compression machine (RCM), the ignition delay results for methanol have been obtained. The modeling predictions were compared with the experimental results, and underpredictions of the ignition delays were found for the investigated conditions.

A detailed methanol oxidation mechanism consisting of 21 species and 115 reactions has been developed by combining existing mechanisms for H_2, CO, CH_2O, and CH_3OH species at 40 torr covering a wide range of lean to rich flames (Hamdane et al. 2012). There was a good agreement between model predictions and measured mole fraction profiles for reactants, products, and intermediates species. Reaction pathway analysis showed the predominant reaction consuming methanol in lean flames was $CH_3OH+OH=CH_3O+H_2O$. In the case of stoichiometric and rich flames the most important methanol consumption reaction was found to be the reaction $CH_3OH+H=CH_2OH+H_2$. In all cases, the methanol consumption gave two isomers hydroxymethyl(CH_2OH) and methoxy (CH_3O) radicals.

Measurements of ignition delay times for methanol oxidation using shock tube and a rapid compression machine have been carried out over a wide range of pressures 2-50 atm, temperature range of 820-1650 K, and equivalence ratios of 0.5, 1.0, and 2.0 (Burke et al. 2016). Using a jet-stirred reactor (JSR) species concentrations have been also measured at equivalence ratios of 0.2-2.0, in the temperature range of 800–1200 K, at pressures of 1-20 atm and with residence times 0.05-2.00 s. A detailed chemical kinetic model for methanol oxidation was proposed and developed. The mechanism consists of 1011 reactions and 173 species. The mechanism was able to predict all of the validation data with a reasonable accuracy.

Inal and Senkan (2002b) have studied the effects of oxygenate additives on the formation of polycyclic aromatic hydrocarbons (PAHs) and soot in laminar, premixed, atmospheric pressure, fuel-rich flames of n-heptane at an equivalence ratio of 2.10. Three different oxygenates were used (i.e., methanol, ethanol, and MTBE). The oxygen weight percent in n-heptane/oxygenate mixtures was kept at 2.7 for all oxygenates. The mole

fractions of CO, acetylene (C_2H_2), vinylacetylene (C_4H_4), and other stable-low-molecular-weight species were consistently lower in oxygenate containing flames. It was also reported that the mole fractions of aromatic and PAH species were lower in these flames. The reduction in some of the aromatic and PAH species concentrations were slightly different from one blended flame to another.

The effects of the oxygenate concentration on species mole fractions have been studied in atmospheric pressure, laminar, premixed, fuel-rich n-heptane flames (Inal and Senkan 2005). The equivalence ratio was 1.97 for both flames (i.e., n-heptane/oxygen/argon and n-heptane/oxygenate/oxygen/argon). The oxygenates used were methanol, ethanol, and MTBE. The oxygen weight percents were kept at 2.7 and 3.4 in n-heptane/oxygenate mixtures. It has been found that the reduction in the aromatic and polycyclic aromatic hydrocarbon species mole fractions increased when the oxygenate concentration increased.

The effects of methanol addition to iso-octane on the performance of spark ignition engines and their emissions have been studied by Yanju et al. (2008). Various methanol volume percentage were used (i.e., 10%, 20%, and 85%). It has been claimed that as methanol ratio in gasoline increased the ignition delay was shortened and the CO emission decreased. At the low methanol ratio in iso-octane no significant effect on reducing the NO_x emission has been observed while at the 85% of methanol the reduction was about 80%.

Zhang et al. (2011) have investigated the combustion characteristics of methanol-gasoline blended fuels in spark ignition engines. A detailed comprehensive methanol oxidation mechanism was combined with an oxidation mechanism of gasoline surrogate (n-heptane, iso-octane and toluene) in order to obtain a methanol-gasoline blended mechanism. The methanol-gasoline mechanism was validated by the jet stirred reactor, flow-reactor, and shock-tube experimental data. The modeling results of the mechanism have showed a good agreement with the experimental data.

A chemical kinetic mechanism and a skeletal model for oxidation of n-heptane/methanol fuel blends were proposed by Xu, Yao, and Xu (2012). The created skeletal kinetic model includes only 38 reactions and 30 species. It was used to predict the ignition delay of methanol/n-heptane blends as well as each pure fuel. Under various equivalence ratios, initial temperatures, and pressures, good predictions were shown by the skeletal model for the ignition delay of the n-heptane, methanol, and the blends as well.

Three different oxygenated fuels (methanol, dimethoxymethane DMM, and dimethyl carbonate DMC) have been added to laminar, premixed n-heptane flames in order to study their effects on n-heptane oxidation (Chen et al. 2012). The overall C/O ratio was 0.507, and the equivalence ratio was 1.6 for all the flames. The concentrations of major and intermediate species were measured experimentally and parallel computations were carried out with a generated model of the n-heptane/oxygenates oxidation. Satisfactory predictions for the species mole fractions have been achieved. A Reaction Flux Analysis was performed near the burner surface and indicated that the peak value of normalized formaldehyde (CH_2O) mole fraction was increased for the blended fuels. The mole fractions of most C_1-C_5 hydrocarbon intermediates were reduced by 10–30% as oxygenated fuels were added. Moreover, the benzene reduction was about 40%.

Chen et al. (2013) have also investigated the influences of methanol on premixed fuel-rich n-heptane flames experimentally using two laminar premixed n-heptane/O_2/Ar flames ($\varphi = 1.60$, (C/O = 0.51), and $\varphi = 1.80$, (C/O = 0.57)) and one laminar premixed n- heptane/methanol/O_2/Ar flame ($\varphi = 1.80$, (C/O = 0.51)). A modeling work was also carried out, and it has been found that the concentrations of C_2–C_7 hydrocarbon intermediates were reduced significantly as methanol was added. It was reported that when the equivalence ratio increased the maximum temperature was reduced by 100 K.

Xu et al. (2013) have studied experimentally the effects of methanol and ethanol addition on the laminar, premixed, n-heptane/toluene flames by using synchrotron photoionization and molecular-beam mass spectrometry techniques at an equivalence ratio of 2.0 and pressure of 30 torr. Parallel simulations were performed, and the model predictions of species concentrations agreed well with the experimental measurements. It was reported that the experimental and modeling results showed sharp decrease in PAH species mole fractions by the addition of alcohols. The formaldehyde and acetaldehyde concentrations (degradation intermediates) were high in the presence of methanol and ethanol, respectively.

2.3. Formation of First Aromatic Ring

Since the first aromatic ring is the main source of the formation and growth of PAHs during combustion of non-aromatic fuels, there are many suggestions for its formation. Frenklach and Wang (1994) have the simple suggestion of the formation of

the first aromatic ring in flames of non-aromatic fuels. They have reported that the formation of first aromatic ring starts usually with vinyl addition to acetylene. At high temperatures, it forms vinylacetylene followed by acetylene addition to n-C_4H_3 radical formed by the H-abstraction from the vinylacetylene. The addition of acetylene to vinyl, at low temperatures, results in n-C_4H_5 which reacts with acetylene and forms benzene ring. The following reactions show the high and low temperature routes for the formation of first aromatic ring:
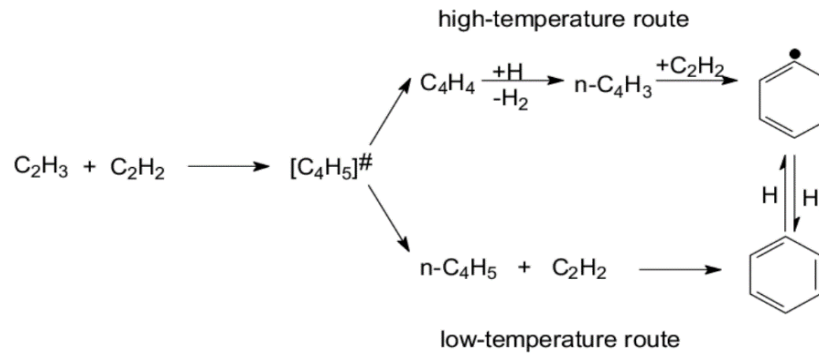
It has been also suggested that the formation of first aromatic ring occurs by the addition of the 1,3-butadienyl (C_4H_5) radical to acetylene C_2H_2 (Cole et al. 1984).

$$C_4H_5 + C_2H_2 = C_6H_6 + H$$
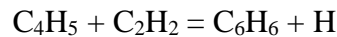
Frenklach and Warnatz (1987) have suggested four-reaction sequence leading to the first aromatic ring:

$$n\text{-}C_6H_5 \rightarrow phenyl$$

$$i\text{-}C_8H_5 \rightarrow C_6H_4C_2H$$

$$n\text{-}C_8H_5 \rightarrow C_6H_4C_2H$$

$$n\text{-}C_6H_7 \rightarrow benzene + H$$
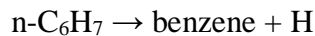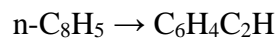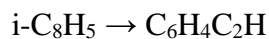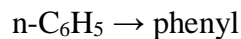
Another important suggestion of benzene formation mechanism has been also proposed by Stein et al. (1991), Melius, Miller, and Evleth (1992), and Marinov et al. (1996). They proposed that benzene is formed through recombination of two propargyls followed by isomerization and cyclization steps that lead to phenyl and H-atom. Then the reaction of phenyl radical with hydrogen atom leads to benzene.

$$C_3H_3 + C_3H_3 \rightarrow C_6H_5 + H$$

$$C_6H_5 + H \rightarrow C_6H_6$$
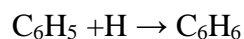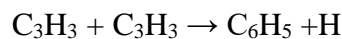
2.4. Formation of Polycyclic Aromatic Hydrocarbons (PAHs)

Polycyclic aromatic hydrocarbons are high molecular weight species that have two or more fused benzene rings, and PAHs are the potential precursors to soot formation. Frenklach et al. (1985), and Frenklach and Warnatz (1987) have claimed that the formation and growth of PAHs in hydrocarbon pyrolysis and oxidation starts after the first aromatic ring formation. A sequence of growth happens by a repeated two-step process, involving hydrogen abstraction followed by subsequent acetylene addition to form the next highest order ring. This process is known as the Hydrogen Abstraction Acetylene Addition (HACA). The continuation of HACA leads to the sequential formation of multi-ring structures such as naphthalene (A_2), phenanthrene (A_3), pyrene (A_4) and higher order rings;

$$A_i + H = A_{i-} + H_2$$

$$A_{i-} + C_2H_2 = A_iC_2H_2$$

$$A_iC_2H_2 + C_2H_2 = A_{i+1} + H$$
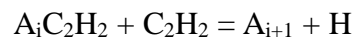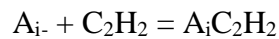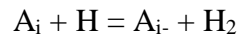
where A_i is the aromatic species with i number of aromatic rings, and A_{i-} the unsaturated (needs one hydrogen atom) aromatic species with i number of aromatic rings.

Appel et al. (2000) have deduced that the addition of vinylacetylene (C_4H_4) to unsaturated aromatic species (A_{i-}) contributes the most to the production of naphthalene (A_2).

$$A_{i-} + C_4H_4 \longleftrightarrow AiC_4H_4 \rightarrow A_{i+1}$$
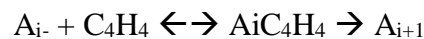
Similar to the naphthalene formation process, the phenanthrene (A_3) is formed based on the combination of cylcopentadienyl (C_5H_5) with indenyl (Marinov et al. 1998).

Marinov et al. (1996) have proposed the pathways of indene formation. It starts with the hydrogen abstraction reaction by H radical of naphthalene as follows:

$$C_{10}H_8 + H = C_{10}H_7 + H_2$$

$$C_{10}H_7 + O_2 = C_{10}H_7O + O$$

$$C_{10}H_7O = lndenyl + CO$$

$$Indenyl + H = Indene$$
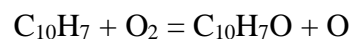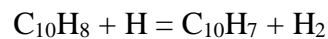
The hydrogen abstraction methyl addition (HAMA) mechanism was claimed to contribute the formation and growth of polycyclic aromatic hydrocarbons (PAHs). Methyl radicals can form side chains, form five-membered ring structures and convert five-membered into six-membered ring structures (Shukla, Miyoshi, and Koshi 2010, Hansen et al. 2017).

An experimental study was conducted regarding the formation pathways of aromatic and polycyclic aromatic hydrocarbon (PAH) species up to five aromatic rings (Marinov et al. 1998). A premixed, atmospheric pressure, rich, n-butane/oxygen/argon flame at an equivalence ratio of 2.6 was used to understand the formation of PAHs. Also a detailed chemical kinetic modeling work has been carried out. A fair agreement between the modeling and experimental results has been achieved. To identify the most important reaction leading to PAH growth and destruction in the n-butane flame, sensitivity analysis was used. Benzene was mainly formed by two propargyl (C_3H_3) recombination reaction in the n-butane flame. In addition, benzene was also formed by combination reaction between allyl and propargyl to produce fulvene and the conversion of fulvene by H-atom catalysis lead to benzene.

The formation of PAH species has been described by a semi-detailed chemical mechanism of toluene reference fuel by An et al. (2015). The mechanism consists of 219 species and 1229 reactions. The validation work was done for ignition delay time in a temperature range of 750 to 1280 K, pressure range of 15 to 60 bar, and equivalence ratios range from 0.5 to 2.0. The mechanism was also validated against laminar flame speeds with various pressures. To investigate the most effective reactions in the formation of benzene, rate of production analysis was done. It was deduced that the reaction rates of benzene formation depend on temperature. At low and high temperatures, the reactions n-C_4H_5 + C_2H_2 = A_1 + H (A_1 refers to benzene) and C_3H_3 + C_3H_3 = A_1 + H, respectively, are the most dominant reactions for the formation of benzene.

The effects of methanol and ethanol addition on the formation of polycyclic aromatic hydrocarbons (PAH) in counterflow, diffusion, fuel-rich ethylene flames were investigated experimentally (Yan et al. 2019). A detailed chemical kinetic model was developed by including benzene formation and PAH growth pathways up to coronene. It has been found that methanol and ethanol were efficient in reducing PAHs and soot emissions.

CHAPTER 3

METHOD

3.1. Detailed Chemical Kinetic Modeling

The improvements of computational technology have resulted in increasing the usage of chemical kinetic modeling in the last decades. The detailed chemical kinetic modeling (DCKM) approach is a computational solution that deals with high number of elementary reactions and species. It is the appropriate method to better understand the combustion chemistry. Chemical kinetic model is a very important key to understand the mechanisms, the chemical kinetics of the reactions, and the formations/decompositions of the stable/radical species.

The predominant and the appropriate software that solves the complex chemical kinetic problems is Chemkin-Pro (Chemkin-Pro® 2018). The Chemkin-Pro input data format is an evolving standard for describing the reactions, the rate parameters, and the thermodynamic, and transport properties of each species. It is used worldwide in the combustion, chemical processing, and automotive industries. Chemkin is a collection of databases and subroutines written in text files for solving problems involving gas-phase kinetics, thermodynamic, and transport properties. The continuity equations for mass, momentum, and energy should be solved all together to model chemically reactive flow systems. The kinetic terms in many oxidation systems valuate the characteristic scales of space and time over which the equations must be solved. In defining the chemistry used in a Chemkin simulation, thermodynamic data for each species in the chemical system must be first supplied. These data are in the form of polynomial fits to temperature, for species enthalpy, entropy, and specific heat capacity. Once these data are defined, they are used during a Chemkin simulation to determine species thermodynamic properties, thermal transport properties, and reaction equilibrium constants. Chemkin solves design equations of the various combustion systems (i.e., reactor, flame, and engine) by utilizing the chemical kinetic data, thermodynamic, and transport properties.

3.2. Chemical Rate Expression

The chemical rate expressions database is utilized to introduce all the species and their elementary reactions to the software to calculate the reaction rates of these elementary reactions, and to determine the rate of production of the species. Each single species and all elementary reactions in the mechanism are defined in the chemical rate expressions database. Each species in a reaction must have the thermodynamic data which are used to determine the equilibrium constant and reverse-rate coefficient for that reaction. By this concept, the chemical rate expressions build on the thermodynamic expressions. The reverse reaction rate constant can be determined by using equilibrium rate constant that is provided by thermodynamic data. The forward reaction rate constant is calculated by the following modified Arrhenius equation:

$$k_{fi} = A_i \, T^{\beta i} \, \exp\left(\frac{-E_i}{RT}\right) \qquad (3.1)$$

where A_i is the pre-exponential collision frequency factor, β_i the temperature exponent, and E_i the activation energy. The forward reaction rate k_{fi} depends on the temperature, at low and moderate temperatures the temperature exponent equals zero. At high temperatures, some reactions can exhibit non– Arrhenius behaviour so the temperature exponent need to be described by additional variation with temperature.

The forward elementary reaction rate constants can be calculated by specifying the kinetic parameter values for each elementary reaction in the chemical rate expressions database. The reverse reaction rate constants are determined using the thermodynamic data for the species and the forward rate constants;

$$k_{ri} = \frac{k_{fi}}{K_{ci}} \qquad (3.2)$$

where K_{ci} is the equilibrium constant (in concentration unit).

The elementary reactions involving K chemical species can be described as;

$$\sum_{k=1}^{K} v'_{ki} X_k \leftrightarrow \sum_{k=1}^{K} v''_{ki} X_k \qquad (3.3)$$
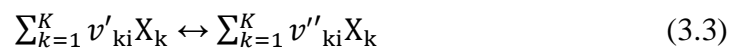
where v_{ki} is the stoichiometric coefficient, X_k the mole fraction for the species (from 1 to K), superscript ′ means forward reactions and ″ means reverse reactions.

The rate-of-progress variable q_i for a reaction is calculated by the forward and reverse reaction rates, and the molar concentration of kth species $[X_k]$;

$$q_i = k_{fi}\prod_{k=1}^{K}[X_k]^{v'_{ki}} - k_{ri}\prod_{k=1}^{K}[X_k]^{v''_{ki}} \tag{3.4}$$

The production rate of kth species ($\dot{w}_k$) can be determined by the summation of progress variables of all reactions;

$$\dot{w}_k = \sum_{k=1}^{K} v_{ki}\, q_i \tag{3.5}$$

where v_{ki} can be calculated by the difference between stoichiometric coefficients of the species for the forward and reverse reactions.

Fundamentally, all the species and their elementary reactions with modified Arrhenius parameters are included in the kinetic database. By using this kinetic database, the forward reaction rate constants of the elementary reactions can be calculated. The reverse reaction rate constants are calculated by using equilibrium constants of the thermodynamic expression. Figure 3.1 shows the chemical kinetic input parameters (i.e., reactions, pre-exponent factor, temperature exponent, and activation energy).

```
Reactions                    Ai          Bi       Ei
2H+H2  = 2H2                 9.000E+16   -0.600    0.0
2H+H2O = H2+H2O              6.000E+19   -1.250    0.0
2H+CO2 = H2+CO2             5.500E+20   -2.000    0.0
H+OH+M = H2O+M              2.200E+22   -2.000    0.0
```

Figure 3.1. Example of chemical kinetic database input data format

3.3. Thermodynamic Expression

The thermodynamic database is an essential element in chemical kinetic that provide the thermodynamic properties of all the chemical species in the mechanism (enthalpy H_k^0, entropy S_k^0, and specific heat capacity cp_k^0). Once these data are defined,

they can be used to determine other thermodynamic properties, transport properties, and reaction equilibrium constants.

$$cp_k^0 = \sum_{m=1}^{M} a_{mk} T_k^{(m-1)} \tag{3.6}$$

$$H_k^0 = \int_0^{Tk} cp_k^0 \, dT + H_k^0(0) \tag{3.7}$$

$$S_k^0 = \int_{298}^{Tk} \frac{cp_k^0}{T} \, dT + S_k^0(0) \tag{3.8}$$

The above equations are polynomial fit equations. The gas-phase kinetics package is designed to work with thermodynamic data in the form used in the NASA chemical equilibrium. In this case, seven coefficients are needed for each of two temperature ranges. An example of input data format used in Chemkin is shown in Figure 3.2. In the input file (Figure 3.2), the first line consists of species name, reference, atomic composition, and phase while the other lines are divided in two seven coefficient of NASA polynomial coefficients, (first for higher temperature ranges second for lower temperature ranges).

```
H2                000000N  0H   2O   0C   0G       300       3000      1000      1
 3.33727920E+00-4.94024731E-05 4.99456778E-07-1.79566394E-10 2.00255376E-14      2
-9.50158922E+02-3.20502331E+00 2.34433112E+00 7.98052075E-03-1.94781510E-05      3
 2.01572094E-08-7.37611761E-12-9.17935173E+02 6.83010238E-01                     4
H2O               000000N  0H   2O   1C   0G       300       3000      1000      1
 3.03399249E+00 2.17691804E-03-1.64072518E-07-9.70419870E-11 1.68200992E-14      2
-3.00042971E+04 4.96677010E+00 4.19864056E+00-2.03643410E-03 6.52040211E-06      3
-5.48797062E-09 1.77197817E-12-3.02937267E+04-8.49032208E-01                     4
CO2               000000N  0H   0O   2C   1G       300       3000      1000      1
 3.85746029E+00 4.41437026E-03-2.21481404E-06 5.23490188E-10-4.72084164E-14      2
-4.87591660E+04 2.27163806E+00 2.35677352E+00 8.98459677E-03-7.12356269E-06      3
 2.45919022E-09-1.43699548E-13-4.83719697E+04 9.90105222E+00                     4
```

Figure 3.2. Example of thermodynamic properties input data format

3.4. Transport Expression

Transport properties are also important in most of the reactive-flow models that are not kinetically limited. Laminar premixed and diffusion flames, as well as many chemical vapour deposition systems, need to have transport properties database. In order

to characterize the transport properties of species in a multicomponent gaseous mixture, the evaluation of diffusion coefficients, viscosities, and thermal conductivities are required. Chemkin addresses both the mixture-averaged approach and the full multicomponent approach to transport properties depending on the computational effort. The transport package is designed for use with the Chemkin thermodynamic Database and the gas-phase kinetics utilities.

An example of the transport properties input data format is given in Figure 3.3. The transport database includes the molecular parameters for each species. 0, 1 and 2 can specify the geometry whether the molecule is monoatomic, linear or nonlinear, respectively. The Lennard-Jones potential well depth ε/kB, the Lennard-Jones collision diameter D_k, the dipole moment σ, the polarizability α, the rotational relaxation collision number, and the single component viscosity η are all specified in the input file. Some of the equations used for the calculation of transport properties are listed below:

$$\eta_k = \frac{5}{16} \frac{\sqrt{\pi m_k K_B T}}{\pi \sigma_k^2 \Omega^{(2.2)*}} \tag{3.9}$$

$$T_k^* = \frac{K_B T}{\varepsilon_k} \tag{3.10}$$

$$\sigma_k^* = \frac{1}{2} \frac{\mu_k^2}{\varepsilon_k \sigma_k^3} \tag{3.11}$$

$$m_{jk} = \frac{m_j m_k}{m_j + m_k} \tag{3.12}$$

$$D_{kj} = \frac{3}{16} \frac{\sqrt{2\pi m_k k_B{}^3 T^3 / m_{jk}}}{P\pi \sigma_{jk}^2 \Omega^{(1.1)*}} \tag{3.13}$$

where * refers to the reduced properties.

species Name	Geometry	ε/kB	δ	μ	α	Zort
AR	0	136.500	3.330	0.000	0.000	0.000
C	0	71.400	3.298	0.000	0.000	0.000
C2	1	97.530	3.621	0.000	1.760	4.000
C2O	1	232.400	3.828	0.000	0.000	1.000
CN2	1	232.400	3.828	0.000	0.000	1.000
C2H	1	209.000	4.100	0.000	0.000	2.500
C2H2	1	209.000	4.100	0.000	0.000	2.500

Figure 3.3. Example of transport properties input data format

3.5. Design Equations for Flame Modeling

The governing conservation equations used for modeling the 1-dimensional premixed, laminar flame with uniform inlet conditions are given below.

The mass continuity;

$$\dot{M} = \rho u A \tag{3.14}$$

The Conservation of Energy;

$$\dot{M}\frac{dT}{dx} - \frac{1}{cp}\frac{d}{dx}\left(\lambda A\frac{dT}{dx}\right) + \frac{A}{cp}\sum_{k=1}^{K}\rho Y_k V_k cp_k\frac{dT}{dx} + \frac{A}{cp} = \sum_{k=1}^{K}\dot{w}_k h_k W_k + \frac{A}{cp}\dot{Q}_{rad} = 0 \tag{3.15}$$

Species;

$$\dot{M}\frac{dY_k}{dx} + \frac{d}{dx}(\rho A Y_k V_k) - A\dot{w}_k W_k = 0 \qquad (k=1, \ldots, K_g) \tag{3.16}$$

Equation of State;

$$\rho = \frac{P\overline{W}}{RT} \tag{3.17}$$

where;

cp: constant pressure heat capacity of the mixture

cp_k: constant pressure heat capacity of the kth species

h_k: specific enthalpy of kth species

$\dot{M}$: mass flow rate

$\dot{Q}_{rad}$: heat loss due to gas and particle radiation

V_k: diffusion velocity of kth species

x: the spatial coordinate

Y_k: mass fraction of the kth species

$\dot{w}_k$: molar rate of production of the kth species per unit volume

$\overline{W}$: mean molecular weight of the mixture

λ : thermal conductivity of the mixture

The temperature profile was entered as an input so that fixed temperature solution method was used to solve for species concentration predictions in modeling the premixed laminar n-heptane and n-heptane/methanol flames.

3.6. Target Flame Model

The target flame that will be modelled has been studied experimentally by Inal and Senkan (2002b). The study concerned one-dimensional, laminar, premixed, fuel-rich flames (at equivalence ratio of 2.10) of n-heptane/O_2/Ar and n-heptane/methanol/O_2/Ar at atmospheric pressure with 2.7 percent (weight) of oxygen in n-heptane/methanol mixture. The experimental conditions of the study are given in Table 3.1.

The major, minor, and trace species were sampled from the flame by a heated quartz-microprobe at different heights above the burner. The characterization of the species concentration profiles was done by GC/TCD for major species, and GC/MS for minor and trace species. Species concentrations were determined either by direct calibration standards or by the use of mass spectral ionization cross-section method. The accuracy of the mole fractions for species determined by the direct calibration was estimated to be ± 15 %. However, ionization cross-section has been reported to be accurate within a factor of 2 (Inal and Senkan 2002b). Argon gas has been used for two functions; to dilute the mixture in both flames and to protect the flames from surroundings effects (shield gas). The temperature measurements were carried out by the rapid insertion technique with a silicon oxide-coated Pt-13% Rh/Pt, 0.075 mm thermocouple. The temperature profiles reported in the study correspond to direct thermocouple readings and were not corrected for radiation losses. The accuracy of the temperature measurements was estimated to be ± 50 °K (Inal and Senkan 2002a). The experimental setup is shown in Figure 3.4. The details of the experimental setup are given elsewhere (Inal and Senkan 2002b).

Table 3.1. The experimental conditions of the target flames (Inal and Senkan 2002b)

Conditions	n-Heptane	n-Heptane/Methanol
Equivalence ratio	2.10	2.10
Pressure (atm)	1	1
Inlet velocity (cm/sec)	5.17	5.157
n-C_7H_{16} mole fraction	0.055	0.0520
CH_3OH mole fraction	-	0.0107
O_2 mole fraction	0.2879	0.2803
Ar mole fraction	0.6571	0.6570
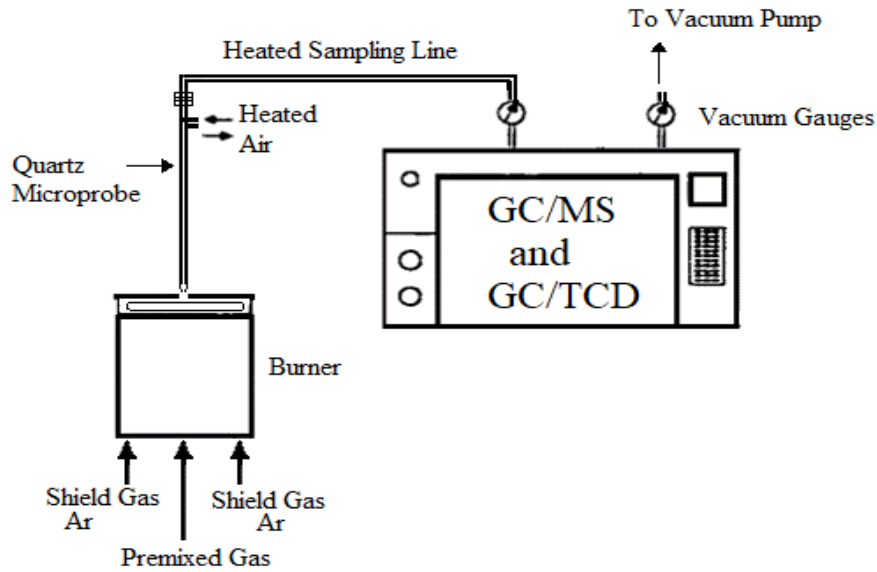
Figure 3.4.   Experimental setup of premixed flames (Inal and Senkan 2002b)

3.6. Radiation Corrections for Flame Temperature Measurements

When a thermocouple junction is suddenly immersed into a flame, the soot deposition on the thermocouple junction surface can cause a considerable difference in the measured temperature from the desired local gas temperature (Eisner and Rosner 1985). As a result of the heat loss from the thermocouple junction, the thermocouple temperature measurements could be lower than the actual gas temperatures by several hundred Kelvin.

It was claimed that there were soot covering at the thermocouple junction in the target flame (Inal 1999). Since the temperature profile is an important input for the model predictions of the species mole fractions using Chemkin, a proposed analysis for the radiation correction of thermocouple measurements in combustion environments was followed to obtain the corrected temperature profile (Chan 2011).

The energy balance is applied around the thermocouple junction in a quasi-steady balance, the heat flows by convection from the surrounding gas into the junction balanced with the heat by conduction and radiation through the junction.

$$\dot{q}_{convection} = \dot{q}_{radiation} + \dot{q}_{conduction} \tag{3.13}$$

By assuming the length of the thermocouple wire is much higher than the diameter of the wire (Collis and Williams 1959), the heat transfer by conduction can be neglected.

$$\dot{q}_{convection} = \dot{q}_{radiation} \tag{3.14}$$

$$q''_{convection} = q''_{radiation} \tag{3.15}$$

By defining each side of the previous equation:

$$q''_{convection} = \overline{h}\ (T_{gas} - T_{tj}) \tag{3.16}$$

$$q''_{radiation} = \varepsilon\sigma\ (T_{tj}^4 - T_{surr}^4) \tag{3.17}$$

where:

$\overline{h}$ = heat transfer coefficient, W/m^2K

T_{gas}= gas temperature, K

T_{tj}= thermocouple junction temperature, K

σ = Stefan-Boltzmann constant; $5.67 \times 10^{-8}\ W/m^2K^4$

ε= emissivity of thermocouple junction

T_{surr}= surrounding temperature, K

The heat transfer coefficient can be calculated by $\overline{h} = \dfrac{Nu * K_{g0}}{d_{tc}}$ and $Nu = f(Re, Pr)$. The junction was assumed to be in spherical geometry and an empirical relation was used to calculate Nu number (Collis and Williams 1959). This assumption is valid when d_j/d_w (The diameter of junction and wire) is large. The empirical relation used for Nu number is, (Acrivos and Taylor 1962)

$$Nu = 2 + 0.5Pe + 0.25Pe^2 \ln Pe + 0.03404Pe^2 + 0.0625Pe^3 \ln Pe \tag{3.18}$$

where:

d_{tc} = thermocouple junction diameter, m

k_{g0} =assumed constant, $\dfrac{k_{gas}}{T_{gas}} = 6.54 \times 10^{-5}\ W/mK^2$

Pe (Peclet number) = *Re* (Reynolds number) × *Pr* (Prandtl number)

In order to calculate *Re* and *Pr* numbers, physical, thermodynamic, and transport properties are required such as gas mixture thermal conductivity, gas mixture viscosity, specific heat, axial velocity, and mixture mass density. These properties were obtained from Chemkin by using measured temperature profiles.

The T_{surr} term can be omitted because T_{gas} is much higher than T_{surr}, so the final energy balance equation becomes:

$$\epsilon \sigma T_{tj}{}^4 = \frac{k_{g0} \times Nu}{2 d_{tc}} (T_{gas}{}^2 - T_{tj}{}^2)$$
(3.19)

Before using the final energy balance equation, the emissivity had to be determined. Because no soot covers the thermocouple junction at the first 2 mm, it was assumed that the emissivity to be equal to the emissivity value of the Pt-13% Rh/Pt, 0.075-mm thermocouple junction which corresponds to 0.1. The emissivity increased according to the linear relation with soot volume fractions since the thermocouple was covered by the soot for both flames (Inal and Senkan 2002b) (Figure 3.5 and Figure 3.6).
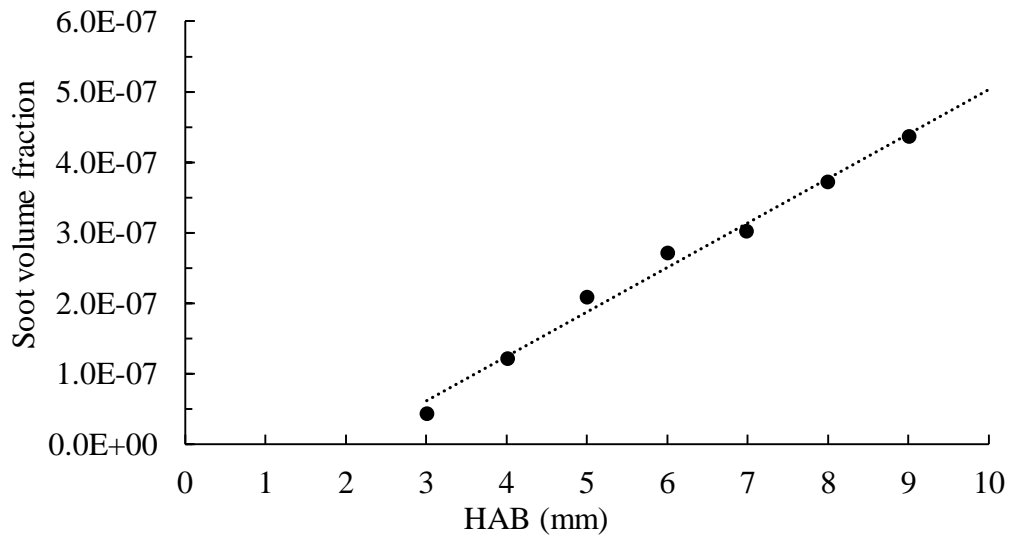
Figure 3.5. Soot volume fractions for the n-heptane flame (Inal and Senkan 2002a)
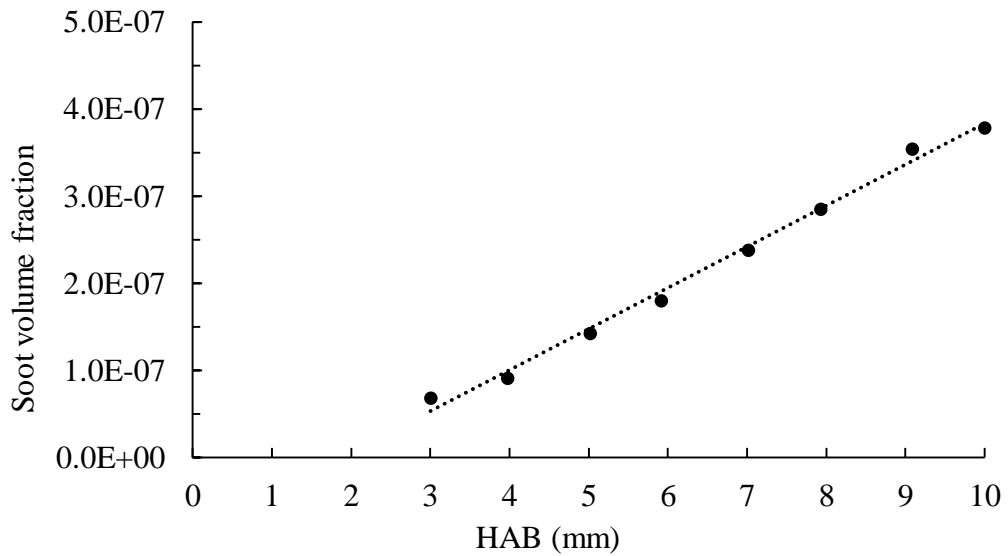
Figure 3.6. Soot volume fraction for the n-heptane/methanol flame (Inal and Senkan 2002b)

The corrected temperatures were obtained using the final energy balance equation and by solving for T_{gas}. Figure 3.7 and Figure 3.8 show the difference between the measured and the corrected temperatures for both n-heptane and n-heptane/methanol flames, respectively. The maximum differences between corrected and measured temperatures for n-heptane and n-heptane/methanol flames were roughly 287K and 292 K, respectively.
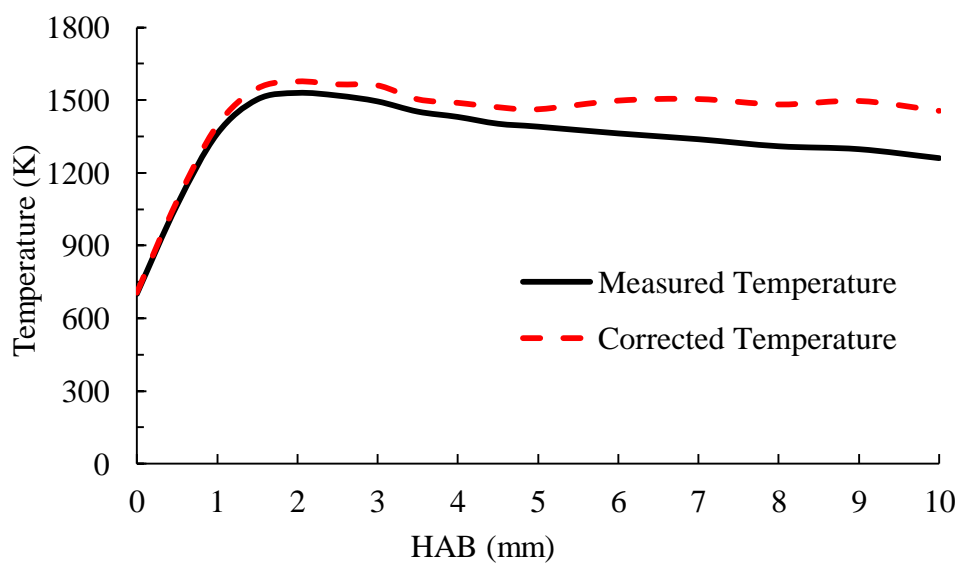
Figure 3.7. Measured and corrected temperature profiles of n-heptane flame
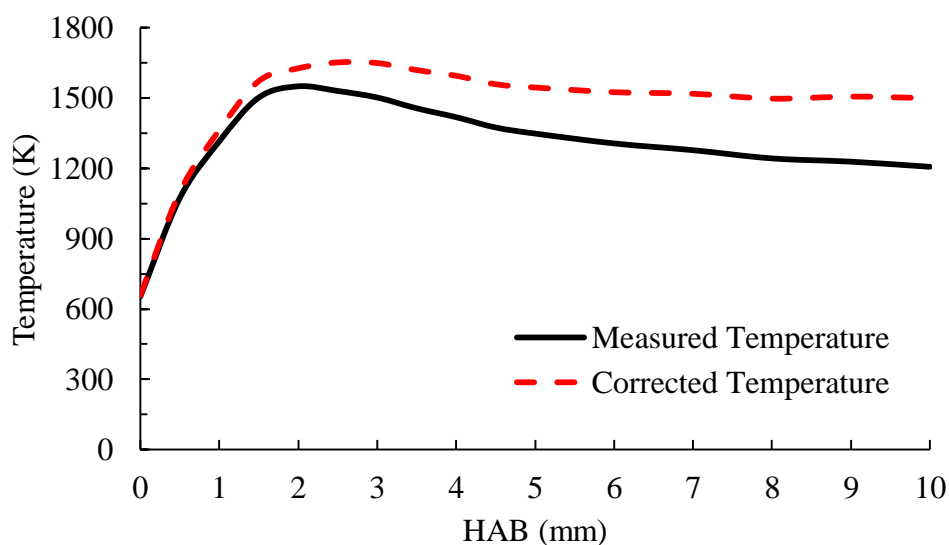
Figure 3.8.   Measured and corrected temperature profiles of n-heptane/methanol flame

The corrected temperature profile was used as an input for the modelling work using Chemkin to see its effect on the model predictions of species mole fractions. The difference of the model predictions using the measured and corrected temperature profiles are given in the next chapter.

3.7. Mechanism Generation

A recent mechanism proposed for the oxidation of n-heptane by Degirmenci (2018) has been chosen as a Base Mechanism for the modeling work. This Base Mechanism was established by an updated mechanism available in the literature, Lawrence Livermore National Laboratory LLNL (Version 3.1) mechanism (Mehl et al. 2011) as a starting mechanism. Since the LLNL mechanism does not include some reactions of C_4-C_6 species and PAHs formation, several mechanisms have been merged with the LLNL mechanism. These mechanisms are Marinov's mechanism (Marinov et al. 1998), Wang and Frenklach mechanism (Wang and Frenklach 1997), Richter and Howard mechanism (Richter and Howard 2000), and additional reactions from Park et. al. mechanism (Park et al. 2017). In addition, some reaction rate parameters have been modified using recent kinetic data available in the literature to improve the mechanism

predictions. The Base Mechanism is a detailed mechanism for the oxidation of n-heptane. It includes the decomposition pathways of n-heptane and the formation of PAHs up to A_4. However, the Base Mechanism does not have the whole reactions of the methanol oxidation. Therefore, a comprehensive and recent mechanism of the methanol oxidation (Burke et al. 2016) as a Donor Mechanism has been merged with the Base Mechanism. The Donor Mechanism includes the chemical reaction for all major species C_1–C_4 and the H_2–O_2 sub-chemistry. Table 3.2 illustrates the general features of the Base, Donor, and Master Mechanisms.

Table 3.2. Basic features of base, donor, and master mechanisms

	Number of Reactions	Number of Species	Reference
Base Mechanism	4185	893	(Degirmenci 2018)
Donor Mechanism	1011	173	(Burke et al. 2016)
Master Mechanism	**4480**	**945**	**This study**

3.8. Sensitivity Analysis and Alteration of Reaction Rate Parameters

Some reactions have considerable amount of uncertainty on their rate parameters due to the uncertainties in the experimental measurements of these parameters at different conditions. So these parameters need to be optimized to improve the model predictions. Sensitivity analysis is a way that can decide the most effective reactions on the formation and decomposition of particular species. Upon that analysis the reaction rate parameters of the effective reactions can be updated.

Sensitivity analyses across the flame for precursor species were performed to investigate the most sensitive reactions that play a significant role for the formation and decomposition of these species. The reaction rate parameters of sensitive reactions need to be updated to improve the model mole fraction predictions of the species. Sensitivity analysis for selected species (i.e., acetylene, propadiene, diacetylene, vinalacetylene and benzene), can present the most sensitive reactions for the formation and decomposition

of these species. These species were selected because their experimental data are available, and they were considered as playing important role for the formation of aromatics and polycyclic aromatic hydrocarbons. The sensitive reactions that have been updated in the Base Mechanism (Degirmenci 2018) will not be updated in this study for all the investigated species.

The sensitivity analysis of acetylene across the flame is given in Figure 3.9. The reaction $C_2H_4+H=C_2H_3+H_2$ was found as an important reaction for the formation of acetylene. The increase in the forward rate constants in this reaction would increase the acetylene mole fractions and improve the model predictions on the flame. Figure 3.10 shows the modified Arrhenius fit rate parameters proposed by different studies obtained from Reaction Mechanism Generator online database (RMG) (Green and West 2019).

The modified Arrhenius fit rate parameters for the reaction $C_2H_4 + H = C_2H_3 + H_2$ have been proposed by different studies (Peeters and Mahnen 1973, Tsang and Hampson 1986, Weissman and Benson 1988, Knyazev et al. 1996) (Figure 3.10). The Arrhenius fit rate parameters of Peeters and Mahnen (1973) were higher than the Arrhenius fit parameters of the Master Mechanism (shown as Chemkin in Figure 3.10). These higher Arrhenius fit rate parameters were used for modeling the flame but it had no significant effect on the predictions of the acetylene mole fractions (Figure 3.11).
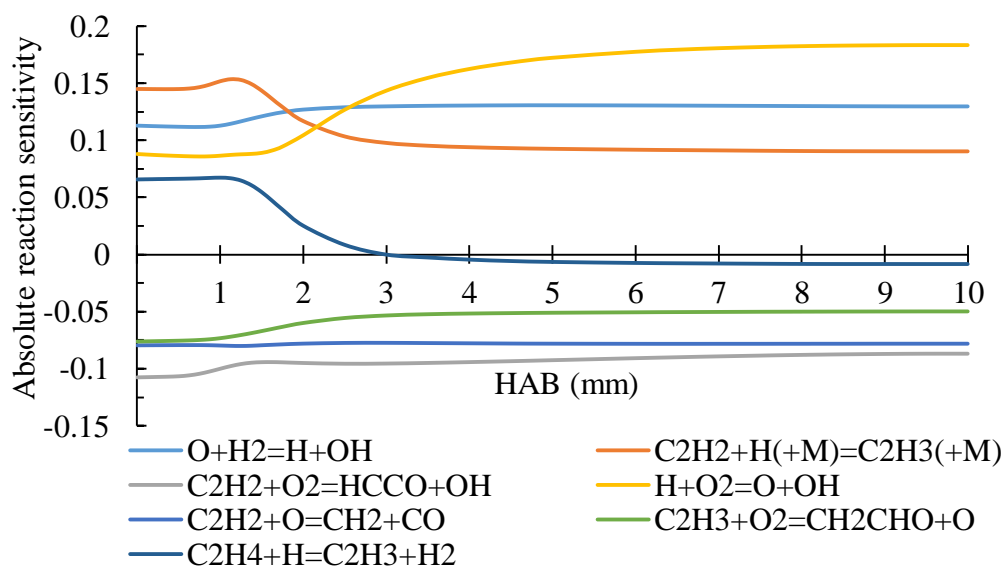

Figure 3.9. Sensitivity analysis of C_2H_2 across the flame
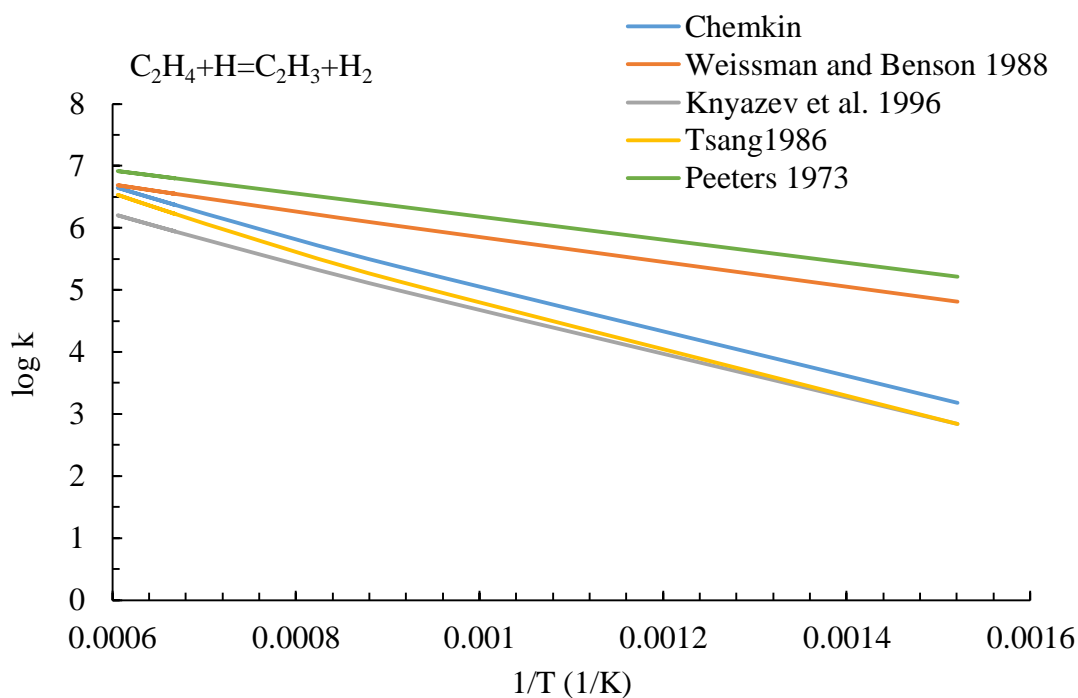
$C_2H_4+H=C_2H_3+H_2$

Figure 3.10. Forward logarithmic rate constant versus inverse temperature for $C_2H_4 + H = C_2H_3 + H_2$ reaction

The reaction $C_2H_2+H(+M) =C_2H_3(+M)$ was found as an important reaction for the consumption of acetylene. To improve the model predictions of acetylene mole fractions, the forward rate parameter was required to be lowered which could decrease the rate of the decomposition of acetylene. Figure 3.12 shows the modified Arrhenius fit rate parameters that suggested by different studies obtained from Reaction Mechanism Generator online database (RMG).

The modified Arrhenius fit rate parameters for the reaction $C_2H_2+H(+M)$ $=C_2H_3(+M)$ have been suggested by different studies (Baulch et al. 1992, Knyazev et al. 1996) (Figure 3.12). The Arrhenius fit rate parameters of RMG Group were lower than the Arrhenius fit parameters of the Master Mechanism (shown as Chemkin in Figure 3.12). They were used for modeling the flame and underpredictions were achieved at 0-5 mm HAB. At 5 mm and higher HAB, the model predictions of C_2H_2 mole fraction were nearly the same as the model predictions by the Master Mechanism. (Figure 3.13).

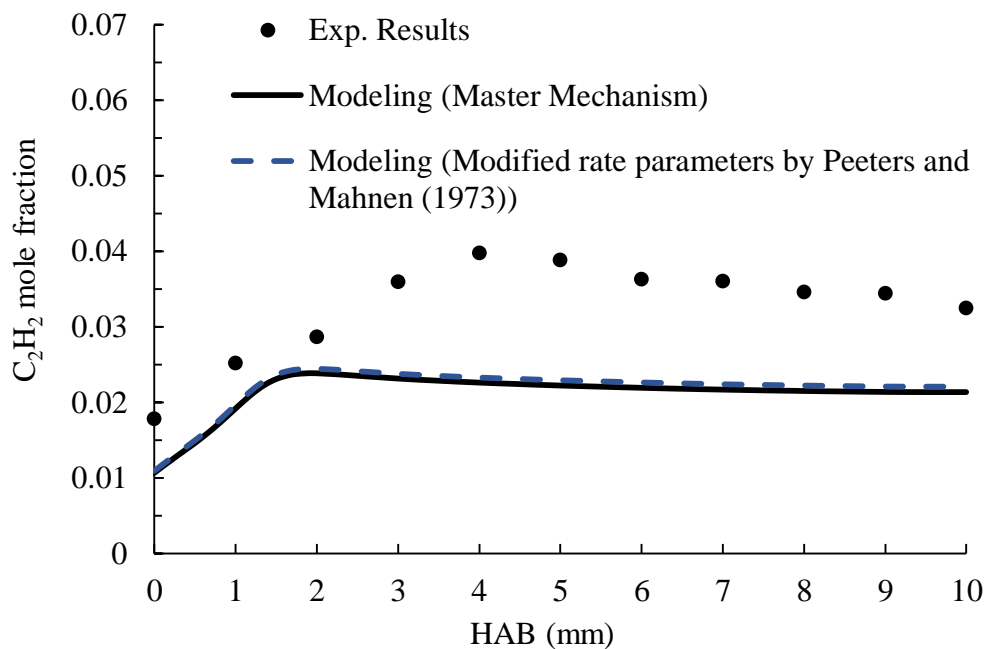Figure 3.11. The effect of the modified reaction rate parameter of $C_2H_4 + H = C_2H_3 + H_2$ on C_2H_2 mole fraction predictions

Figure 3.12. Forward logarithmic rate constant versus inverse temperature for $C_2H_2 + H(+M) = C_2H_3(+M)$ reaction

Figure 3.13. The effect of the modified reaction rate parameter of $C_2H_2+H(+M)$ $=C_2H_3(+M)$ on C_2H_2 mole fraction predictions

The sensitivity analysis of propadien (C_3H_4-A) across the flame is given in Figure 3.14. The sensitive reaction C_3H_4-P+H=C_3H_3+H_2 has been found as an effective reaction for the consumption of propadien. The forward rate parameters were required to be decreased which could decrease the rate of propadien consumption. As a result, the model predictions of propadien mole fractions would be improved. Figure 3.15 shows the modified Arrhenius fit rate parameters suggested by different studies obtained from Reaction Mechanism Generator online database (RMG).

The modified Arrhenius fit rate parameters for the reaction C_3H_4-P+H=C_3H_3+H_2 have been suggested by different studies (Lopez et al. 2009, Dooley et al. 2010, Bugler et al. 2016). The Arrhenius fit rate parameters of Dooley et al. (2010) were lower than the Arrhenius fit parameters of the Master Mechanism (shown as Chemkin in Figure 3.15). No significant difference in the model predictions of propadien mole fraction has been found when the Arrhenius fit rate parameters of Dooley et al. (2010) were used (Figure 3.16).

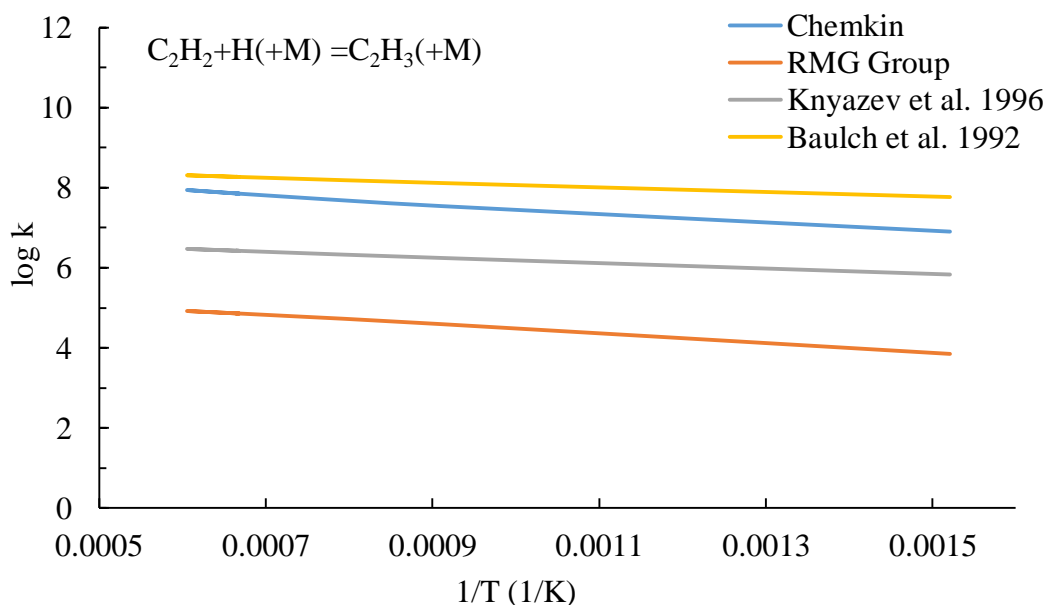Figure 3.14. Sensitivity analysis of C_3H_4-A across the flame

Figure 3.15. Forward logarithmic rate constant versus inverse temperature for C_3H_4-P $+H=C_3H_3+H_2$
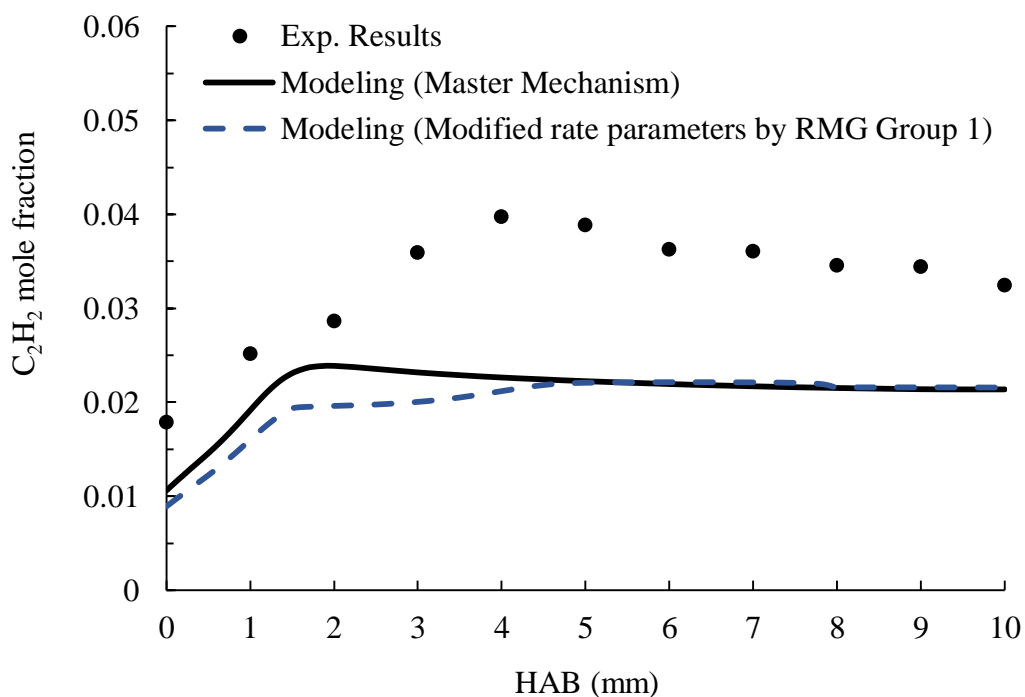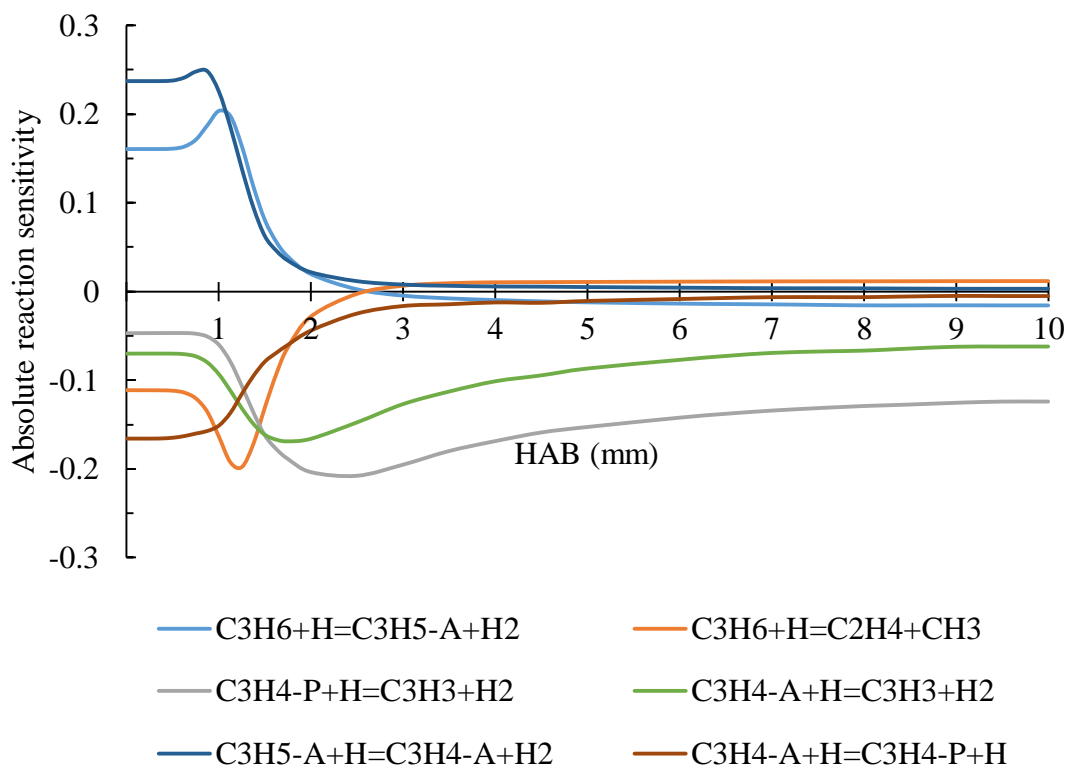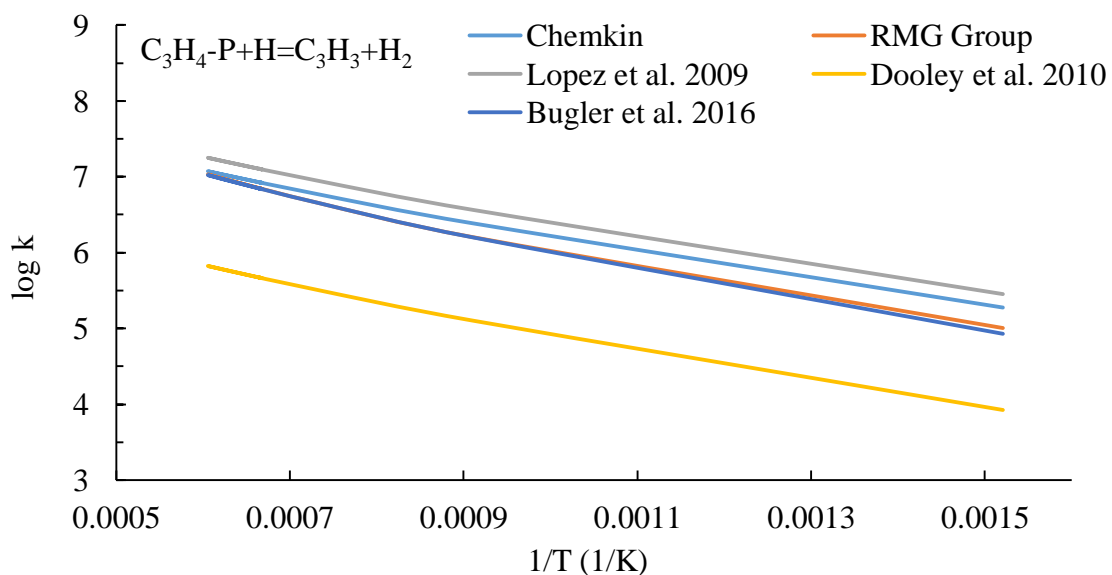
Figure 3.16. The effect of the modified reaction rate parameter of C_3H_4-P+H $=C_3H_3+ H_2$ on C_2H_2 mole fraction predictions

The sensitivity analysis of diacetylene (C_4H_2) across the flame is given in Figure 3.17. The reaction $C_2H_2+OH=C_2H+H_2O$ was found as an important reaction for the consumption of diacetylene. To improve the model predictions of diacetylene mole fractions, the forward rate parameter was required to be decreased which could decrease the rate of the consumption of diacetylene. Figure 3.18 shows the modified Arrhenius fit rate parameters proposed by different studies obtained from Reaction Mechanism Generator online database (RMG) for $C_2H_2+OH=C_2H+H_2O$.

The modified Arrhenius fit rate parameters for the reaction $C_2H_2+OH=C_2H+H_2O$ have been suggested by different studies (Eiteneer and Frenklach 2003, Acarl et al. 2005). The Arrhenius fit rate parameters of RMG Group were lower than the Arrhenius fit parameters of the Master Mechanism (shown as Chemkin in Figure 3.18) and they were used for modeling the flame. The previously mentioned reaction was also found as an important reaction for the consumption of acetylene, therefore the model predictions of acetylene mole fraction have been investigated. No significant differences in the model predictions of acetylene and diacetylene mole fractions have been achieved when the modified Arrhenius fit rate parameters of RMG Group were used (Figures 3.19 and 3.20).

Figure 3.17. Sensitivity analysis of C$_4$H$_2$ across the flame

Figure 3.18. Forward logarithmic rate constant versus inverse temperature for C$_2$H$_2$+OH =C$_2$H+H$_2$O
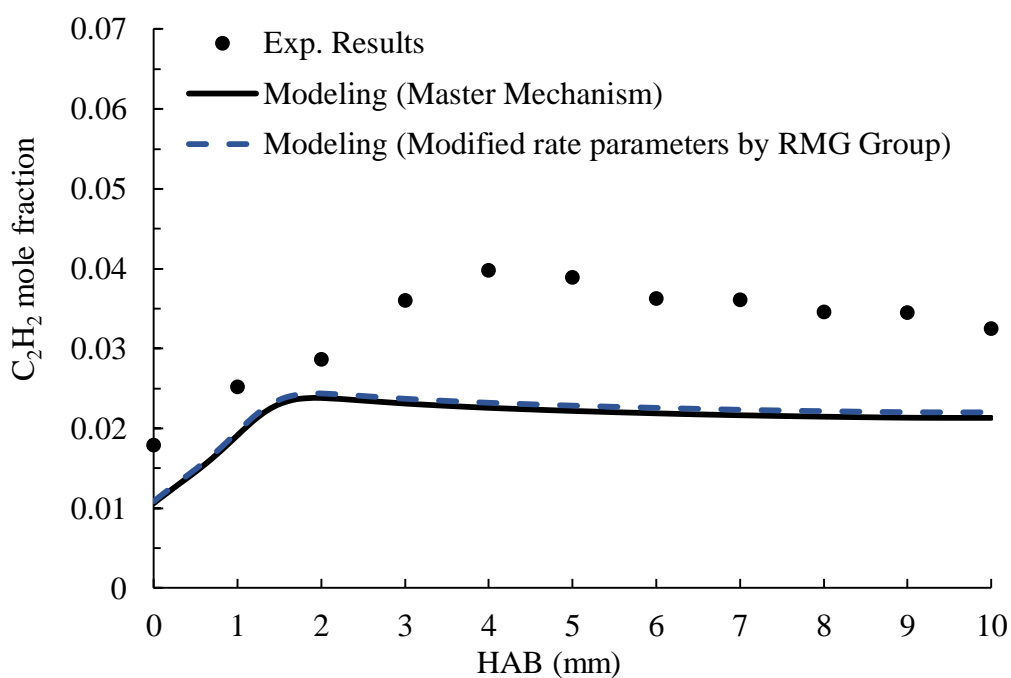
Figure 3.19. The effect of the modified reaction rate parameter of $C_2H_2+OH=C_2H+H_2O$ on C_2H_2 mole fraction predictions
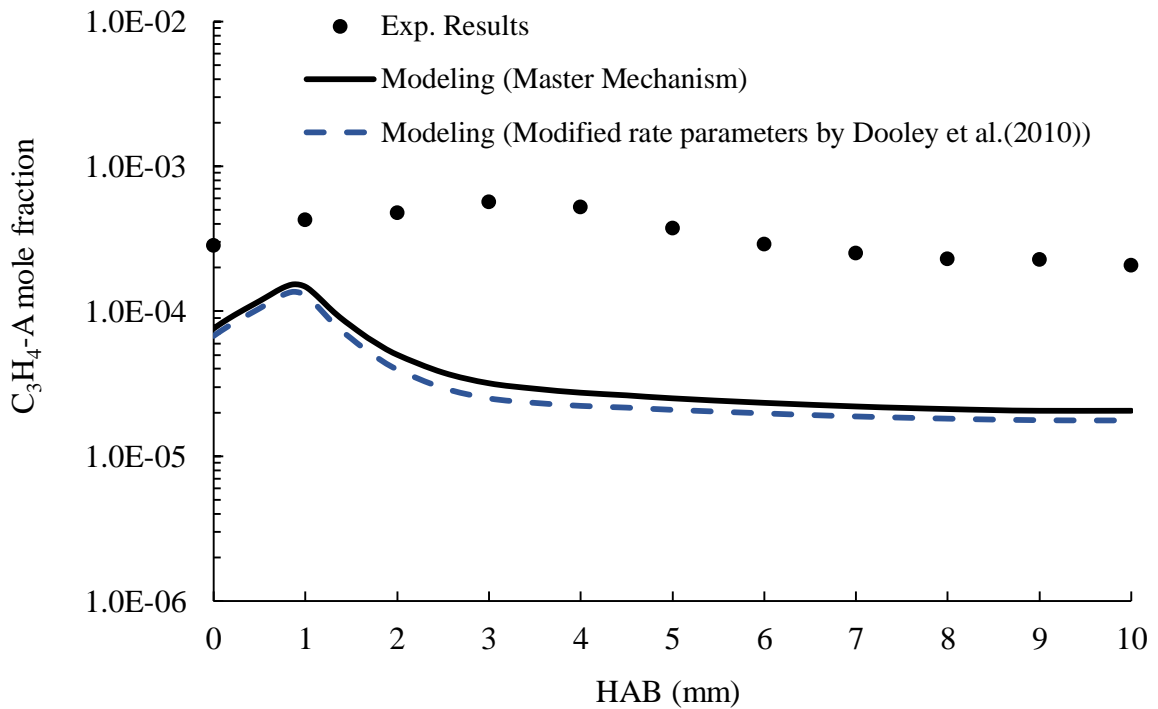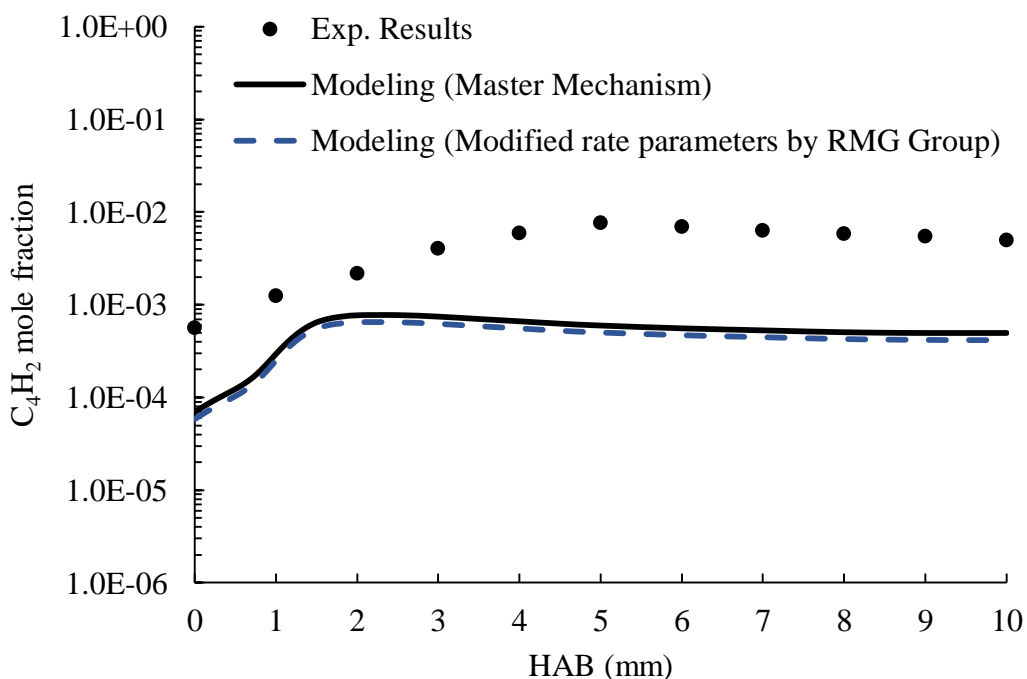

Figure 3.20. The effect of the modified reaction rate parameter of $C_2H_2+OH=C_2H+H_2O$ on C_4H_2 mole fraction predictions

The sensitivity analysis of vinylacetylene (C_4H_4) across the flame is given in Figure 3.21. The reaction $C_4H_4+H=i-C_4H_3+H_2$ has been found as an effective reaction for the consumption of vinylacetylene. The forward rate parameter of the reaction needed to be decreased, therfore the model predictions of vinylacetylene mole fractions would be improved. Figure 3.22 shows the modified Arrhenius fit rate parameters given by different studies (Bugler et al. 2016, RMG-Group1 2019, RMG-Group2 2019). The Arrhenius fit rate parameters of RMG Group 1 were the lowest so they were used for modeling the flame. The modified Arrhenius fit rate parameters had almost no effect on the predictions of the C_4H_4 mole fraction (Figure 3.23). Since there was no significant difference in the model predictions, these rate parameters have not been used in the Master Mechanism.
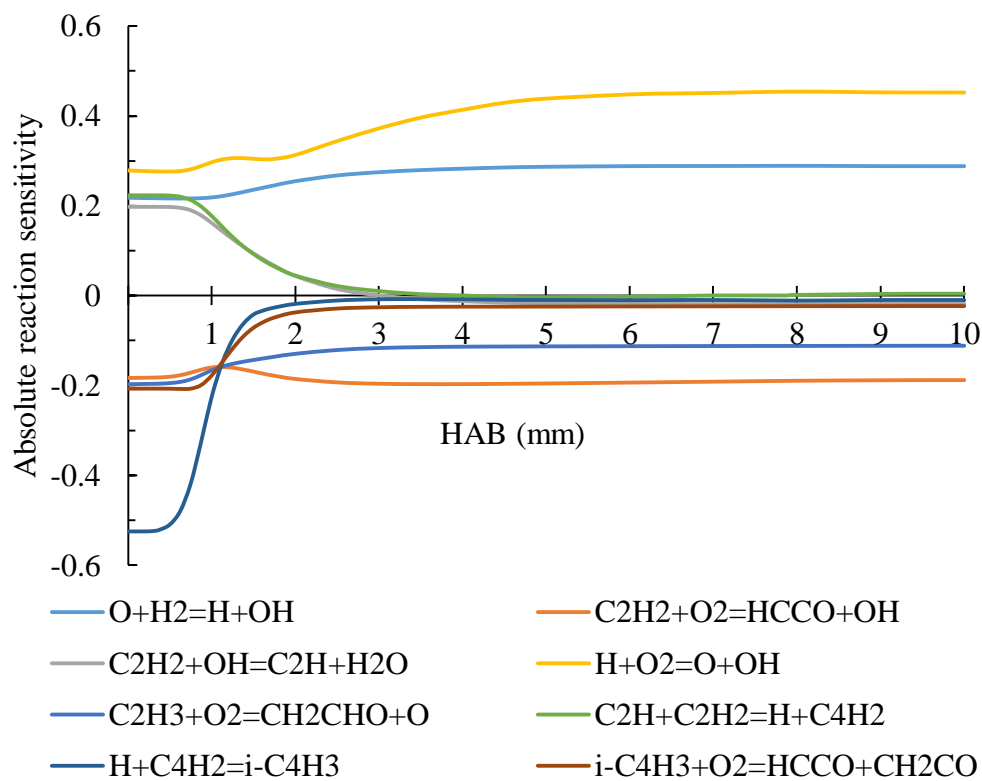

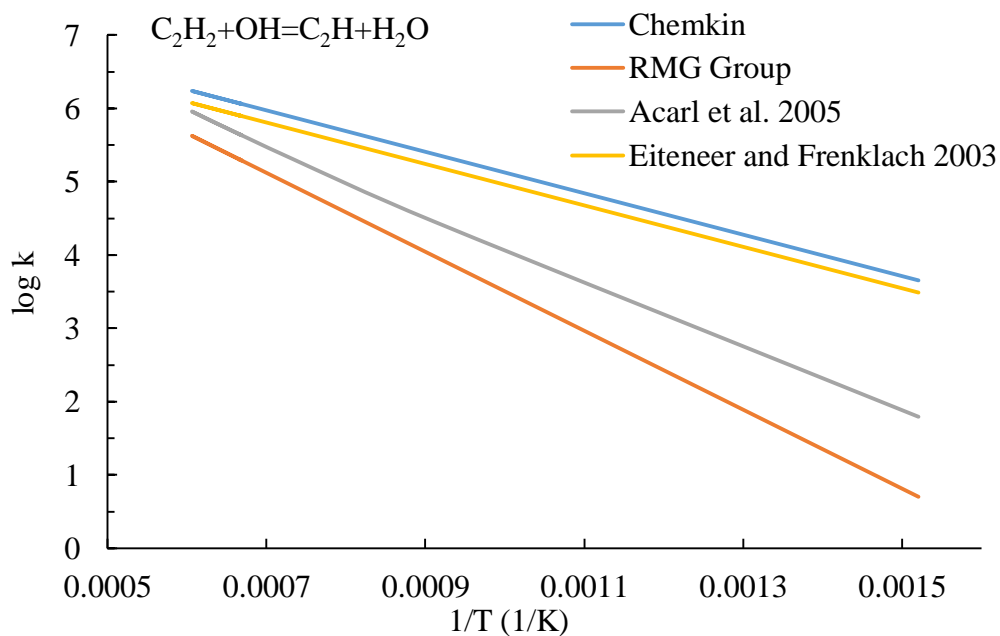Figure 3.21. Sensitivity analysis of C_4H_4 across the flame

Figure 3.22. Forward logarithmic rate constant versus inverse temperature for C_4H_4 $+H=i\text{-}C_4H_3+H$

Figure 3.23. The effect of the modified reaction rate parameter of $C_4H_4+H=i\text{-}C_4H_3+H_2$ on C_4H_4 mole fraction predictions

The sensitivity analysis of benzene (C_6H_6) across the flame is given in Figure 3.24. The reaction $C_3H_3+OH=C_2H_3+HCO$ has been found playing a role for the destruction of

benzene. The forward rate parameters were required to be increased to avoid the overpredictions of C_6H_6 mole fractions and improve model predictions on the flame. The model overprdicted the benzene mole fractions specifically at high distances above the burner. Figure 3.25 shows the modified Arrhenius fit rate parameters proposed by different studies (Lopez et al. 2009, Bugler et al. 2016) . The Arrhenius fit rate parameters of Bugler et al. (2016) were higher than the Arrhenius fit parameters of the Master Mechanism (shown as Chemkin in Figure 3.25). As these parameters used for modelling work, it had better effect on the predictions of the C_6H_6 mole fractions specifically at high distances above the burner (Figure 3.26). These rate parameters have not been used in the Master Mechanism, since there was no significant difference in the overall model predictions.

The sensitivity analysis has been carried out for precursor species and benzene, and updated reaction rate parameters have been tested. When the updated reaction rate parameters have been altered in the mechanism, no significant improvements for the model predictions have been achieved. This might be attributed to the developments made on the Base Mechanism (Degirmenci 2018) using altered parameters for different sensitive reactions. Therefore, no changes have been made for the Master Mechanism regarding the reaction rate parameters of the sensitive reactions.
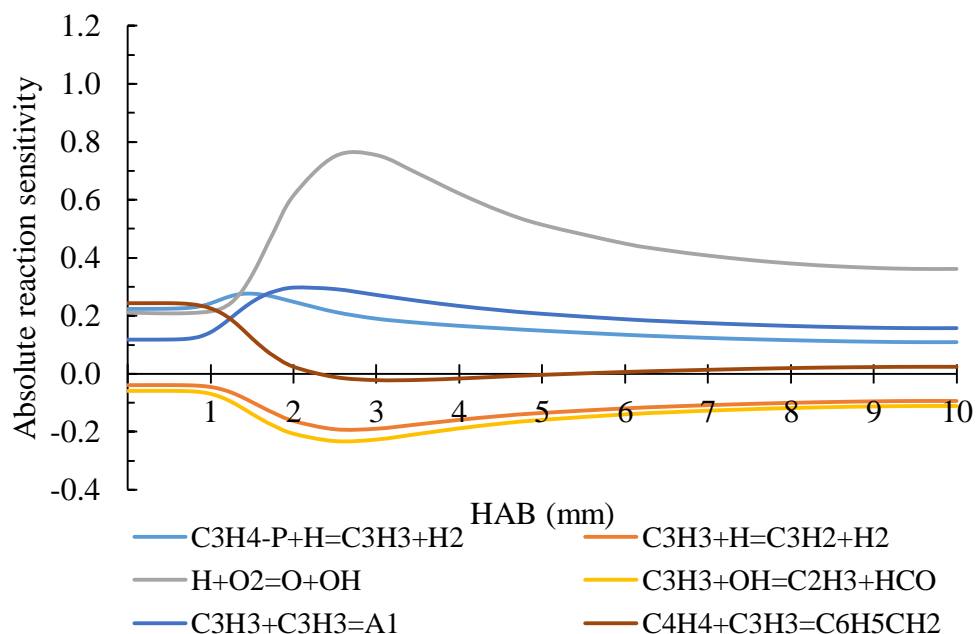
Figure 3.24. Sensitivity analysis of benzene across the flame
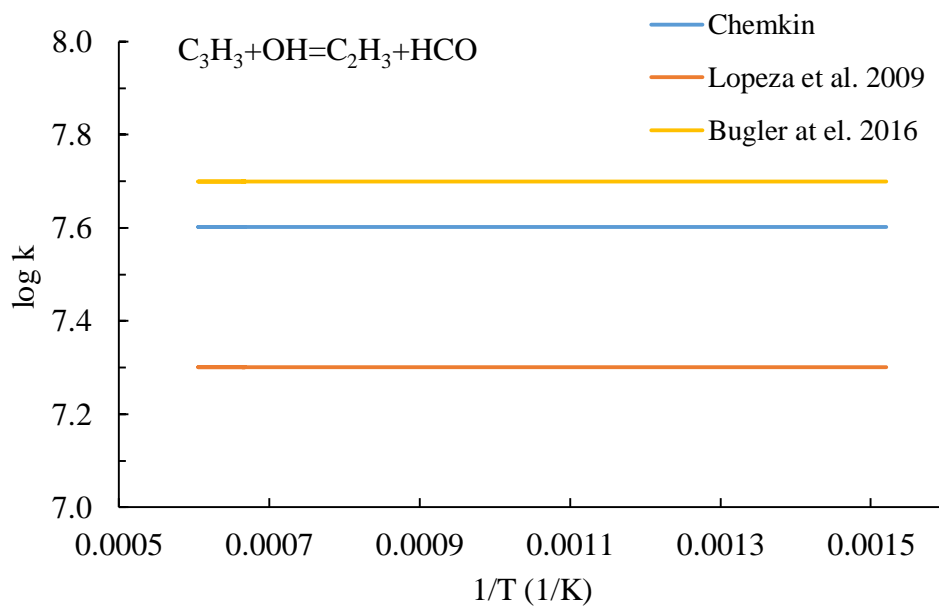
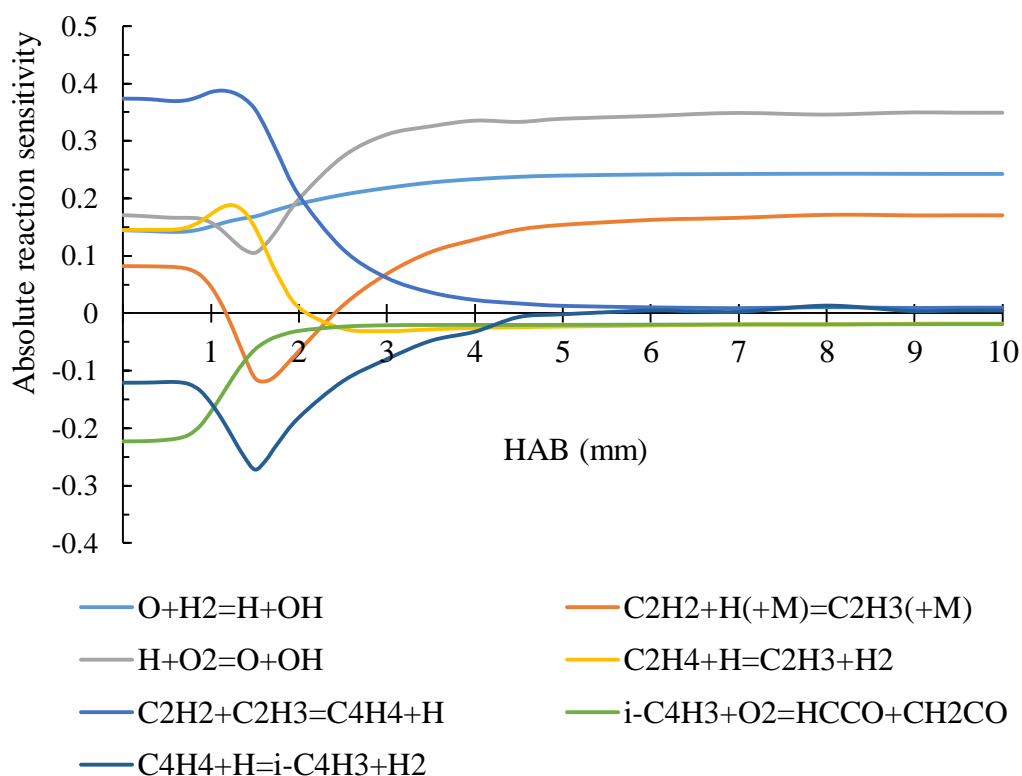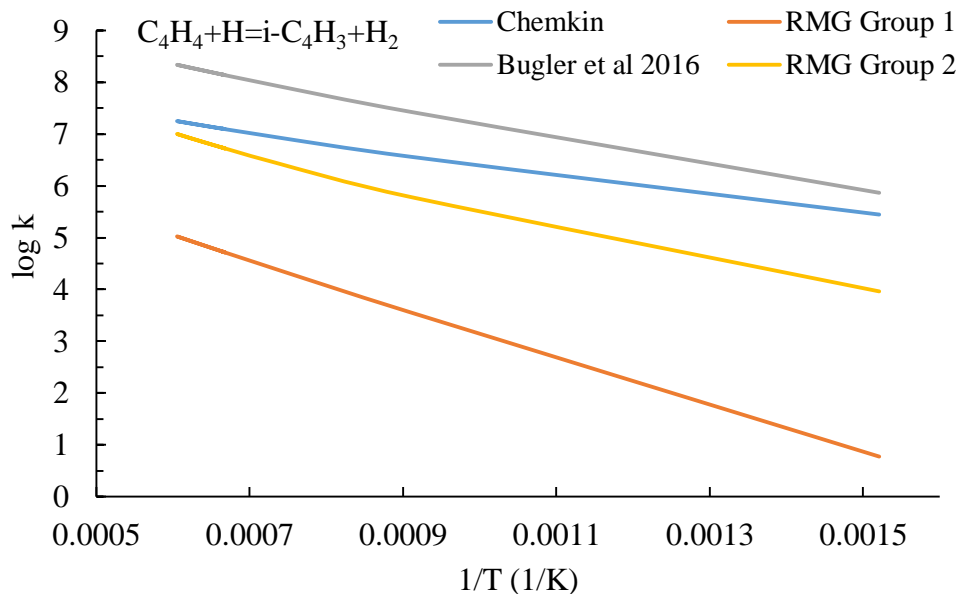Figure 3.25. Forward logarithmic rate constant versus inverse temperature for $C_3H_3+OH=C_2H_3+HCO$

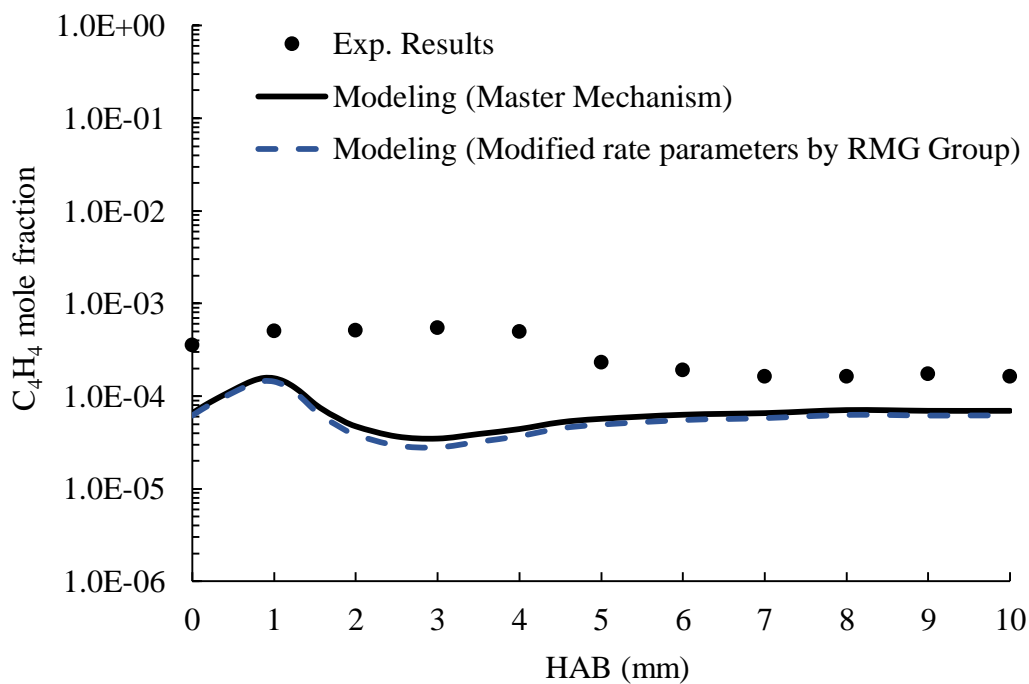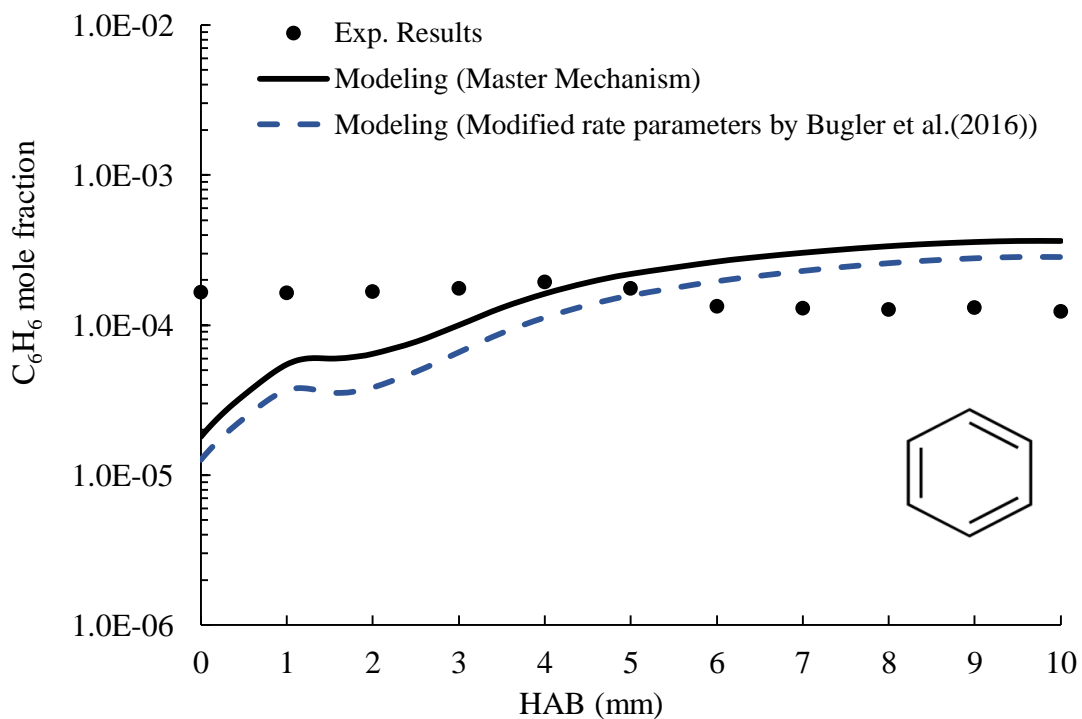Figure 3.26. The effect of the modified reaction rate parameter of $C_3H_4\text{-}P+H=C_3H_3+H_2$ on benzene mole fraction predictions

CHAPTER 4

RESULTS AND DISCUSSION

4.1. Model Validation

To investigate the capabilities of the Master Mechanism, model validation has been carried out using various experimental data available in the literature for different combustion systems. Rapid compression machine (RCM) experimental data (Kumar and Sung 2011) were used to validate the ignition delay time estimations of methanol by the Master Mechanism. The mole fraction profiles of species were validated by experimental data of premixed, laminar n-heptane/methanol flame (Chen et al. 2012). Table 4.1 shows the general characteristics of the two studies that have been used for the model validation.

Table 4. 1. Experimental conditions of the studies used for the model validation

Conditions	Chen et al. (2012)	Kumar and Sung (2011)
System type	Premixed flame	RCM
Temperature (K)	400~ 1980	850-1100
Pressure (atm)	0.04	14.8
Equivalence ratio φ	1.6	1
n-C_7H_{16} mole fraction	0.078	-
CH_3OH mole fraction	0.018	0.1227
O_2 mole fraction	0.549	0.184
Ar mole fraction	0.355	0.693

The model validations were done using ignition delay time experimental measurements of methanol (Kumar and Sung 2011) to understand the capabilities of the Master Mechanism. The ignition delay time is the time between injecting the fuel into the engine cylinder, and the start of combustion (Lakshminarayanan and Aghav 2010). A closed, homogenous batch reactor with a constant volume was used in the modeling as a

rapid compression machine. As seen in Figure 4.1, there were underestimations by the Master Mechanism for the ignition delay times of pure methanol fuel. Kumar and Sung (2011) have also used a kinetic mechanism to predict ignition delay times. The modeling predictions of the Master Mechanism developed in this study were closer to the experimental measurements compared with the performance of their model. The model validation of the Master Mechanism using RCM experimental data has shown that the Master Mechanism is able to predict ignition delay times of pure methanol fuel.
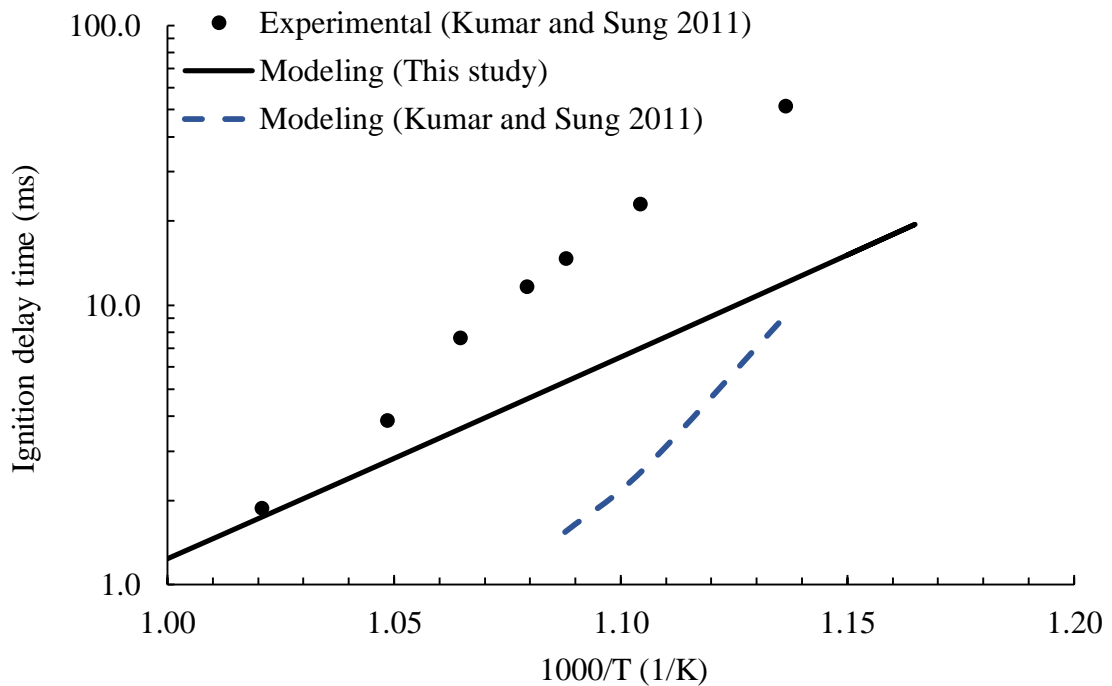
Figure 4. 1.Validations of the Master Mechanism by ignition delay times

Additional model validation has been carried out by one dimensional, laminar, premixed n-heptane/methanol flame of Chen et al. (2012). The fixed temperature solver was used with the measured temperature profile. The comparison between the model predictions and experimental measurements of species concentration profile for H_2 is shown in Figure 4.2. The modeling results of H_2 by the Master Mechanism have fitted most of the experimental results. A good prediction has been achieved by the Master Mechanism for hydrogen mole fractions.
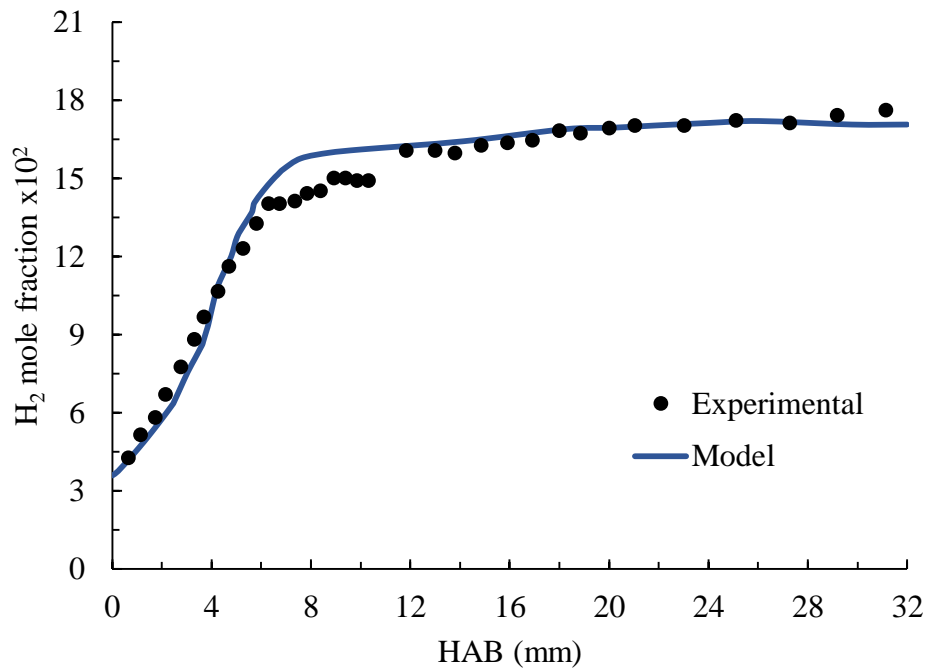
Figure 4. 2. Validation of the Master Mechanism on H_2 mole fraction profiles of a Flame (Chen et al. 2012)
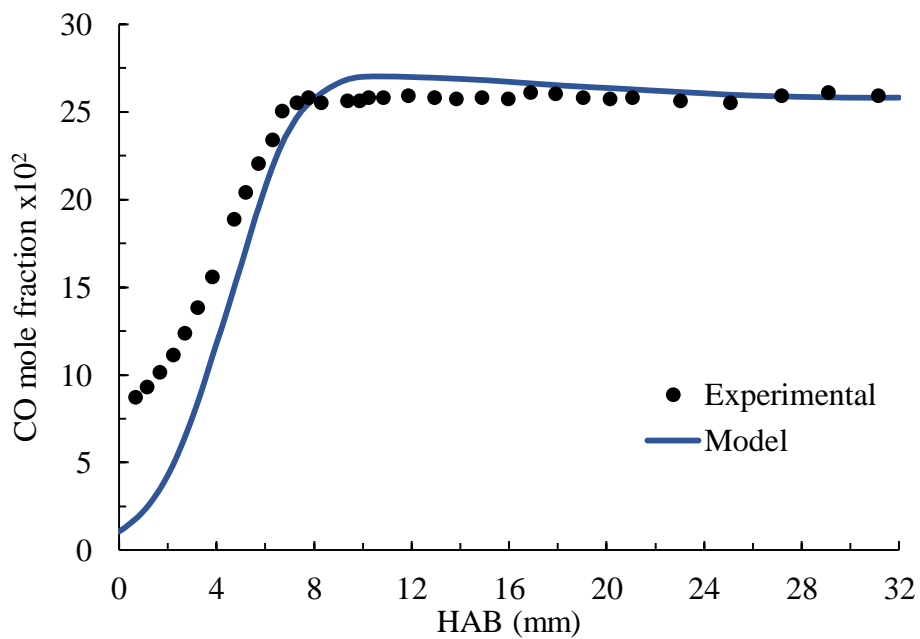
Figure 4. 3. Validation of the Master Mechanism on CO mole fraction profiles of a Flame (Chen et al. 2012)

The model predictions and experimental measurements of CO mole fraction profiles are shown in Figure 4.3. There were underpredictions by the model at low heights

above the burner. At higher distances, the model predicted the experimental measurements very well. The comparison between the model predictions and experimental measurements of species concentration profile for CO_2 is shown in Figure 4.4. It can be seen that, Master Mechanism slightly underpredicted the carbon dioxide mole fraction profile at 0 to 20 mm HAB. However, the Master Mechanism has given proper results at higher distances for the carbon dioxide mole fraction profile.
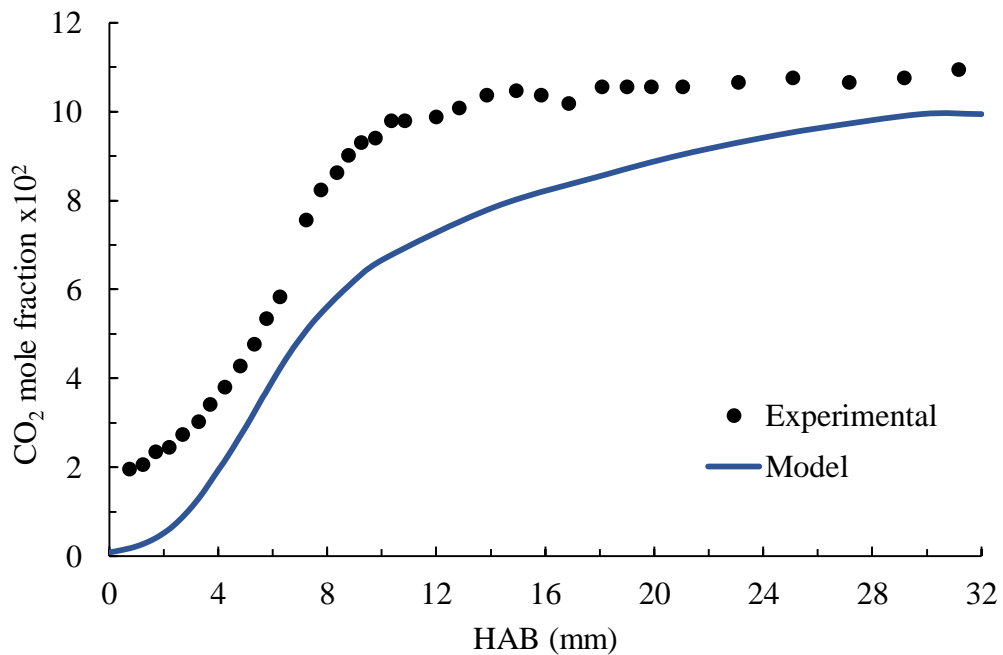
Figure 4. 4. Validation of the Master Mechanism on CO_2 mole fraction profiles of a Flame (Chen et al. 2012)

4.2. Effects of Temperature Correction on the Model Performance

The model predictions of species mole fractions in the target flames (n-heptane and n-heptane/methanol) (Inal and Senkan 2002b) were affected by the temperature corrections. To better understand the difference in the model predictions using the corrected and measured temperature profiles, a comparison of some species mole fractions predictions were carried out.

As seen in Figure 4.5 there was a difference between acetylene mole fraction predictions by the Master Mechanism using corrected and measured temperature profiles. The model with the corrected temperature profile could predict the experimental

measurements of acetylene mole fractions better than the model with the measured temperature profile. Figure 4.6 shows the effect of temperature profile on propadiene mole fractions profiles. The temperature corrections slightly increased the model predictions of propadiene mole fractions at lower heights above the burner surface (HAB < 2 mm). For HAB greater than 2 mm, no significant differences in propadien mole fractions were found (Figure 4.6).
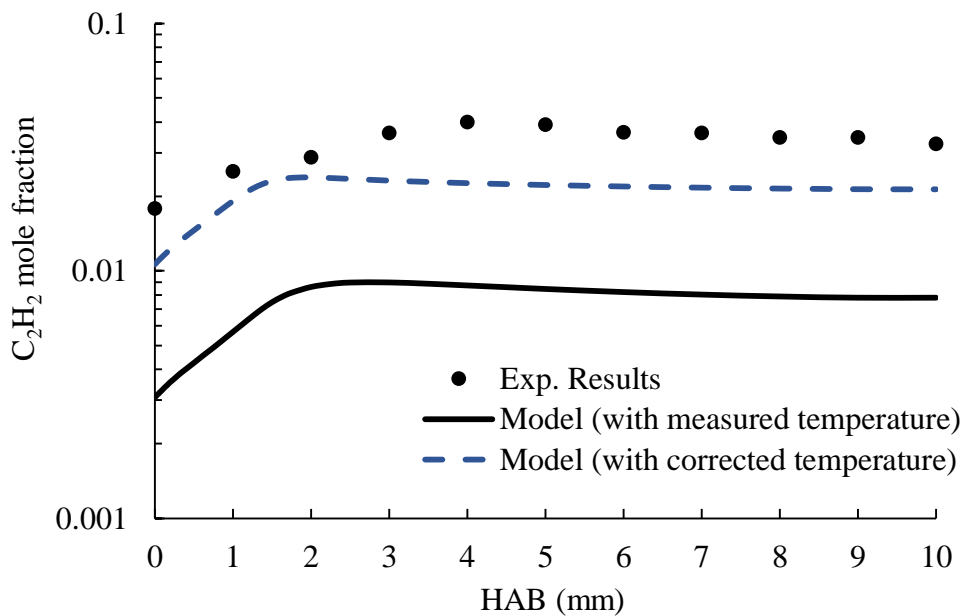
Figure 4. 5. Effect of temperature profile on acetylene mole fractions

The effect of temperature profile on mole fraction predictions of vinylacetylene is given in Figure 4.7. The effect of temperature corrections was greater than the previously mentioned species (propadien). The model with the corrected temperature profile has given closer predictions to the experimental measurements than the model with the measured temperature profile (Figure 4.7). For benzene (Figure 4.8), the effect of temperature correction on the mole fraction profile was not considerable in terms of the benzene mole fraction predictions.

For two aromatic ring species, the effect of temperature profile on naphthalene mole fractions is given in Figure 4.9. The effect of using the corrected temperature profile instead of measured temperature profile improved the model predictions of naphthalene mole fractions specially at HAB greater than 2 mm. At lower heights above the burner

surface (HAB < 2 mm) the temperature corrections did not affect the model predictions (Figure 4.9).
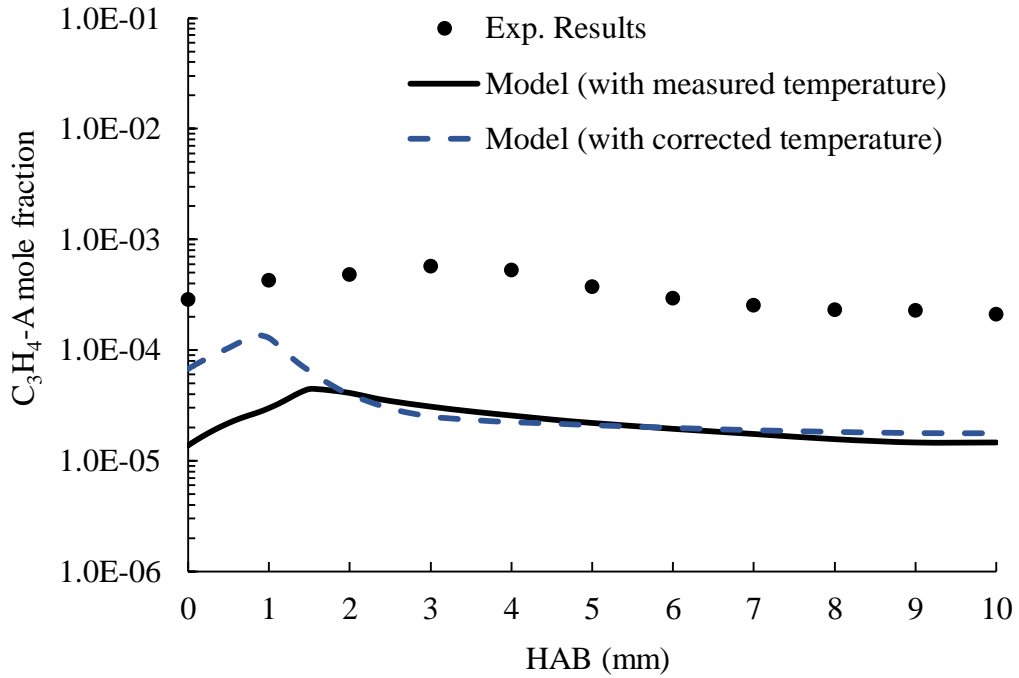
Figure 4. 6. Effect of temperature profile on propadiene mole fractions
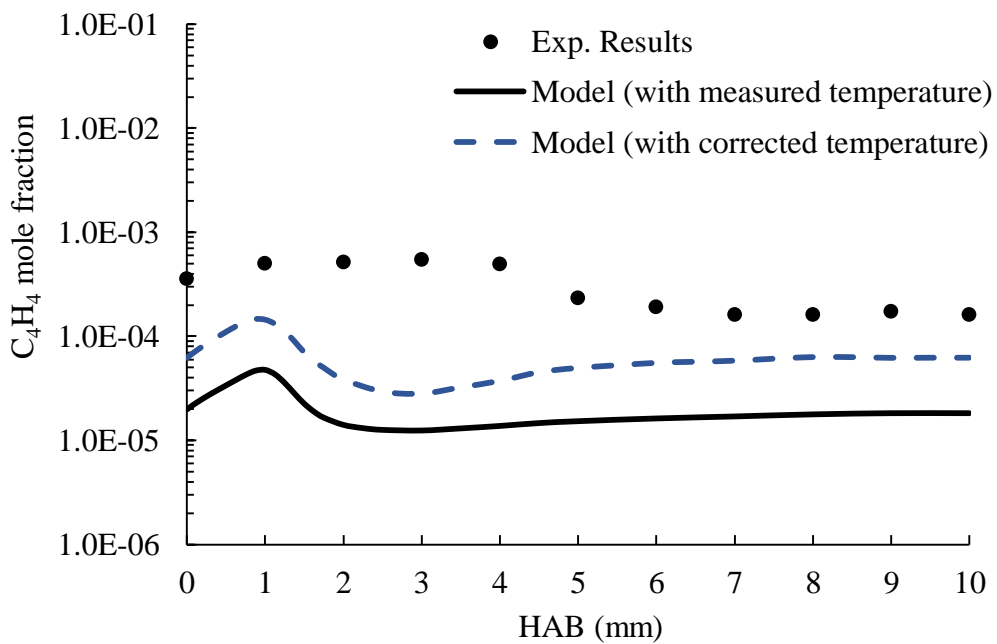
Figure 4. 7. Effect of temperature profile on vinylacetylene mole fractions
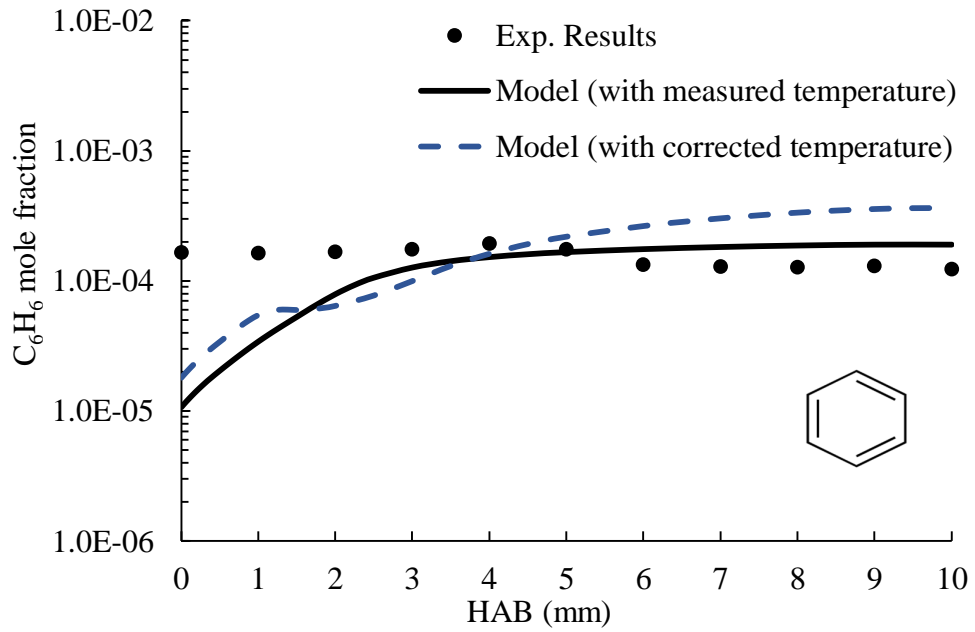
Figure 4. 8. Effect of temperature profile on benzene mole fractions
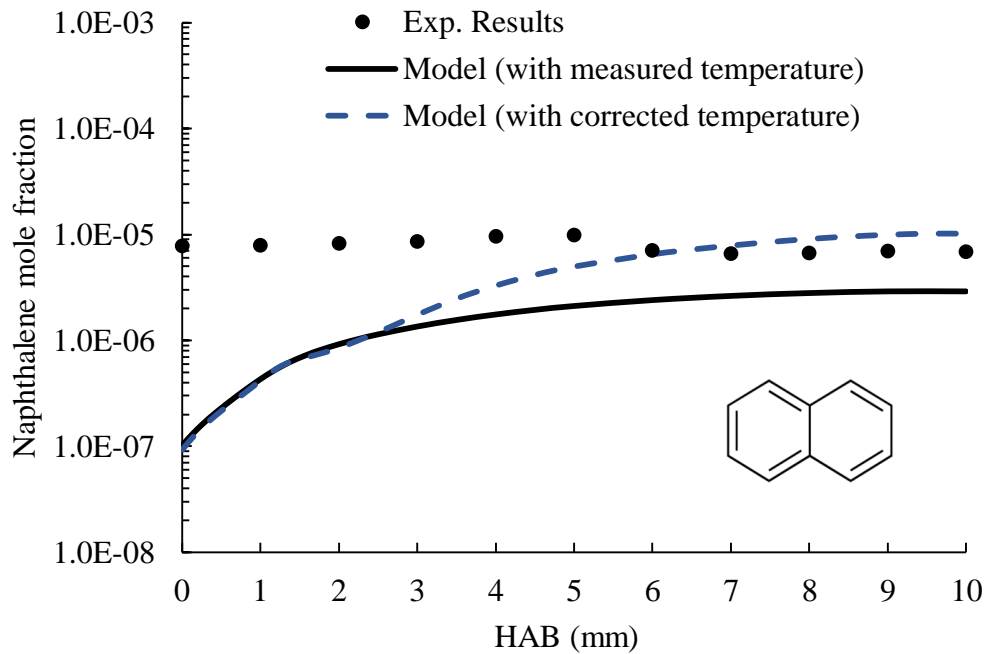
Figure 4. 9. Effect of temperature profile on naphthalene mole fractions

As seen in Figure 4.10, the corrected temperature profile had significant effect on the acenaphthylene mole fraction predictions. The mole fraction predictions of acenaphthylene were much closer to experimental measurements when the corrected

temperature profile was used (Figure 4.10). The difference between the model predictions using the corrected and measured temperature profiles was high and it seemed acenaphthylene was highly sensitive to the temperature.
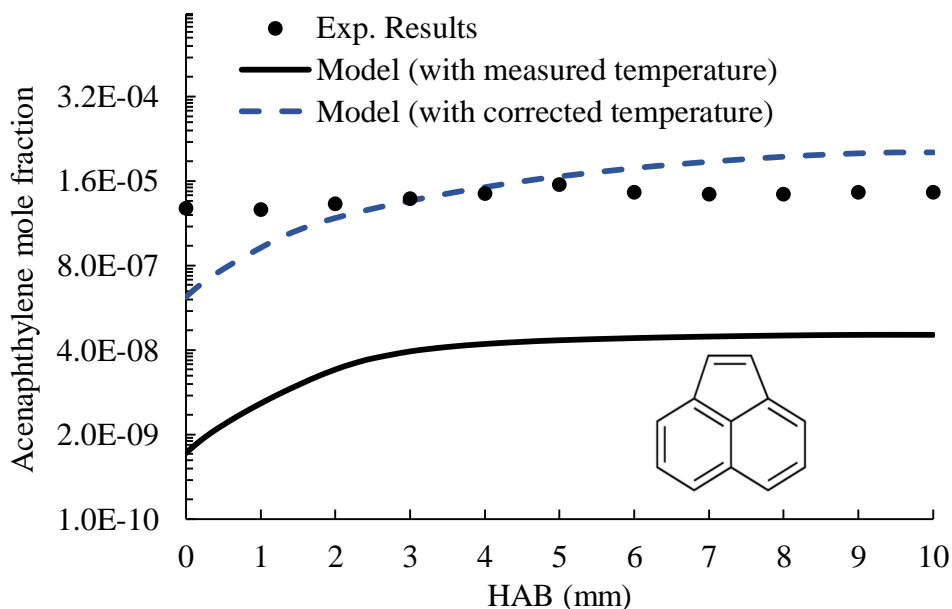
Figure 4. 10. Effect of temperature profile on acenaphthylene mole fractions

The investigations of the effect of the temperature corrections on the model predictions of species mole fractions in the flame have shown that the uncertainties in the temperature measurements can have high influence on the mole fraction predictions for some species.

4.3. Detailed Analysis for the Flames

To analyse the flame in details, rate of production and pathway analyses should be carried out. The aim of doing the rate of production/consumption analysis is to find the elementary reactions that form/decompose the species. While the pathway analysis has been done for some important species (i.e., important precursors and aromatics) to understand the formation or the decomposition pathways of these species. The pathway analysis shows the reaction sequences of the formation or decomposition of the species

based on either carbon, hydrogen or both fluxes. Basically, these fluxes pathways can be drawn using the software by following the carbon and hydrogen elements on the reaction sequences. The thickness of the drawn lines is proportional with the formation ratio of the species for the pathway analysis. The thicker the line is the faster the reaction rate will be. It is worth mentioning that the experimental measurements at low HAB (0 ~2 mm) were considered questionable due to the higher amount of uncertainty at the microprobe sampling caused by the possible interactions between sampling microprobe and the burner surface (Inal 1999). Based on that, the experimental measurements at these heights were considered less reliable, especially for PAHs.
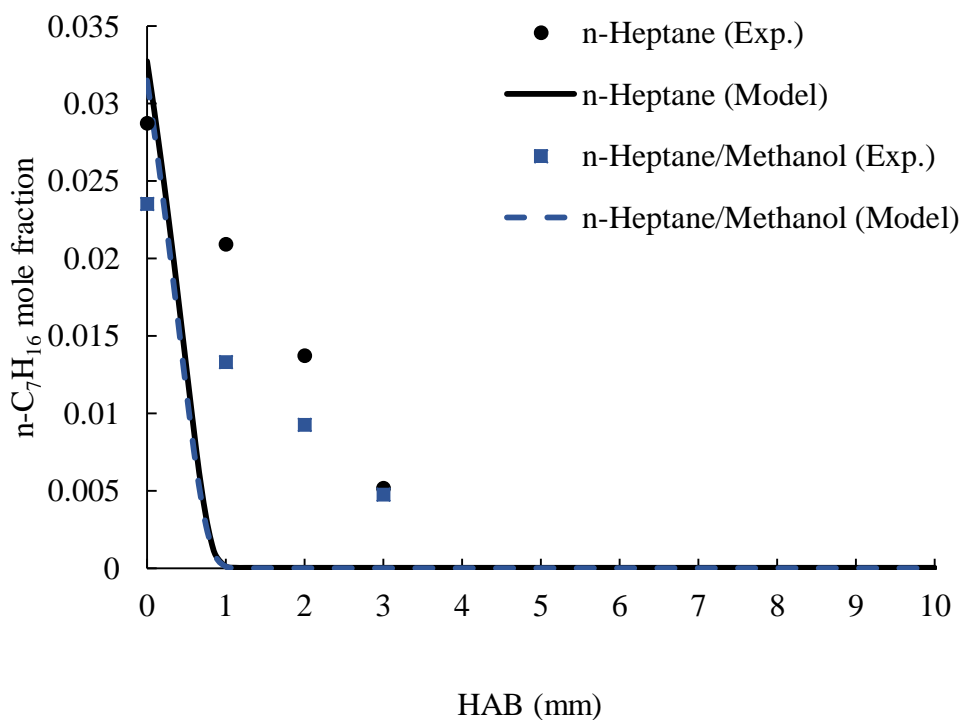
Figure 4. 11. Comparison of species profiles of n-heptane

As seen in Figure 4.11, the Master Mechanism predicted the n-heptane mole fraction profiles in both flames. The fuel completely consumed at HAB ~3 mm according to the experimental measurements while the model predictions showed consumption of n-heptane at lower HAB (~1 mm) for both flames.

According to the rate of production analysis for n-heptane in n-heptane flame (Figure 4.12), the n-heptane consumption occurs at 0 to ~1.25 mm HAB. The main

reactions consuming the n-heptane are either hydrogen abstraction reactions (by H or OH radicals) or third body reactions (these reactions are listed in Figure 4.12). The minimum point of the total consumption rate of n-heptane for n-heptane flame corresponds to 0.8125 mm. This point has been chosen to do the pathway analysis for both carbon and hydrogen fluxes. Based on the decomposition analysis, the most dominant reactions are $NC_7H_{16}+H=C_7H_{15}-2+H_2$ and $NC_7H_{16}+H=C_7H_{15}-3+H_2$ ($C_7H_{15}-2$ and $C_7H_{15}-3$ refer to 2-heptyl and 3-heptyl radicals, respectively). The same reactions have been reported as the most dominant reactions for the oxidation of fuel-rich n-heptane in a jet-stirred flow reactor in the temperature range of 950-1200 K at atmospheric pressure (Chakir et al. 1992). The decomposition reactions of n-heptane (i.e., $n-C_7H_{16}(+M)=C_5H_{11}-1+C_2H_5(+M)$ and $n-C_7H_{16}+OH=C_7H_{15}-2+H_2O$) were also found as important decomposition reactions, which is consistent with a study of laminar premixed low pressure n-heptane/methanol flame at an equivalence ratio of 2 by Xu et al. (2013).

Figure 4. 12. Rate of production analysis for $n-C_7H_{16}$ across the flame (n-heptane)
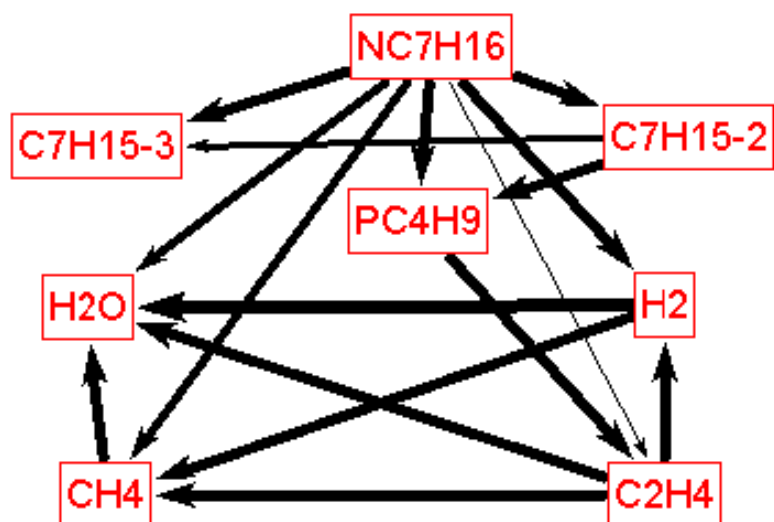
Figure 4. 13. n-Heptane decomposition pathways at HAB=0.8125mm (both H and C
fluxes) (n-heptane flame)

The pathway analysis for the decomposition of n-heptane can be seen in Figure
4.13 (both hydrogen and carbon fluxes). The n-heptane decomposes to 2-heptyl and 3-
heptyl. After that 2-heptyl mainly breaks down to 1-butyl (PC_4H_9) which decomposes to
ethene (C_2H_4) (Figure 4.13). The reaction C_7H_{15}-2= PC_4H_9+C_3H_6 was found as the
thermal decomposition of 2-heptyl radical by β-Scission of C-C bond at high temperatures
(Chakir et al. 1992). The decomposition path for 3-heptyl is not shown in Figure 4.13
since the decomposition rate is very low (-3.20 x10^{-06} mole/cm^3.sec). For the n-heptane
decomposition reactions, the hydrogen abstraction reactions by H radical form H_2 while
hydrogen abstraction reactions by OH radical form H_2O (Figure 4.12). The n-heptyl
radicals, which formed by H-atom abstraction reactions, are assumed to rapidly undergo
thermal decomposition through the β-scission of a C-C bond at high temperatures (Held,
Marchese, and Dryer 1997, Dagaut, Reuillon, and Cathonnet 1994).

C_7H_{15}-1= C_5H_{11}-1 +C_2H_4 (C_5H_{11}-1 refers to 1-pentyl)

C_7H_{15}-2= PC_4H_9+C_3H_6

C_7H_{15}-3= C_6H_{12}-1+ CH_3 (C_6H_{12}-1 refers to 1-hexene)

C_7H_{15}-4= C_5H_{10}-1+C_2H_5 (C_5H_{10}-1 refers to 1-pentene)

The rate of production analysis for n-heptane in n-heptane/methanol flame (Figure
4.14) shows that the n-heptane consumption occurs at 0 to ~1.25 mm HAB. The

consumption of n-heptane in n-heptane and n-heptane/methanol flames occur at the same HAB. The minimum point of the total rate of n-heptane decomposition for n-heptane/methanol flame is different from that one for the n-heptane flame, which corresponds to 0.75 mm HAB. So that means n-heptane consumption starts earlier by having methanol as an oxygenate in the fuel. The pathway analysis for both carbon and hydrogen fluxes has been done at 0.75 mm HAB. The main reactions consuming the n-heptane are either hydrogen abstraction reactions (by H or OH radicals) or third body reactions (these reactions are listed in Figure 4.14). Figure 4.15 shows the pathway analysis of both hydrogen and carbon fluxes for the decomposition of n-heptane for n-heptane/methanol flame. There was no significant difference in the decomposition of n-heptane in both flames (i.e., n-heptane/methanol and n-heptane flames) (Figures 4.13 and 4.15). The main difference that has been found between these two flames is the rate of consumption of the reaction $NC_7H_{16}+H=C_7H_{15}-1+H_2$ becomes slightly higher for n-heptane/methanol flame (Figure 4.14).
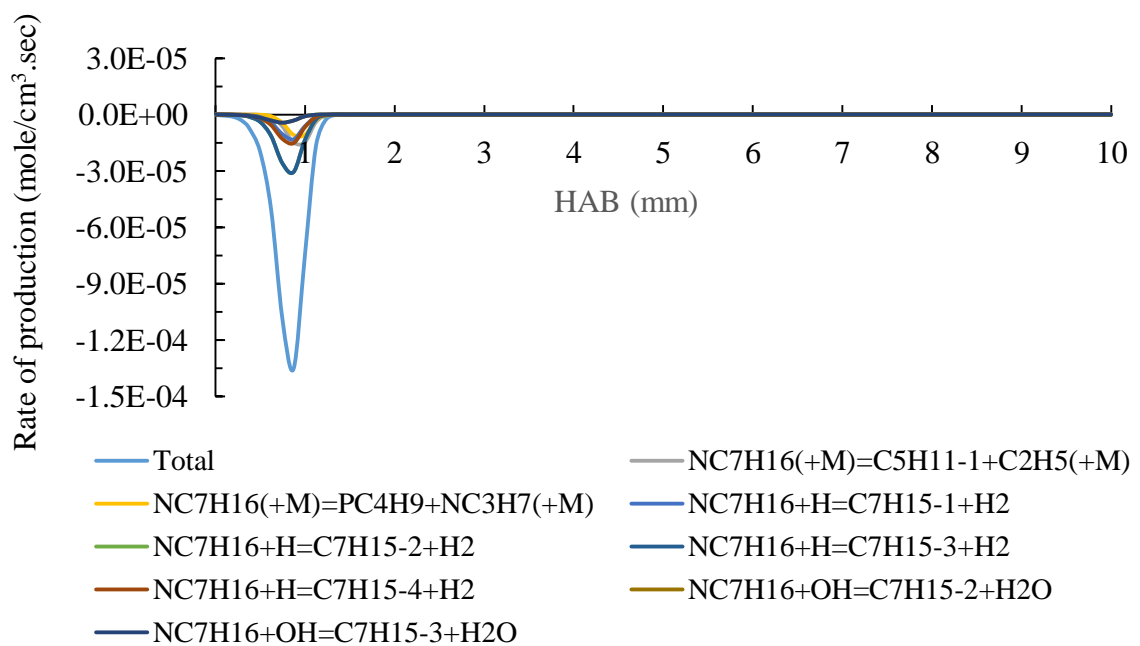

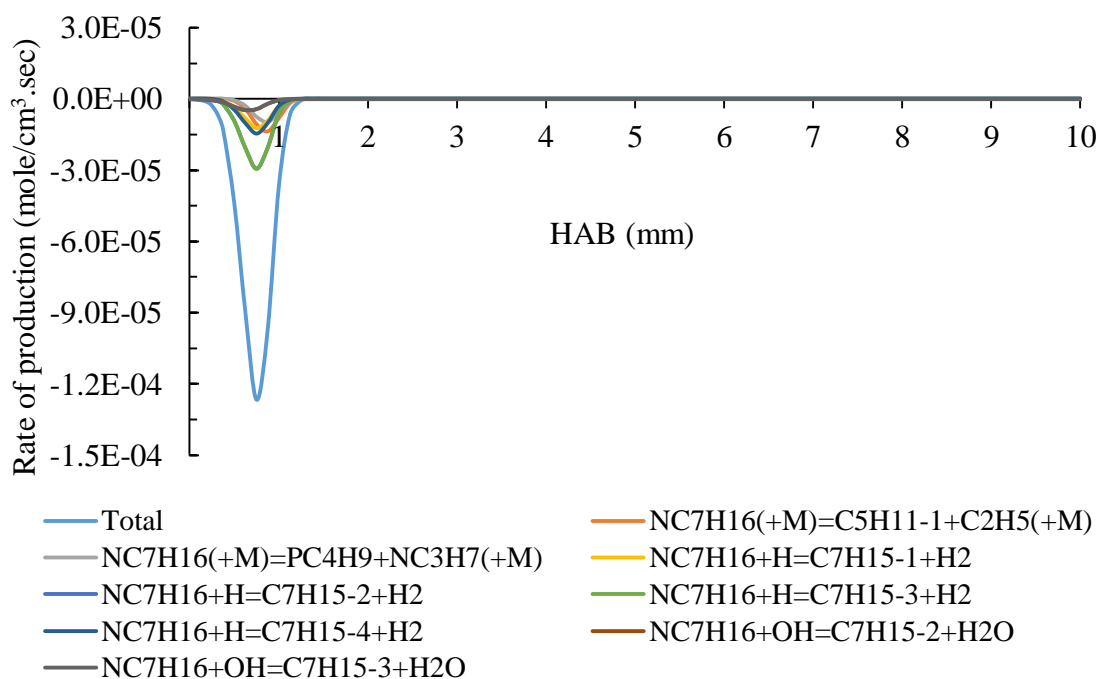Figure 4. 14. Rate of production analysis for NC_7H_{16} across the flame (n-Heptane/methanol)
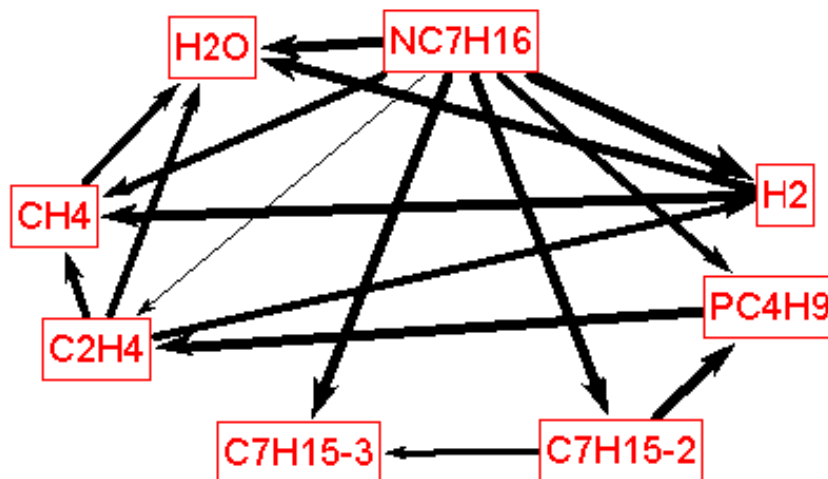
Figure 4. 15. n-Heptane decomposition pathways at HAB=0.75mm (both H and C flux) (n-heptane/methanol flame)

The rate of production analysis for methanol across the flame can be seen in Figure 4.16. The rate of consumption of methanol mainly occurs at 0-2 mm HAB. The minimum point of the methanol total rate of consumption is at 1 mm HAB, and the pathway analysis is carried out at this point for both hydrogen and carbon fluxes. From the pathway analysis (Figure 4.17), the most dominant reactions for the methanol consumption were $CH_3OH+H=CH_2OH+H_2$ and $CH_3OH+H=CH_3O+H_2$. Methanol decomposes majorly to CH_2OH and H_2 as seen from the reactions in Figure 4.16. In JSR fuel-rich methanol study (at atmospheric pressure and temperature range of 633 to 873 K), the same reactions have been reported for methanol consumption paths (Held and Dryer 1998). Methanol decomposes predominantly through H abstraction and produces either hydroxymethyl radical (CH_2OH) or methoxy radical (CH_3O). Subsequently, CH_2OH decomposes mainly to formaldehyde (CH_2O) by hydrogen abstraction reaction, which is the most important intermediate product during methanol oxidation. This leads to have high concentration of CH_2O in n-heptane/methanol flames. Because of the high amount of formaldehyde in methanol consumption paths, most of the carbons in the hydrocarbon species would be oxidized through a route involving formaldehyde (Egolfopoulos, Du, and Law 1992). In addition, the methanol decomposes in less important paths to H_2O and CH_4 (Figure 4.17).
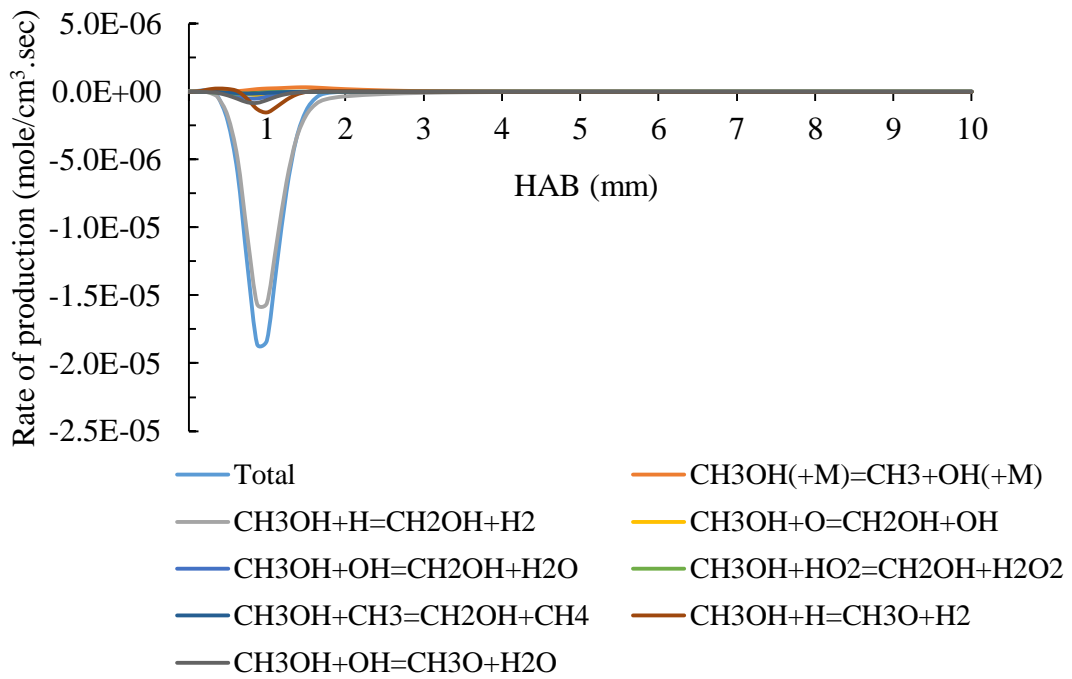
Figure 4. 16. Rate of production analysis for CH$_3$OH across the flame
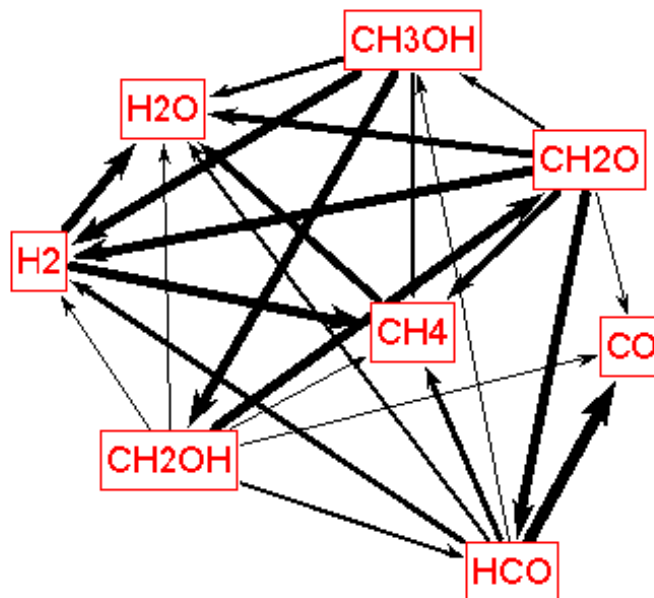
Figure 4. 17. Methanol decomposition pathways at HAB=1mm (both H and C flux)

The modeling results of species mole fractions of n-heptane and n-heptane/methanol flames have been compared against the experimental results of the

target flame. The H_2 mole fraction predictions and experimental measurements profiles are shown in Figure 4.18. There were underestimations by about a factor of 2.5 in the model predictions of hydrogen mole fractions for both n-heptane and n-heptane/methanol flames. The uncertainties of kinetic and thermodynamic properties in the model might be the reason behind the underestimations by the model of both flames.

There were underpredictions by the model of CO mole fractions for both n-heptane and n-heptane/methanol flames, as seen in Figure 4.19. The mechanism has predicted the reduction in mole fractions of CO as methanol included in the flame (Figure 4.19). The CO mole fractions decreased with the addition of methanol, similar results were also found in other studies (Bata and Roan 1989, Yanju et al. 2008). There was a fair agreement between model predictions and experimental measurements for CH_4 mole fractions (Figure 4.20). The model predictions showed underestimations for both flames at 1 mm < HAB < 6 mm, and reductions in CH_4 mole fraction in methanol-blended flame.
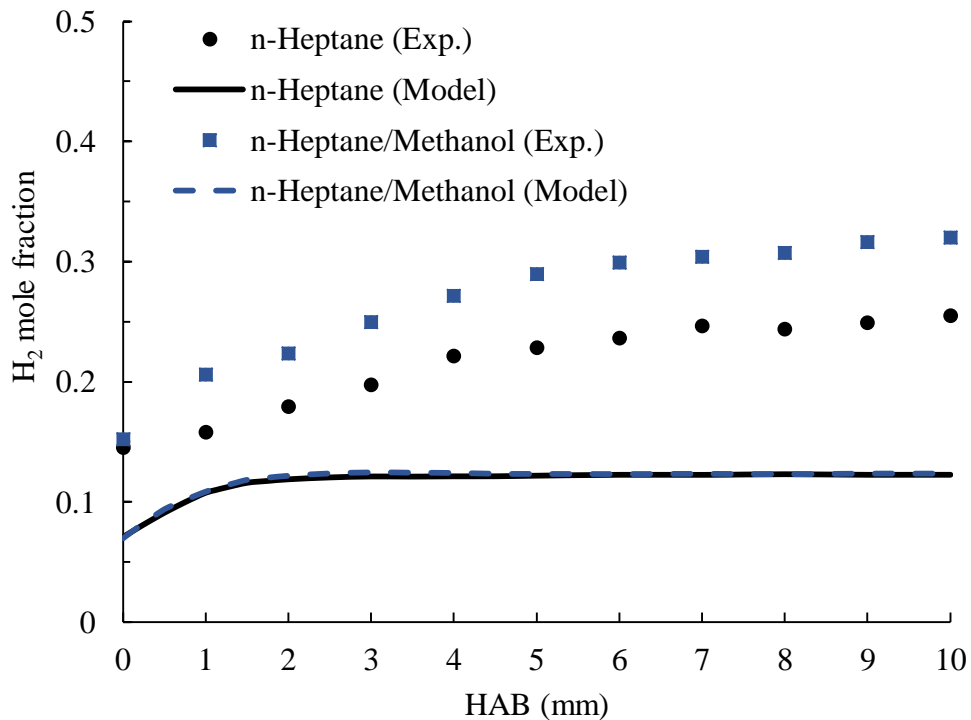
Figure 4. 18. Comparison of species profiles of hydrogen
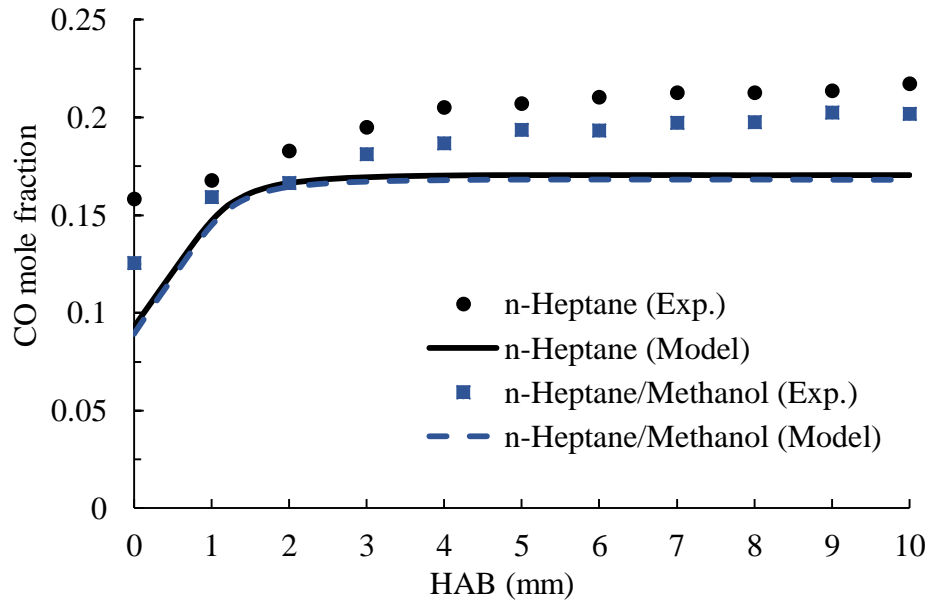
Figure 4. 19. Comparison of species profiles of carbon monoxide

The mole fractions of low molecular weight stable species were also determined since they are important for the formation of first aromatic ring and PAHs. For acetylene, as seen in Figure 4.21 the modeling results showed underestimations for both flames, n-heptane and n-heptane/methanol. There were acetylene mole fraction reductions when methanol was added in both the experimental and modeling data (Figure 4.21).
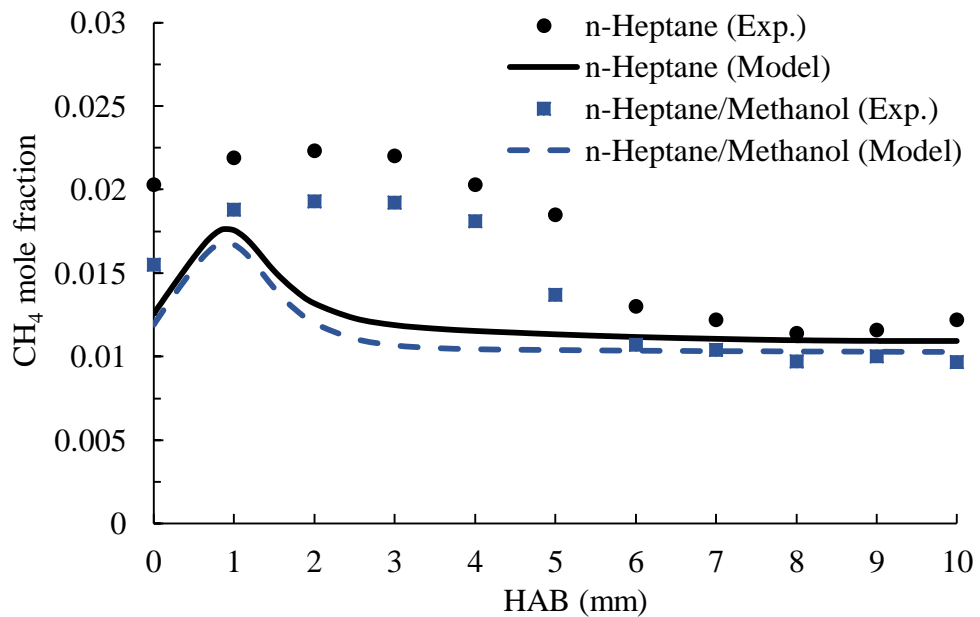
Figure 4. 20. Comparison of species profiles of methane

The acetylene is one of the important precursors for the first aromatic ring formation and PAH growth (Richter and Howard 2000, Frenklach and Wang 1994). Therefore, the rate of production and pathway analyses should be done for acetylene across the flame to gain deeper understanding for the acetylene formation and decomposition. The pathway analysis for acetylene (n-heptane flame) for both hydrogen and carbon fluxes was carried out at 1.5 mm since the peak point of the total rate of production corresponds to this height (Figure 4.22). The major acetylene formation was by the decomposition reaction of vinyl radical (C_2H_3). Acetylene was mainly decomposed by the reaction with O_2 which formed formaldehyde (CH_2O) and OH radical. Based on the pathway analysis the acetylene was mainly formed from vinyl radical by the reverse reaction of $C_2H_2+H(M)=C_2H_3+M$ (Figure 4.23), and it was mainly decomposed by the reaction of $C_2H_2+O_2=HCCO+OH$ and it forms HCCO (Figure 4.24). The same finding has been reported for fuel-rich n-heptane flame (Seidel et al. 2015). The acetylene also decomposes to CH_2 and CO by reacting with O radical whereas H_2O is formed when C_2H_2 reacts with OH radical.

Figure 4. 21. Comparison of species profiles of acetylene

Figure 4. 22. Rate of production analysis for C_2H_2 across the flame (n-heptane)
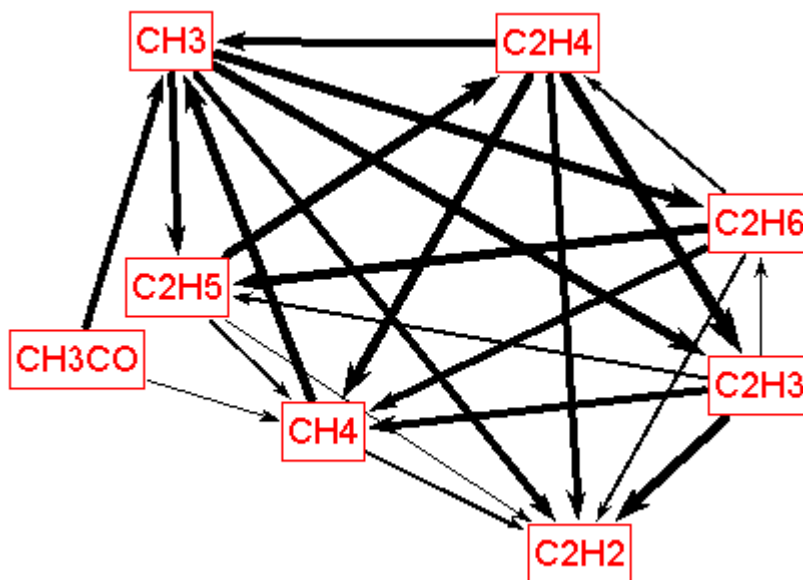
Figure 4. 23. Acetylene formation pathways at HAB=1.5mm (both H and C flux)(n-heptane flame)

Figure 4. 24. Acetylene decomposition pathways at HAB=1.5 mm (both H and C flux)
(n-heptane flame)

The acetylene formation and decomposition pathways in the n-heptane/methanol flame are almost the same according to the rate of production and pathway analyses (Figures 4.25-4.27). The noticeable differences in the pathway analysis of the two flames, n-heptane/methanol and n-heptane is, the reaction rate of $C_2H_3+CH_3=C_2H_2+CH_4$ that forms acetylene becomes less important when methanol is included in the fuel mixture. In addition, a significant difference has been found for the rate of decomposition of acetylene to formaldehyde when methanol was included (i.e., the acetylene decomposition to formaldehyde becomes higher in n-heptane/methanol flame) (Figures 4.22 and 4.25). That increase in formaldehyde coincides with the previously reported results of a fuel-rich laminar n-heptane/methanol flame (Chen et al. 2012).

For both n-heptane and n-heptane/methanol flames, the predictions of the mole fractions of propadiene (C_3H_4-A) were underestimated by the model as shown in Figure 4.28. The modeling results of methanol-blended flame showed an average reduction in propadiene species mole fractions of about 8% whereas the average reduction of propadiene mole fractions was about 22% according to the experimental data.
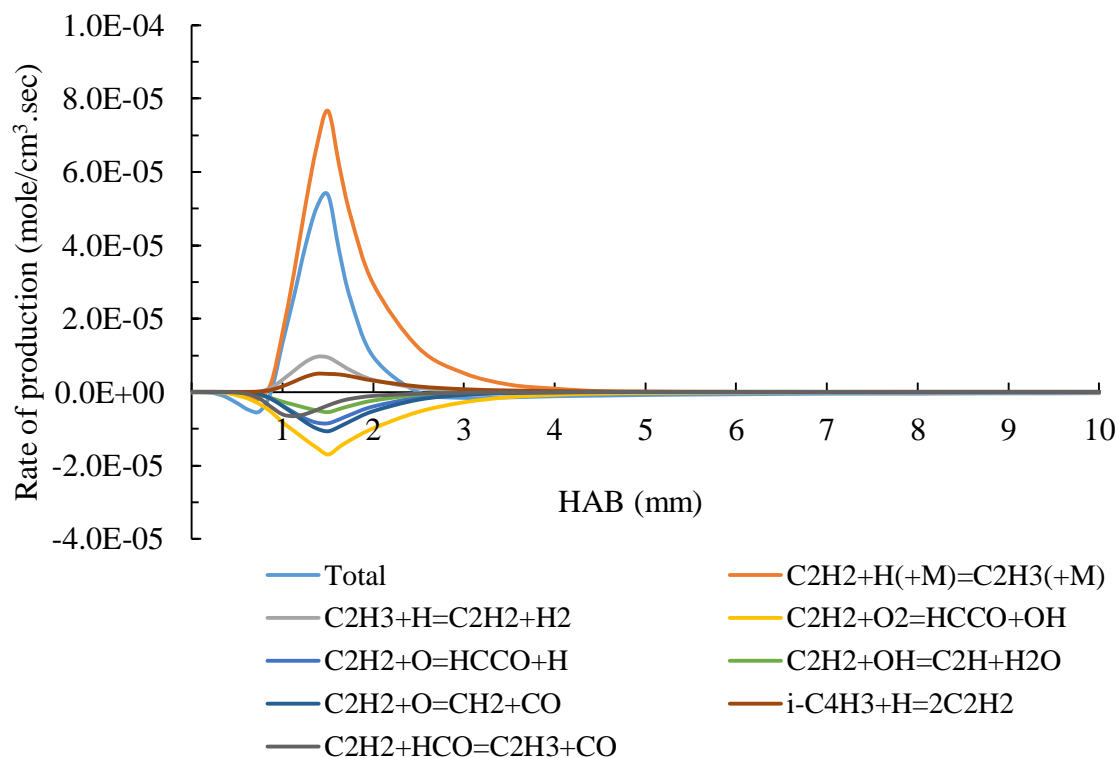
Figure 4. 25. Rate of production analysis for C_2H_2 across the flame (n-heptane/ methanol)
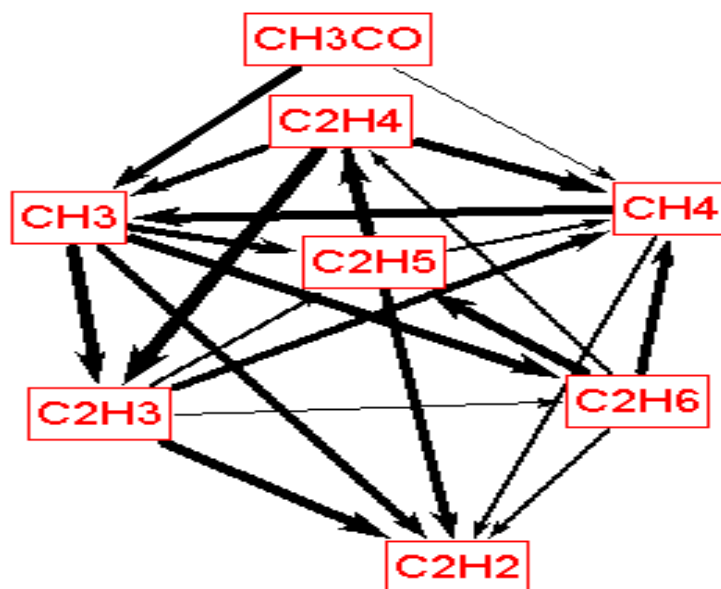
Figure 4. 26. Acetylene formation pathways at HAB=1.5mm (both H and C flux) (n-heptane/methanol flame)
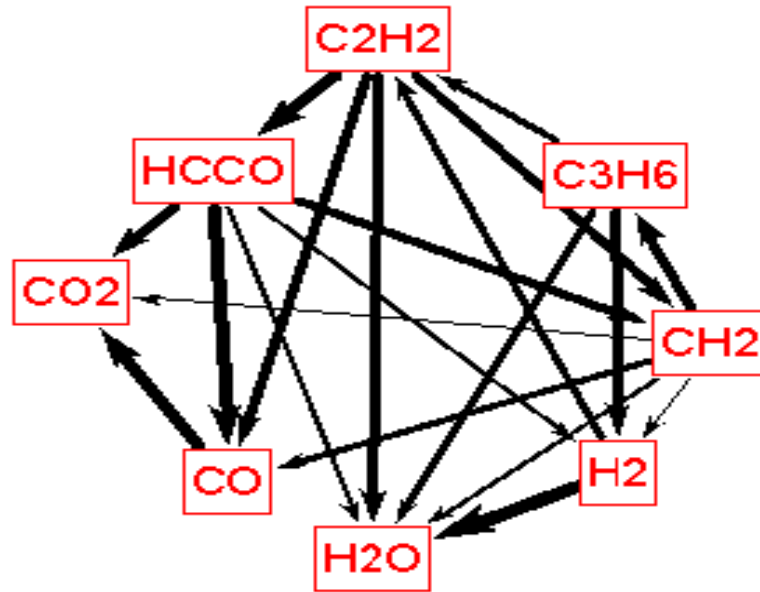
Figure 4.27. Acetylene decomposition pathways at HAB=1.5 mm (both H and C flux)
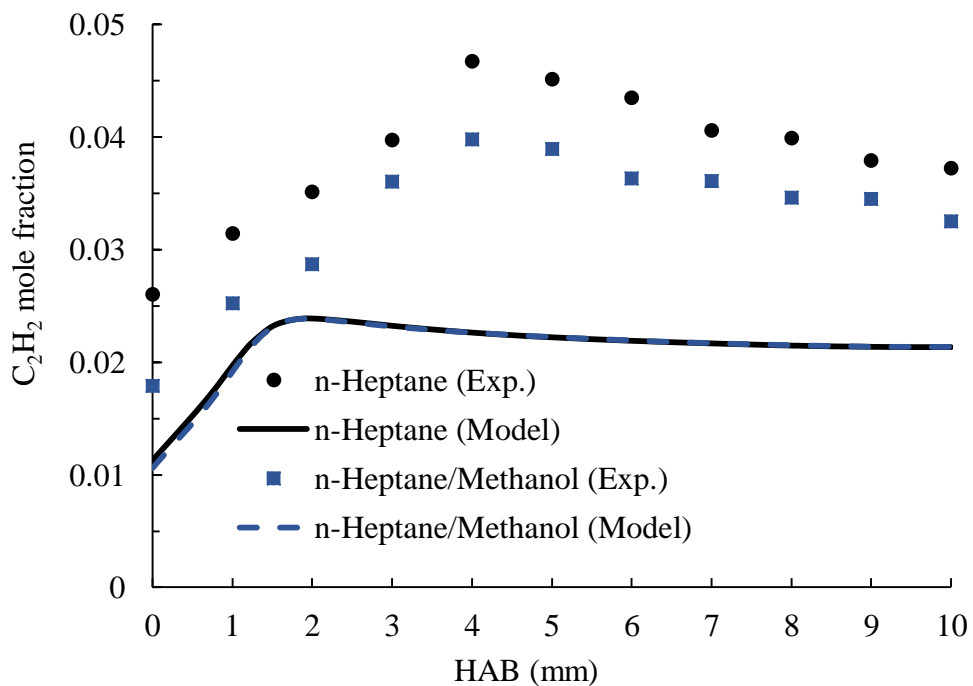(n-heptane/methanol flame)
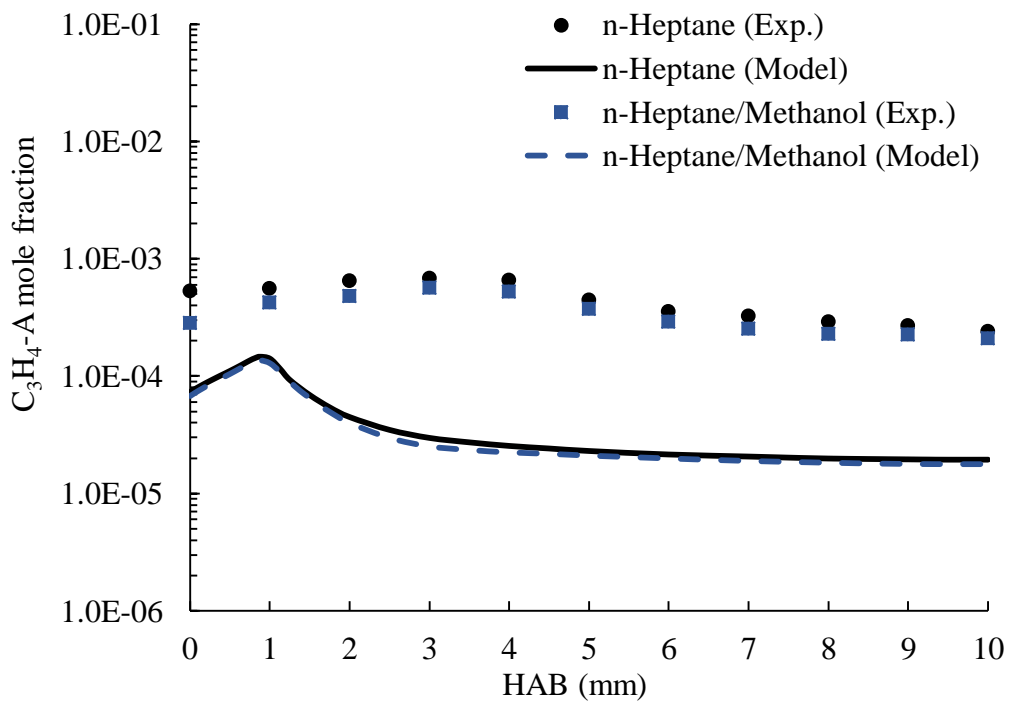
Figure 4.28. Comparison of species profiles of propadiene
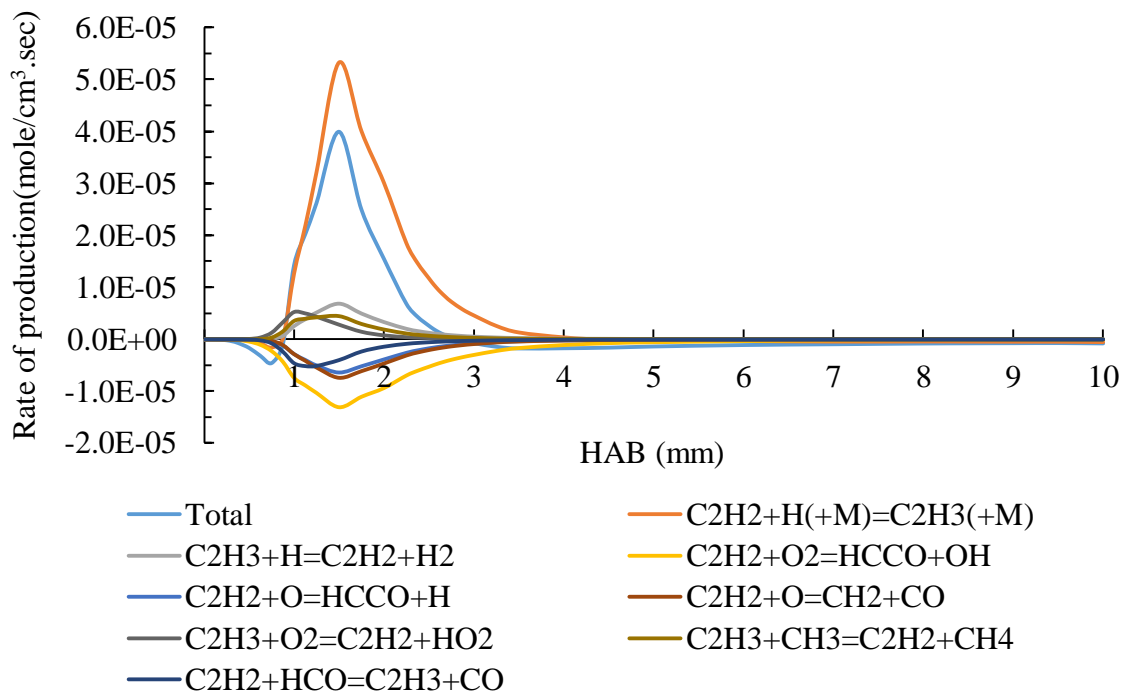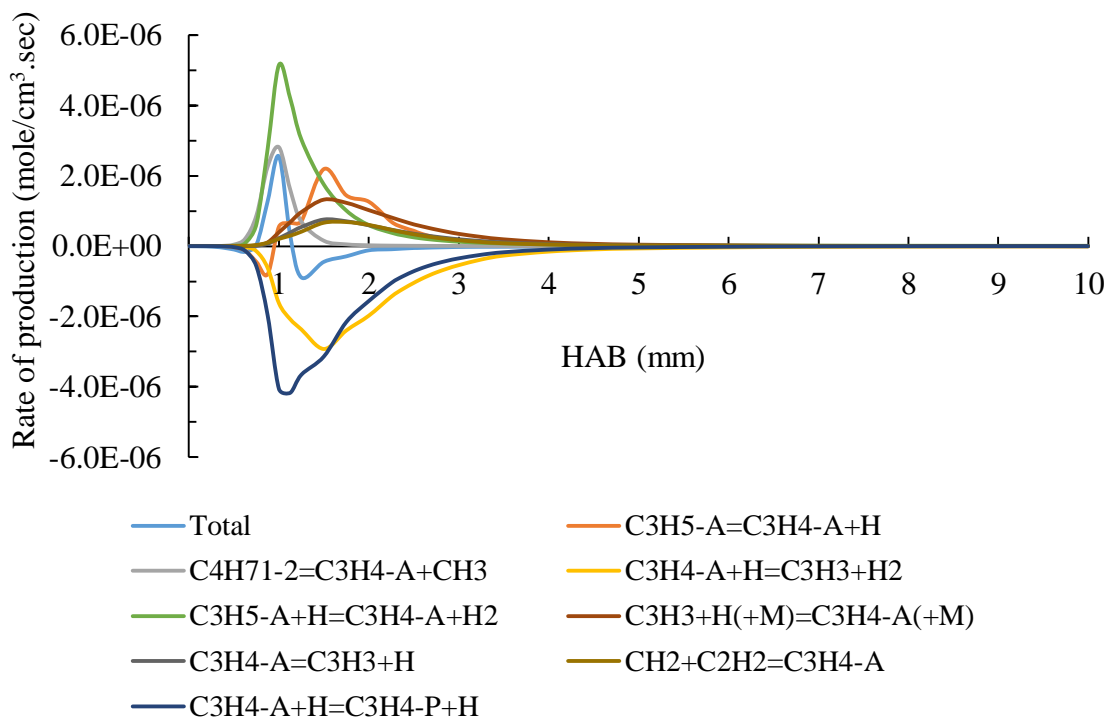
Figure 4.29. Rate of production analysis for C_3H_4-A across the flame (n-heptane)
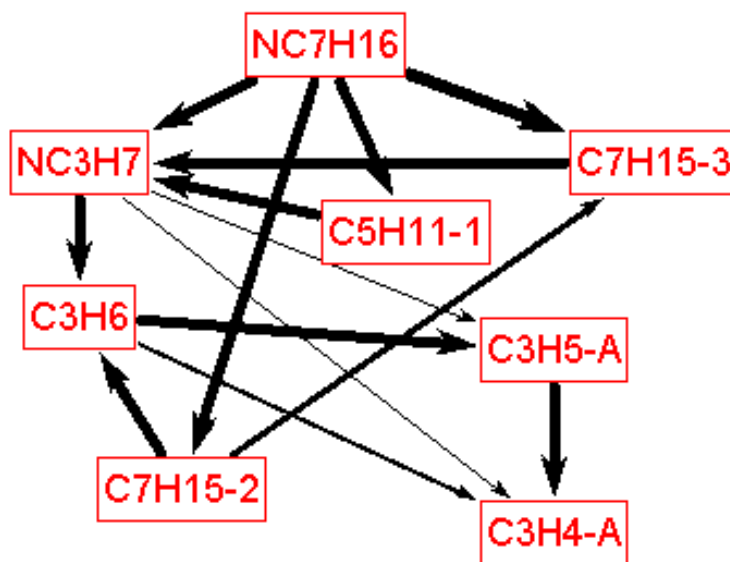
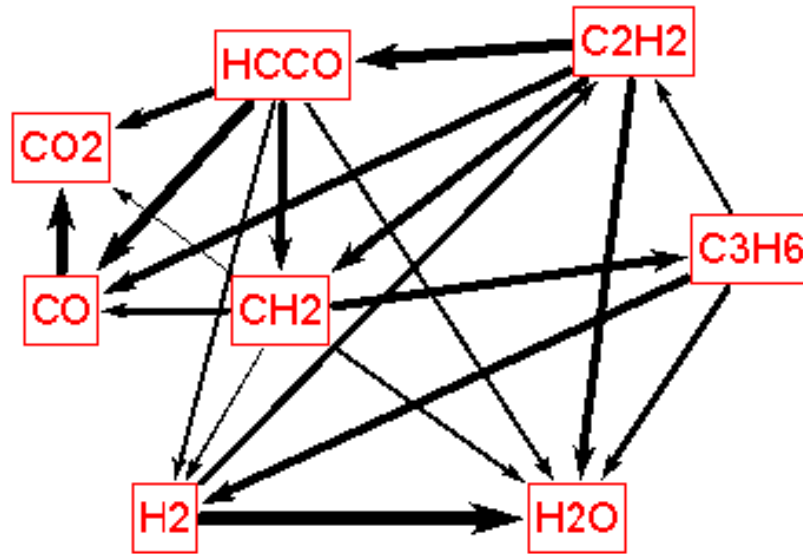Figure 4.30. C_3H_4-A formation pathways at HAB=0.875mm (both H and C flux) (n-heptane flame)

Propadiene (C_3H_4-A), as a precursor specie, plays an important role for the formation of aromatics and polycyclic aromatic hydrocarbons. The rate of production and

pathway analyses were carried out for C_3H_4-A of both n-heptane and n-heptane/methanol flames. C_3H_4-A is formed in the range 0.8~1 mm HAB and decomposed in 1.125~2 mm HAB according to the rate of production analysis in n-heptane flame (Figure 4.29). The peak point of the total rate of production corresponds to 0.875 mm HAB, and it is used for the pathway analysis. The formation pathways of C_3H_4-A at HAB=0.875 mm for n-heptane flame is shown in Figure 4.30. The allene is mostly formed from allyl radical (C_3H_5-A) by the hydrogen abstraction reaction C_3H_5-A=C_3H_4-A+H while the dominant reactions for the destruction of allene are the reverse reactions of C_3H_5-A+H=C_3H_4-A+H_2 and $C_4H_7$1-2=C_3H_4-A+CH_3 ($C_4H_7$1-2 refers to 1-Butene2yl).

The rate of production analysis for C_3H_4-A across the n-heptane/methanol flame is shown in Figure 4.31. By comparing the rate of production and pathway analyses of propadiene for both flames (i.e., n-heptane/methanol and n-heptane flames), there is no significant difference between them (Figures 4.30-4.32). Propyne (p-C_3H_4) and allene (C_3H_{4-}A) are reported previously as crucial species to the formation of the C_3H_3 and a-C_3H_5 which play significant role in the formation of benzene (Hansen et al. 2009). It has been found that when methanol was added to n-heptane, the decomposition reaction of C_3H_4-A= C_3H_3+H became less important which might play a role in the reductions of the mole fractions of aromatics and polycyclic aromatic hydrocarbons. That may be attributed to the addition of methanol which reduces the system reactivity by converting an active hydroxyl radical, OH, into inactive hydrogen peroxide, H_2O_2 by the following set of reactions (Xu, Yao, and Xu 2012);

$$CH_3OH+OH=CH_2OH+H_2O$$

$$CH_2OH+O_2=CH_2O+HO_2$$

$$HO_2+HO_2=H_2O_2$$
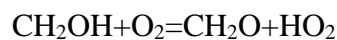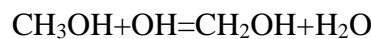
OH is an important radical which plays a decisive role in the fuel ignition stage. When methanol is added to the fuel in laminar, premixed n-heptane/toluene/methanol flame, active OH is converted into inactive H_2O_2 (Xu et al. 2013). This agrees with the result of ethanol converting the active OH into inactive H_2O_2 in the ethanol/PRF fuel mixture study (Haas, Chaos, and Dryer 2009). Therefore, the activity of the system decreases and the ignition is delayed.
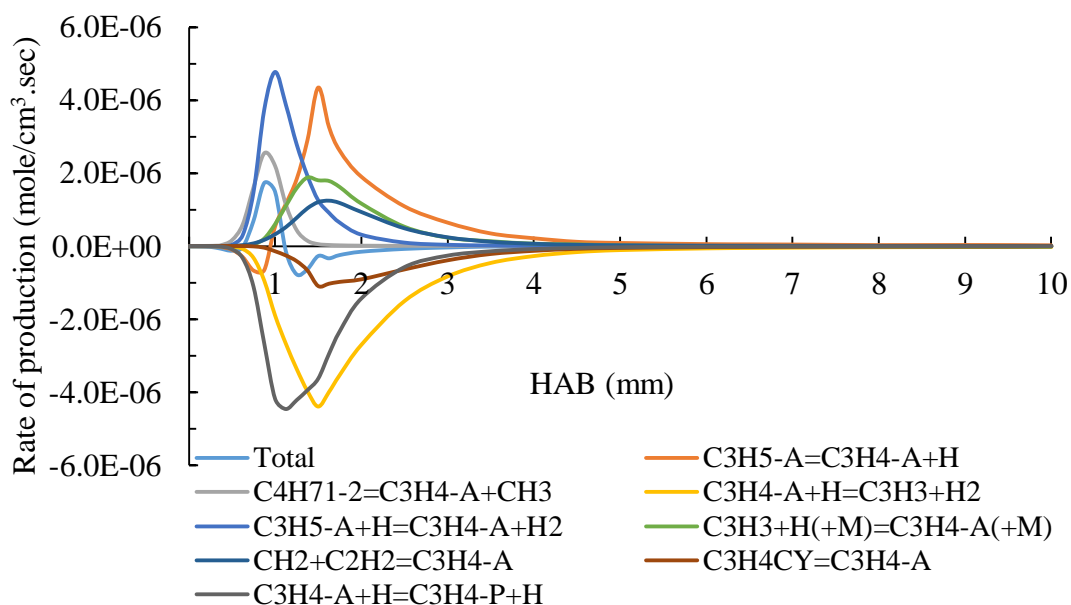
Figure 4.31. Rate of production analysis for C_3H_4-A across the flame (n-heptane/ methanol)

For both n-heptane and n-heptane/methanol flames, the predictions of the mole fractions of diacetylene (C_4H_2), and vinylacetylene (C_4H_4) were underestimated by the model as shown in Figure 4.33 and Figure 4.34, respectively. The modeling predictions of methanol-blended flame showed average reductions in these species mole fractions of about 7% and 5% for diacetylene and vinylacetylene, respectively. On the other hand, the average reductions of the mole fractions of diacetylene and vinylacetylene were about 30% and 35%, respectively according to the experimental data.
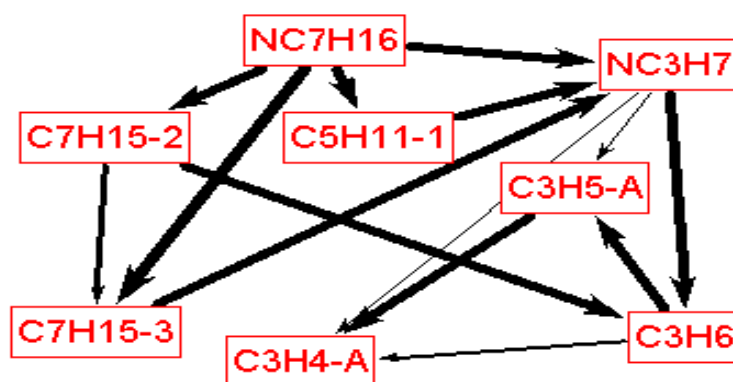
Figure 4.32. C_3H_4-A formation pathways at HAB=0.875mm (both H and C flux) (n-heptane/methanol flame)
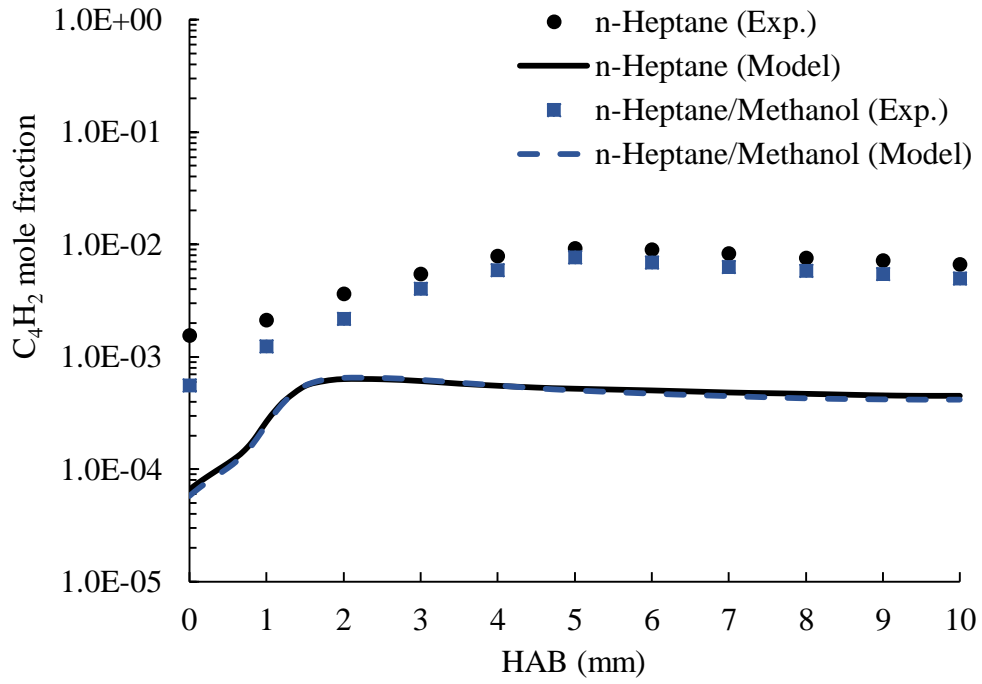
Figure 4.33. Comparison of species profiles of diacetylene
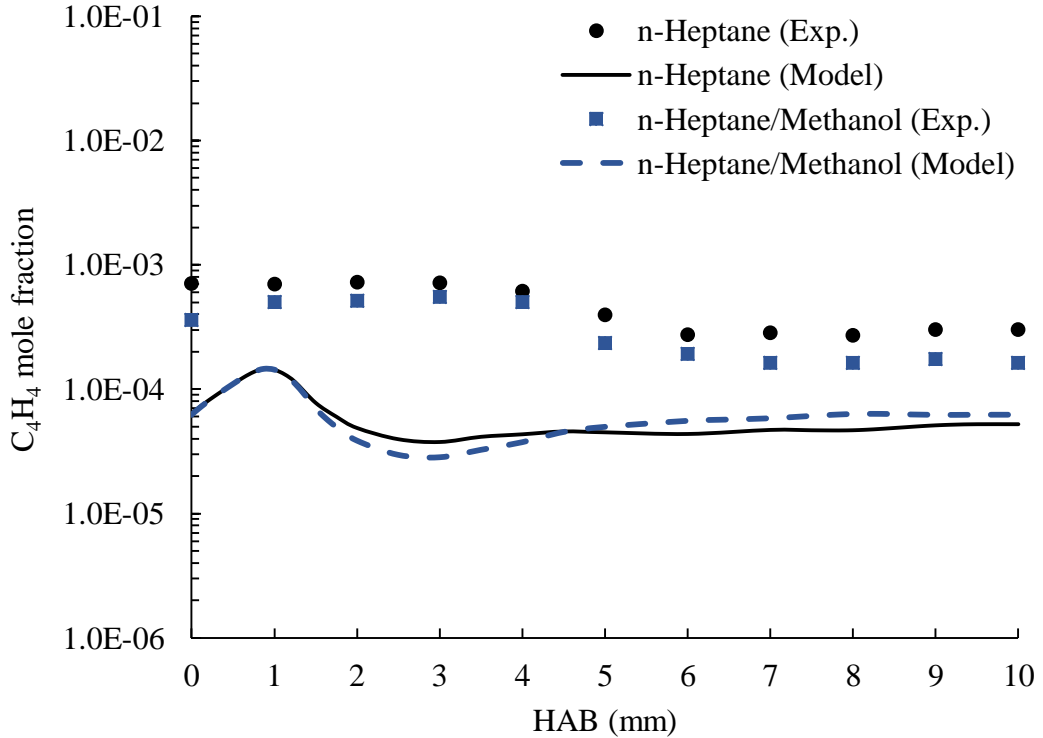
Figure 4.34. Comparison of species profiles of vinylacetylene

Vinylacetylene is considered as one of the precursor of the aromatic and PAHs formation. The rate of production analysis for vinylacetylene across the n-heptane flame can be seen in Figure 4.35. The minimum point for the decomposition of vinylacetylene is roughly at 1.5 mm HAB where the peak point of the formation of vinylacetylene is at 1mm HAB (Figure 4.35). The pathway analysis shows that the dominant reaction for the formation of vinylacetylene is by the reaction of acetylene and vinyl radical $C_2H_2+C_2H_3=C_4H_4+H$ (Figure 4.36). In addition, vinylacetylene can be formed by the combination reaction between ethylene (C_2H_4) and C_2H (ethyne). The main consumption path of vinylacetylene is from hydrogen abstraction reaction by H radical which forms i-C_4H_3 and hydrogen $C_4H_4+H=i-C_4H_3+H_2$ (Figure 4.37). Other less important decomposition paths for vinylacetylene are the reaction of C_4H_4 with O which forms CO, $C_4H_4+O=C_3H_4-P+CO$, and the reaction of propargyl radical (C_3H_3) and vinylacetylene $C_4H_4+C_3H_3=C_6H_5CH_2$.
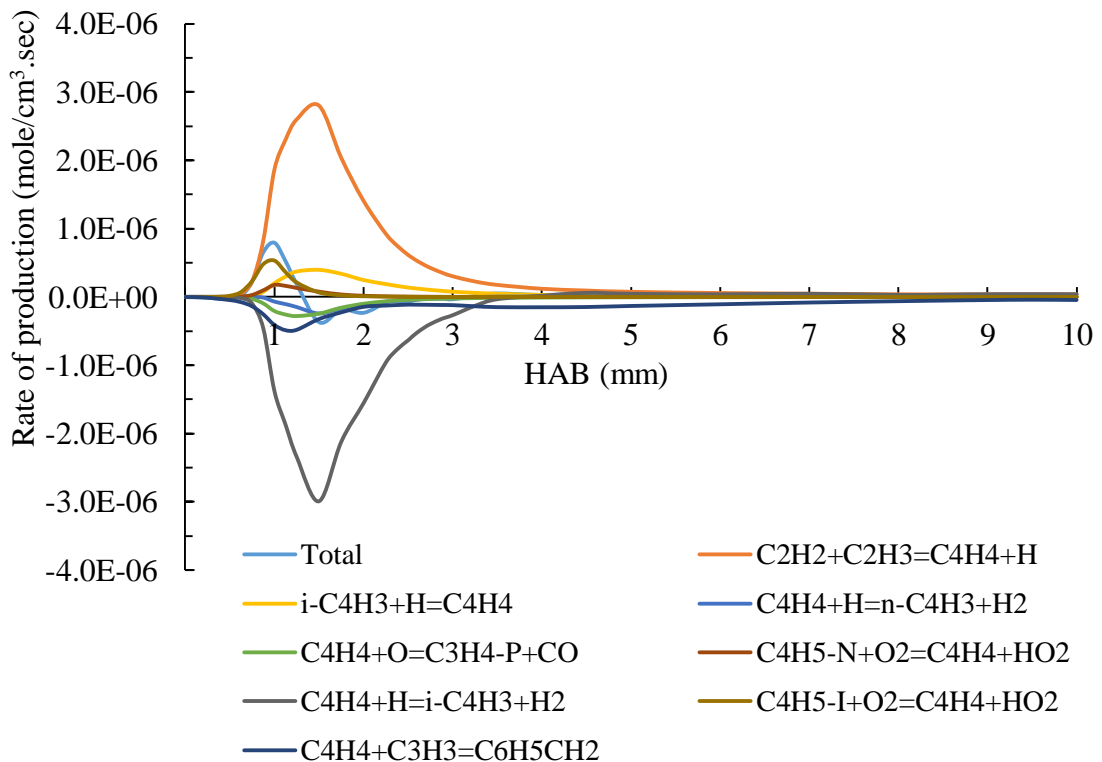
Figure 4.35. Rate of production analysis for C_4H_4 across the flame (n-heptane)
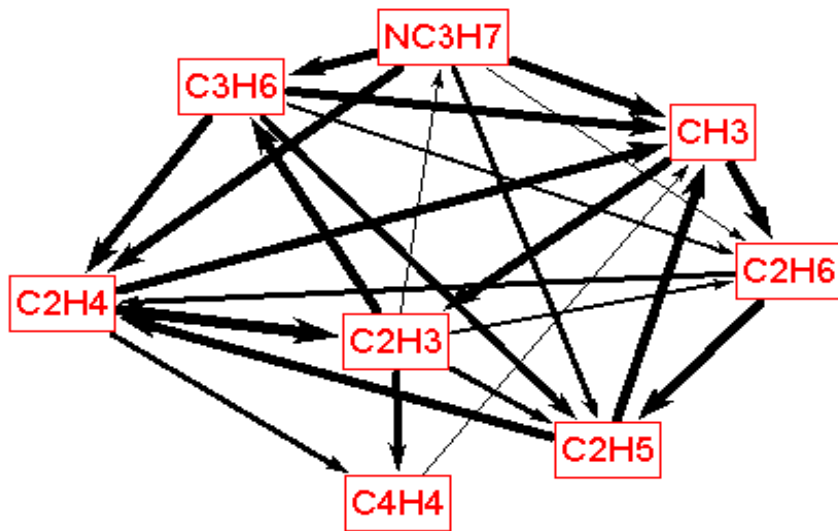
Figure 4. 36. C_4H_4 formation pathways at HAB=1mm (both H and C flux) (n-heptane flame)
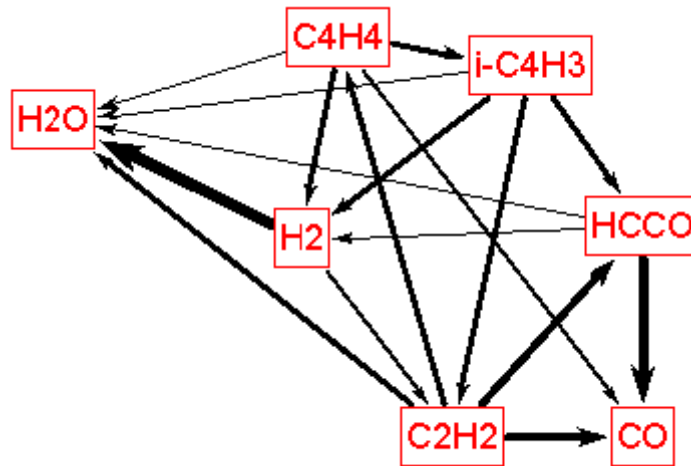
Figure 4. 37. C_4H_4 decomposition pathways at HAB=1.5mm (both H and C flux) (n-heptane flame)

The total rate of production and pathway analyses for the vinylacetylene in the n-heptane/methanol flame are shown in Figures 4.38-4.40. The main differences that have been found in the pathway analysis for C_4H_4 between n-heptane/methanol and n-heptane flames, the reaction of $C_2H_2+C_2H_3=C_4H_4+H$ has higher rate of production (which equals 3.4E-06 mole/cm^3.sec for n-heptane/methanol flame and 2.8E-6 mole/cm^3.sec for n-heptane flame). The rate of destruction of C_4H_4 is slightly different for two flames (-3.0E-

6 mole/cm^3.sec for n-heptane/methanol flame and -3.80E-6 mole/cm^3.sec for n-heptane flame).
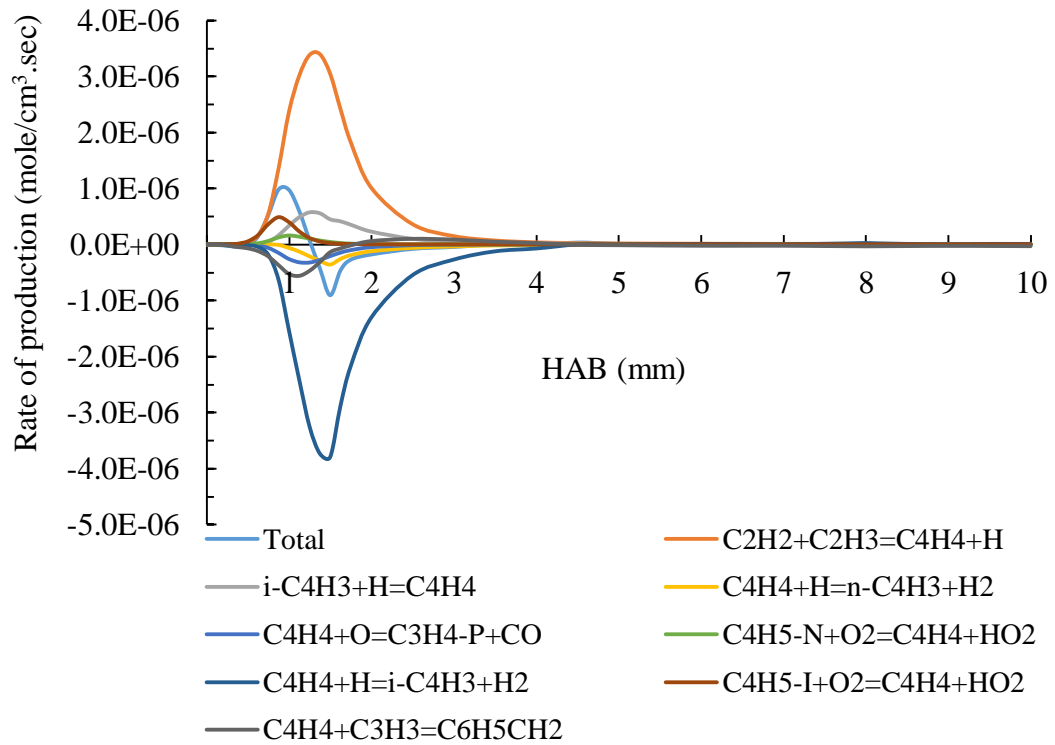
Figure 4. 38. Rate of production analysis for C$_4$H$_4$ across the flame (n-heptane/ methanol)
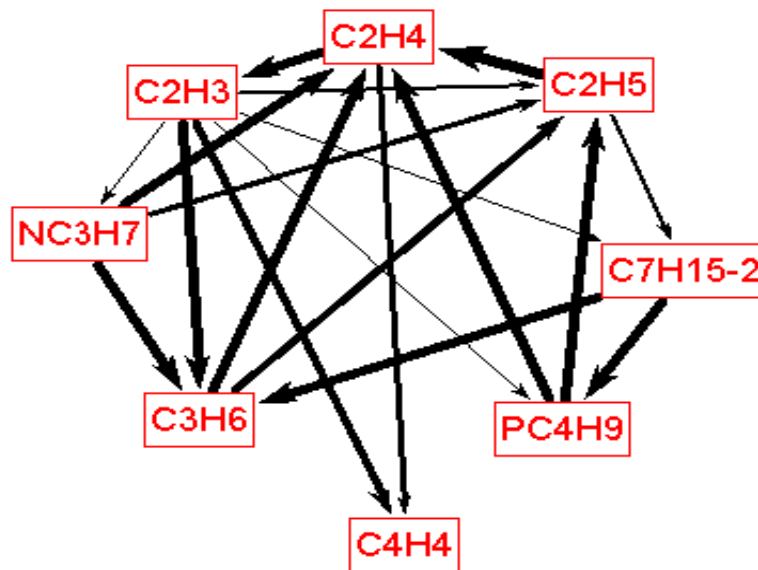
Figure 4. 39. C$_4$H$_4$ formation pathways at HAB=1mm (both H and C flux) (n-heptane/ methanol flame)
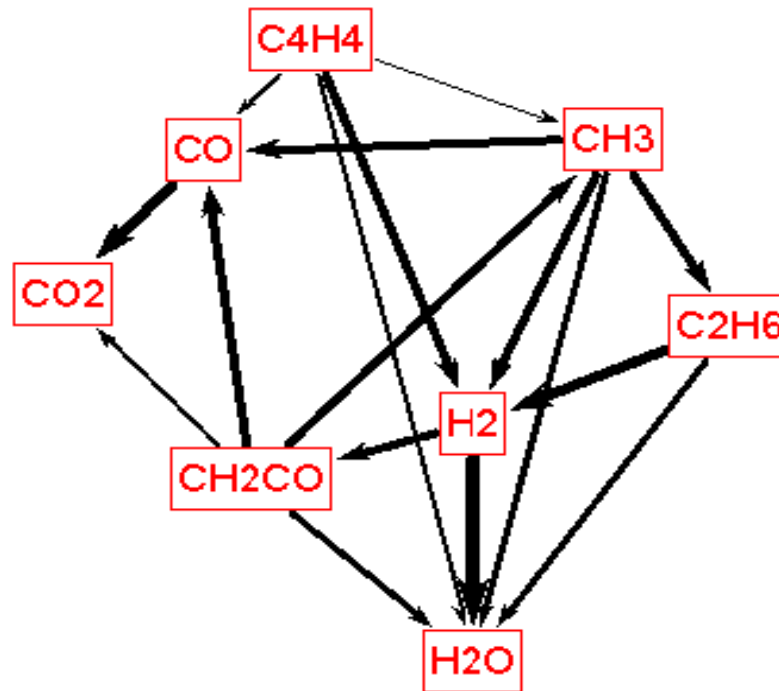
Figure 4. 40. C_4H_4 decomposition pathways at HAB=1.5mm (both H and C flux) (n-heptane/methanol flame)

The mole fractions of benzene decreased in the presence of methanol (Figure 4.41). There was a good agreement between the experimental measurements and modeling predictions of benzene mole fractions. However, at low heights above the burner there were underestimations by the model (due to possible burner surface-sampling probe interaction) while for HAB greater than 4 mm there were overestimations for both n-heptane and n-heptane/methanol flames. The average reductions in benzene mole fractions when methanol was added were 15% for the model predictions and 40 % for the experimental data. Xu et al. (2013) have reported that the average benzene mole fractions reduction was about 12.5% in the presence of methanol, and 33.3% in the presence of ethanol for low-pressure, laminar, premixed n-heptane/toluene/methanol and n-heptane/toluene/ethanol flames, respectively. Reuter et al. (1992) have also reported that the blending of gasoline with ethyl tertiary-butyl ether (ETBE) in a spark ignition engine, reduced the emissions of benzene.
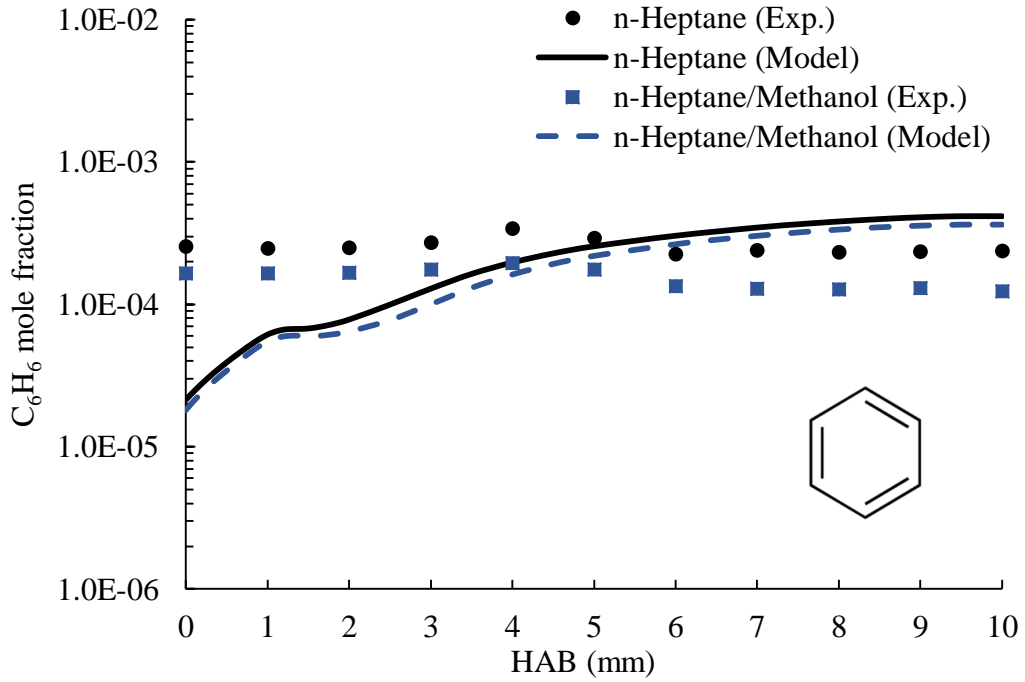
Figure 4. 41. Comparison of species profiles of benzene
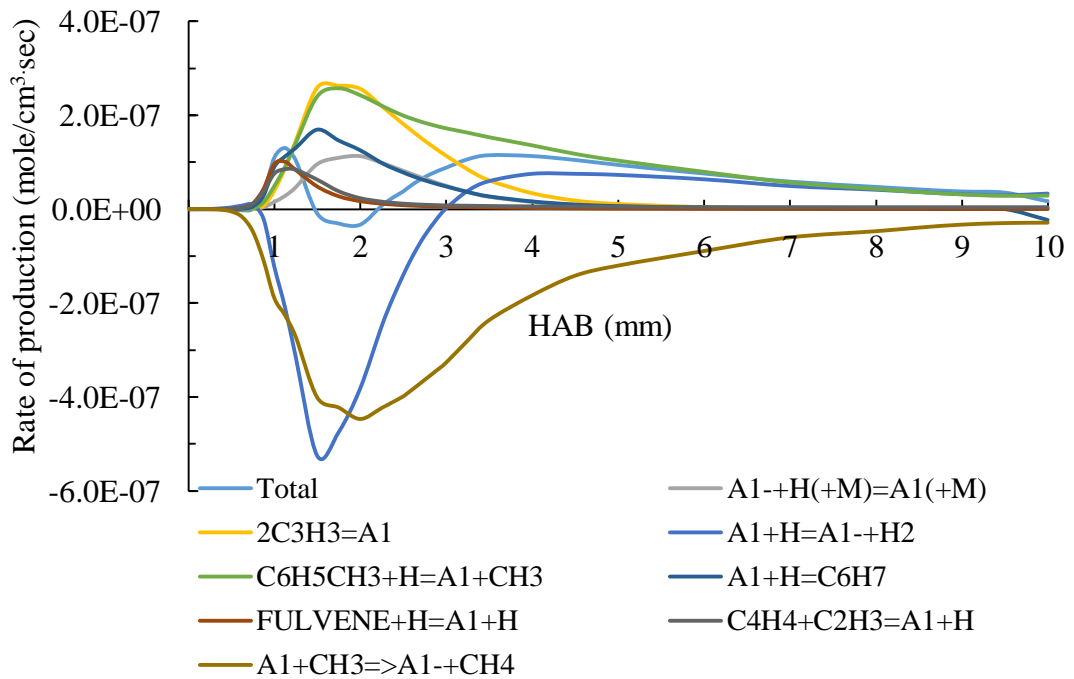
Figure 4. 42. Rate of production analysis for A_1 across the flame (n-heptane)

Benzene is considered as a first aromatic ring in non-aromatic hydrocarbon flames (Richter and Howard 2000) . Therefore, there is a need to carry out the rate of production

analysis for benzene across the flames. The total rate of production of benzene for the n-heptane flame is positive at HAB 0 - 1.5 mm. However, at HAB 1.5 - 2.5 mm it is negative (rate of decomposition is higher) as seen in Figure 4.42. The benzene decomposition and formation reactions are mainly hydrogen abstraction reaction by hydrogen radical (Figure 4.42). To see different formation pathways of benzene for the n-heptane flame, two heights above the burner are used (i.e., HAB ~1.25 mm and ~4 mm) corresponding to the corrected flame temperatures of 1480 K and 1600 K, respectively (Figures 4.43 and 4.44). As seen in Figure 4.43, benzene is mostly formed by a combination reaction of two propargyl radicals (C_3H_3) ($2C_3H_3=A_1$). In addition, benzene is formed by the reaction between vinyl radical and vinylacetylene ($C_4H_4+C_2H_3=A_1+H$). As seen in Figure 4.44, benzene is mainly formed by the reaction of toluene and H radical at 4 mm HAB ($C_6H_5CH_3+H=A_1+CH_3$). The two propargyl radicals combination reaction is also a path of benzene formation reaction at HAB=4.0 mm. Benzene is also formed by the bimolecular reaction between vinylacetylene and vinyl radical ($C_4H_4+C_2H_3=A_1+H$). That consists with the reported pathway of benzene formation by $C_2 + C_4$ reactions (i.e., the reaction between C_2H_2 and $n-C_4H_5/n-C_4H_3$ radicals) (Frenklach and Warnatz 1987, Cole et al. 1984, Raj et al. 2012). Vinylacetylene plays an important role in the formation of benzene by the reaction $C_4H_4+C_2H_3=A_1+H$. Acetylene is the main reactant that forms vinylacetylene and propargyl radical so that it is considered as an important precursor for benzene formation (Richter and Howard 2002).

Figure 4. 43. A_1 formation pathways at HAB=1.25mm (both H and C flux) (n-heptane flame)
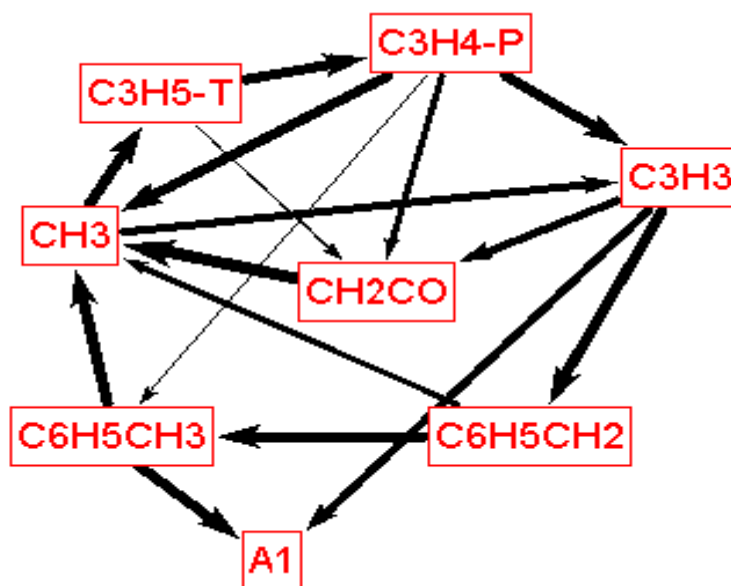
Figure 4. 44. A1 formation pathways at HAB=4mm (for both H and C fluxes) (n-heptane flame)
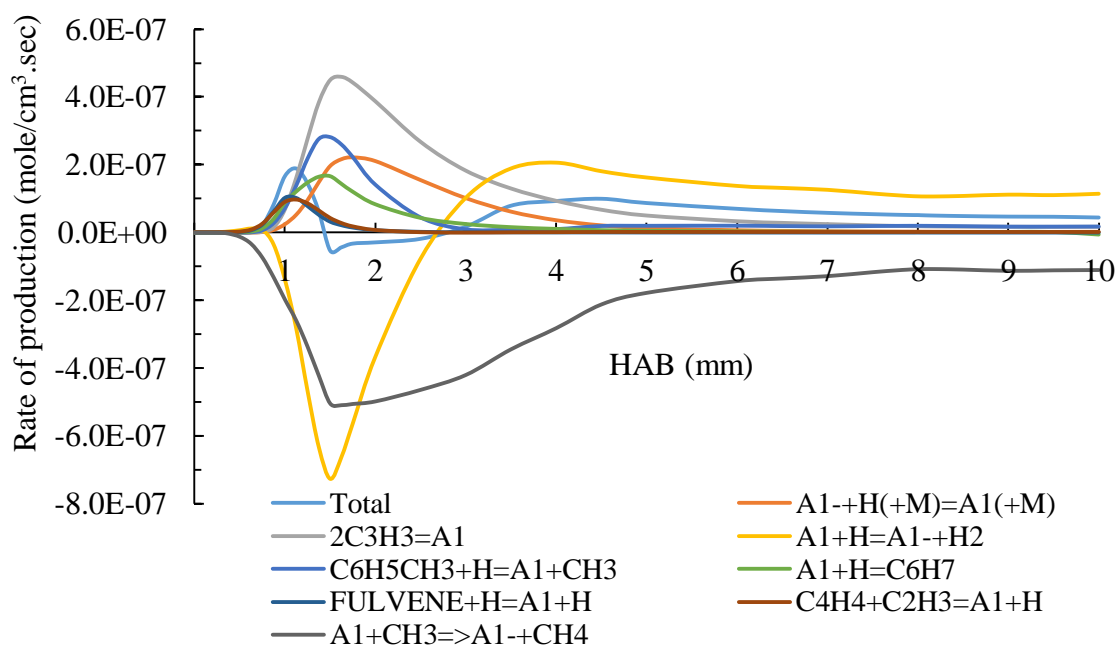
Figure 4. 45. Rate of production analysis for A_1 across the flame (n-heptane/methanol)

The rate of production analysis for benzene across the n-heptane/methanol flame is shown in Figure 4.45. The slight difference in the pathway analyses between n-heptane/methanol and n-heptane flames is the reverse reaction rate of $C_6H_5CH_3+H=A_1+CH_3$ becomes slightly higher (2.40E-07 and 2.82E-07 mole/cm^3.sec for

the n-heptane and n-heptane/methanol flames, respectively). However, at high distances above the burner the reverse reaction rate of $C_6H_5CH_3+H=A_1+CH_3$ is almost the same for n-heptane and n-heptane/methanol flames (Figure 4.45). The reactions of $C_6H_5CH_3+H=A_1+CH_3$ and $2C_3H_3=A_1$ were also reported for premixed fuel-rich n-heptane/methanol flame at equivalence ratio of 1.6 and 30 torr pressure for the benzene formation (Chen et al. 2012). The pathway analysis for benzene in n-heptane/methanol flame at HAB ~1.25 mm and ~4 mm is shown in Figures 4.46 and 4.47. At 1.25 mm HAB, the benzene is mostly formed by $2C_3H_3=A_1$, and a direct path of acetylene also forms benzene (Figure 4.46). However, the reverse reaction of $A_1+H=A_{1-}+H_2$ is the dominant reaction for the formation of benzene at 4mm HAB (Figure 4.47). The reaction rate of $A_1+CH_3=A_{1-}+CH_4$ becomes higher at low distances above the burner when methanol is included in the flame. It is reported that adding oxygenates to flames does not change the reaction flux of benzene (Chen et al. 2012). Chen et al. (2012) have also reported reductions in species mole fractions; like C_3H_3 and a-C_3H_5 decreased by 29% and 22%, respectively so the reduction of C_6H_6 should be attributed to the reduced concentrations of its precursors. The dominant reaction for the destruction of benzene for both n-heptane/methanol and n-heptane flames is the reaction of benzene with the methyl radical which forms methane $A_1+CH_3=A_1-1+CH_4$ (Figure 4.42 and Figure 4.45).
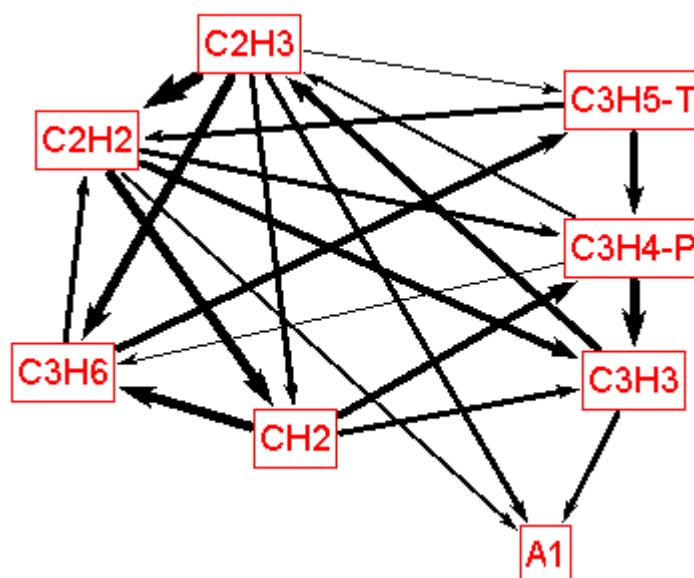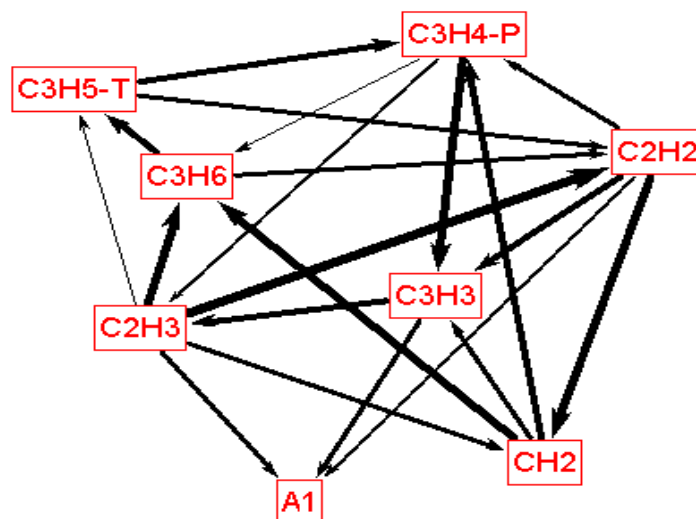

Figure 4. 46. A_1 formation pathways at HAB=1.25 mm (both H and C flux) (n-heptane/ methanol flame)
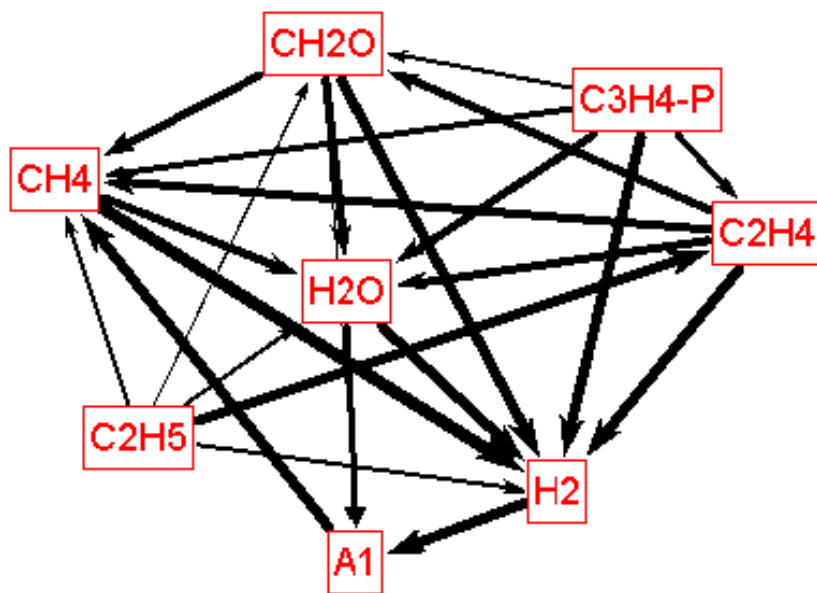
Figure 4. 47. A_1 formation pathways at HAB=4mm (both H and C fluxes) (n-heptane/ methanol flame)
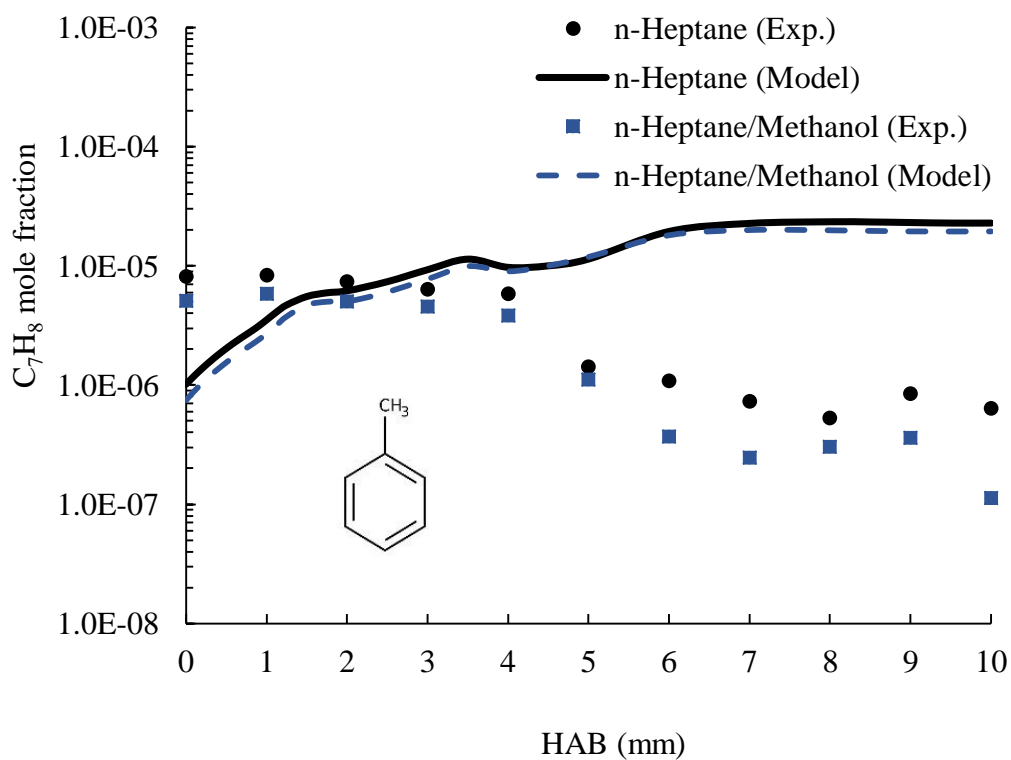
Figure 4. 48. Comparison of species profiles of toluene
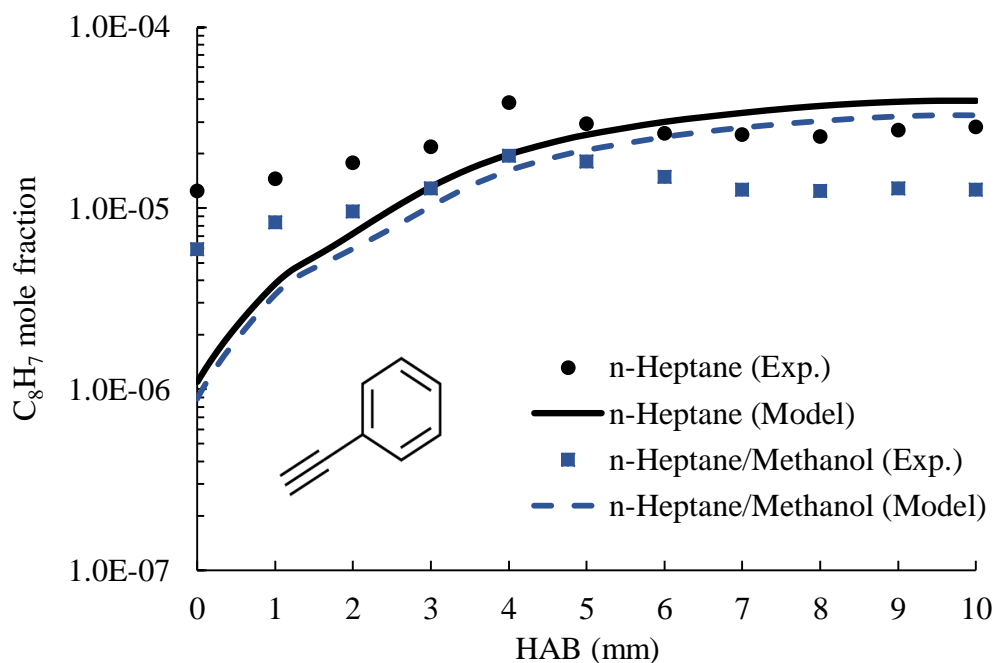
Figure 4. 49. Comparison of species profiles of phenylacetylene

The experimental measurements and model predictions for toluene and phenylacetylene in n-heptane/O_2/Ar and n-heptane/methanol/O_2/Ar flames are shown in Figure 4.48 and Figure 4.49, respectively. As mentioned previously, the experimental mole fractions within 2 mm HAB were considered questionable (Inal 1999). For HAB > 4 mm, there were overestimations by the Master Mechanism for both flames. The average reductions in mole fractions of toluene and phenylacetylene with methanol addition were about of 40% in the experimental measurements. However, the model was able to predict an average of 20% reductions for toluene and 27% reductions for phenylacetylene with the addition of methanol.

The experimental measurements and model predictions mole fraction profiles for indene and naphthalene for n-heptane and n-heptane/methanol flames are shown in Figure 4.50 and Figure 4.51, respectively. For indene mole fractions profiles, the difference between model predictions and experimental measurements decreased as the height above the burner increased (Figure 4.50). The addition of methanol to n-heptane resulted 20% of average mole fraction reductions for indene regarding the modeling results. However, the average mole fraction reductions were about 50% for the experimental measurements. There was a good agreement between the modeling and experimental results of naphthalene mole fractions for both flames (Figure 4.51). Naphthalene mole fractions

were also reduced with the addition of methanol to n-heptane. In the model predictions, there was an average of 27% reduction for naphthalene mole fractions, whereas in experimental measurements the average decrease was around 50%.
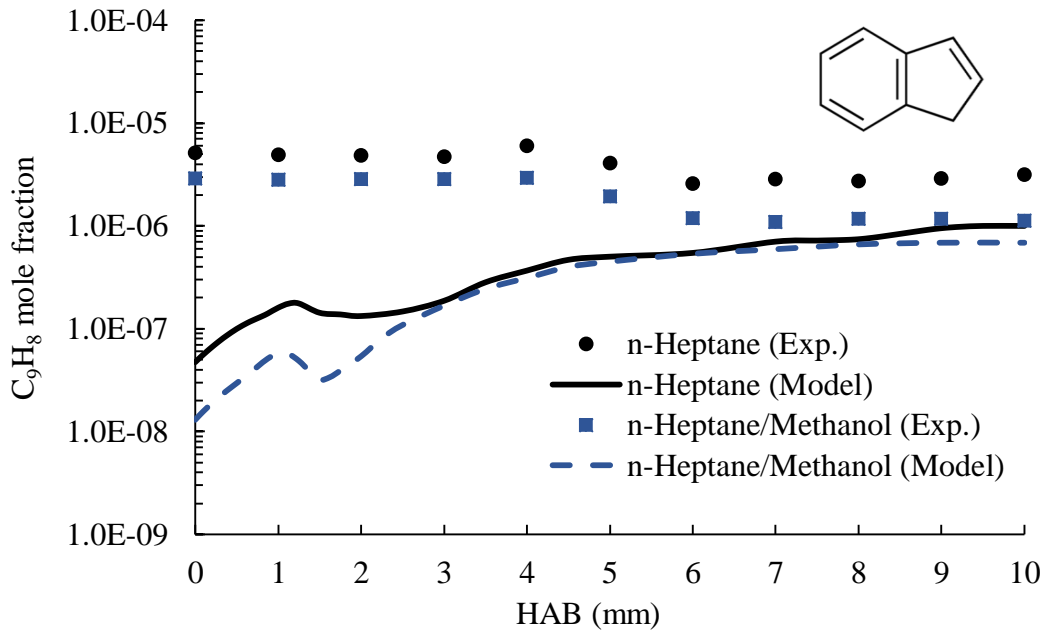
Figure 4. 50. Comparison of species profiles of indene
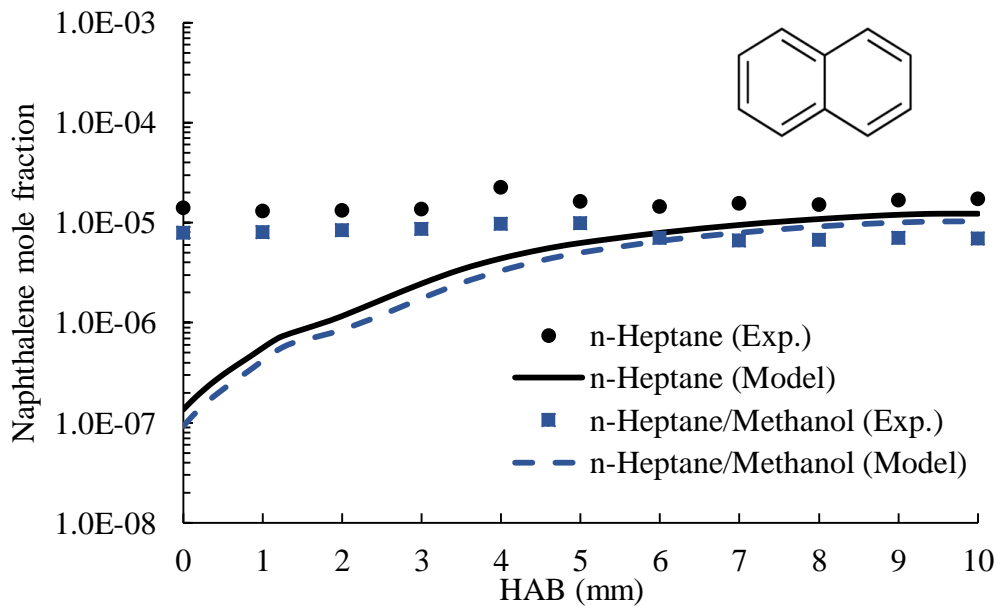
Figure 4. 51. Comparison of species profiles of naphthalene

As a reference for two-ring aromatic hydrocarbon, the rate of production analysis has been carried out for naphthalene (A_2) firstly for n-heptane flame as seen in Figure 4.52. The peak points of the total rate of formation profile of naphthalene in n-heptane flame are at HAB of 1.25 and 4 mm. At these points the pathway analysis for n-heptane flame regarding A_2 was carried out. For the decomposition of naphthalene hydrogen abstraction reactions are responsible for the consumption of naphthalene $A_2+H=A_2-2+H_2$ and $A_2+H=A_2-1+H_2$ (A_2-1 and A_2-2 refer to naphth-1-yl and naphth-2-yl, respectively) (Figure 4.52). The pathway analysis has been carried out for naphthalene (A_2) for n-heptane flame at 1.25 mm and 4 mm HAB as seen in Figures 4.53-4.54. The most important reaction for the formation of naphthalene at 1.25 mm HAB is the reaction between benzyl radical $C_6H_5CH_2$ and propargyl radical C_3H_3 ($C_6H_5CH_2+C_3H_3=A_2+2H$). Another path of acetylene also contributes to naphthalene formation ($C_8H_7+C_2H_2=A_2+H$). Similar to 1.25 mm HAB pathway analysis, the dominant reaction for the naphthalene formation is $C_6H_5CH_2+C_3H_3=A_2+2H$ at 4 mm HAB, which was also reported for a fuel-rich, laminar, premixed, low-pressure n-heptane/methanol flame (Xu et al. 2013). Another study has reported similar path of the recombination of benzyl radical and propargyl radical which has a significant contribution for the formation of naphthalene in fuel-rich premixed n-heptane flame (Seidel et al. 2015). The other reactions of the naphthalene formation are much slower than the previously mentioned reactions.
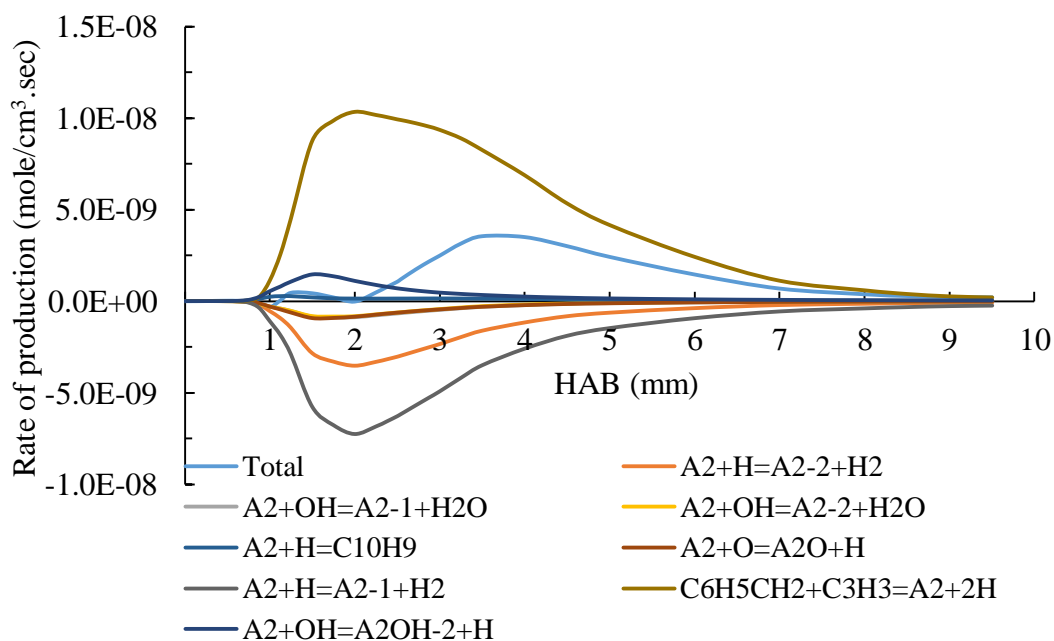
Figure 4. 52. Rate of production analysis for A_2 across the flame (n-heptane)

The total rate of production and pathway analyses for naphthalene in n-heptane/methanol flame have been also carried out (Figures 4.55-4.57). The peak points of the total rate of formation profile of naphthalene in n-heptane/methanol flame are at HAB of 1.5 and 4 mm (Figure 4.55). The peak point of the rate of naphthalene formation by the reaction of $C_6H_5CH_2+C_3H_3=A_2+2H$ is shifted to lower HAB when methanol is included in the flame. The pathway analysis was done for the naphthalene at HAB 1.5 mm and 4 mm to see different formation pathways of naphthalene for the n-heptane/methanol flame (Figures 4.56, 4.57). The most important paths for the formation of naphthalene at 1.5 mm HAB are through benzyl radical $C_6H_5CH_2$, propargyl radical C_3H_3 and acetylene C_2H_2. However, the dominant path for the naphthalene formation at 4 mm HAB is by benzyl radical $C_6H_5CH_2$.
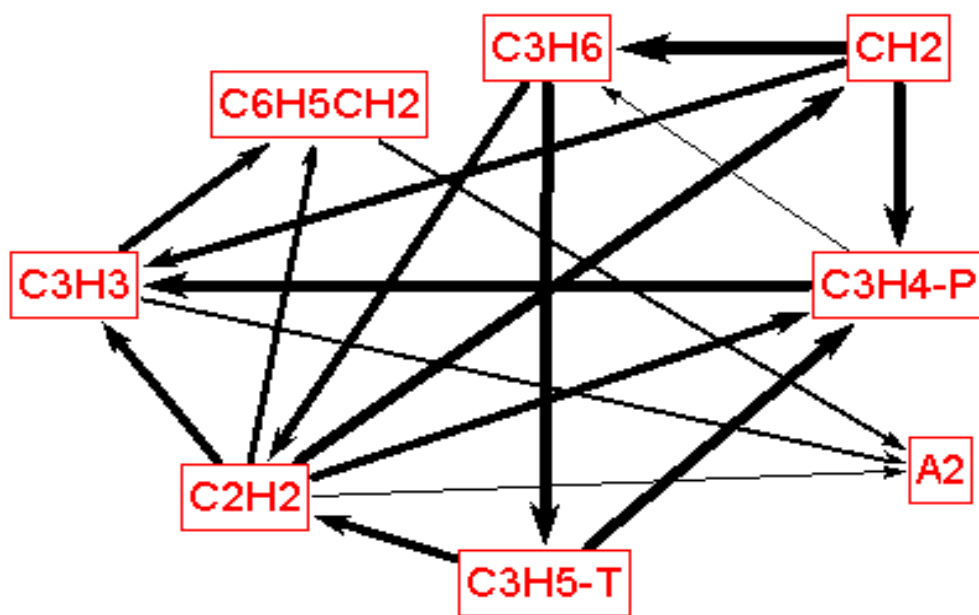
Figure 4. 53. A_2 formation pathways at HAB=1. 25mm (both H and C flux) (n-heptane flame)

Generally, the oxidation of n-heptane and n-heptane/methanol flames show no substantial change for the low-molecular-weight species and PAHs paths after methanol addition, which consists with the study of laminar, premixed n-heptane/toluene flames with oxygenates addition (methanol or ethanol) (Xu et al. 2013).
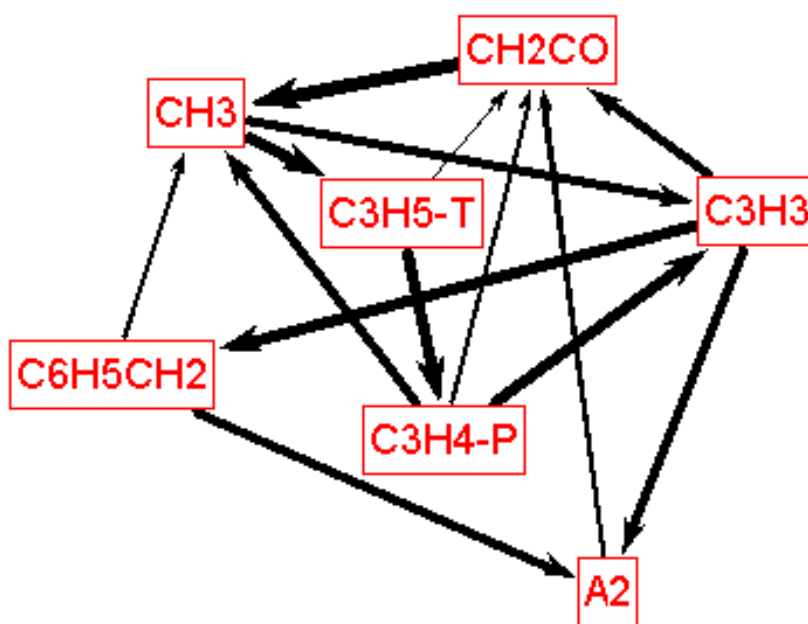
Figure 4. 54. A_2 formation pathways at HAB=4mm (both H and C flux) (n-heptane flame)
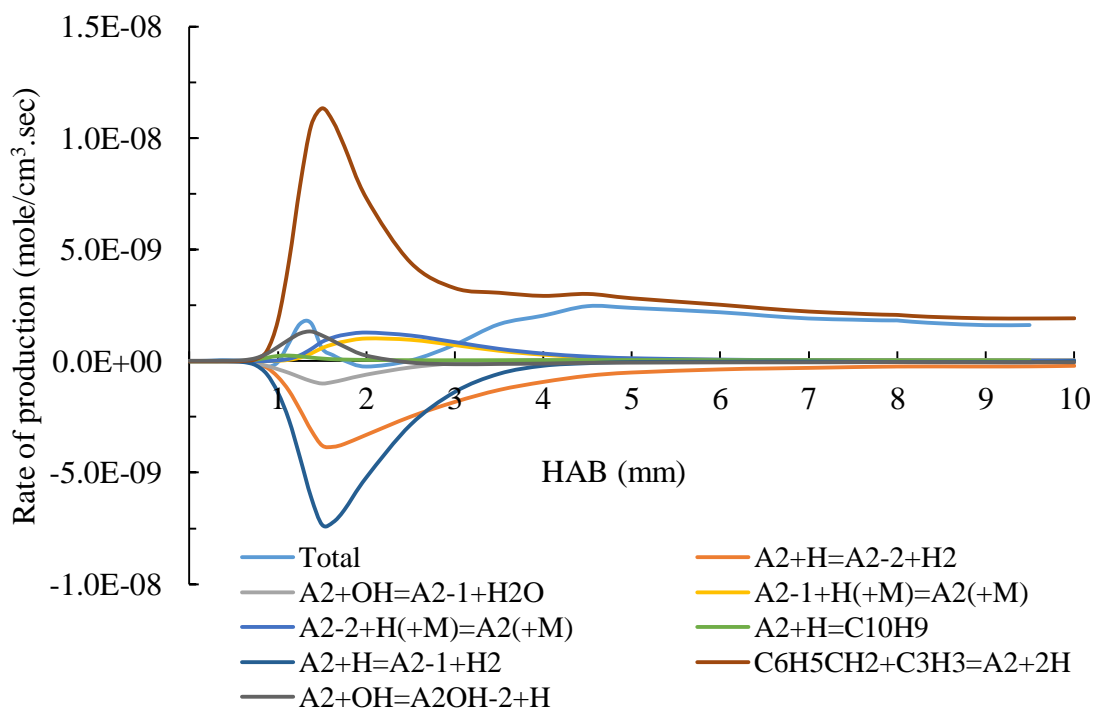
Figure 4. 55. Rate of production analysis for A_2 across the flame (n-heptane/methanol)
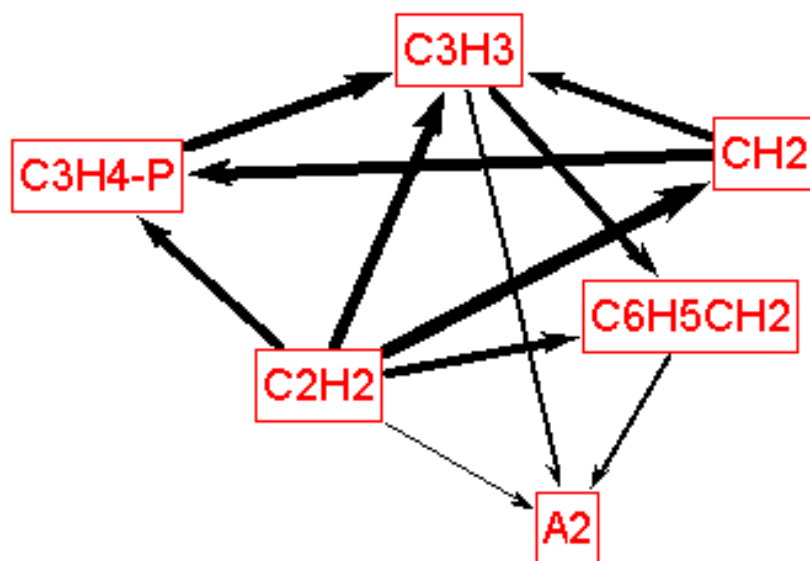
Figure 4. 56. A_2 formation pathways at HAB=1.5mm (both H and C flux) (n-heptane/ methanol flame)

The model predictions and experimental measurements for mole fraction profiles of higher PAHs species (i.e., acenaphthylene and 4H-cyclopenta[def]phenanthrene) for both fames are shown in Figures 4.58 and 4.59, respectively. For acenaphthylene mole fractions, there was a good agreement between experimental measurements and model predictions for both flames (Figure 4.58). The average reductions in mole fractions of acenaphthylene were around 58% for the experimental measurements and 34% for the model predictions when methanol was added. There were underpredictions by the Master Mechanism for the mole fractions of 4H-cyclopenta[def]phenanthrene for both flames by a factor of about 10 (Figure 5.59). The average reduction in mole fractions of 4H-cyclopenta[def]phenanthrene was about 45% for model predictions when methanol was added. However, there was an average of 60% reduction for the experimental data of 4H-cyclopenta[def]phenanthrene mole fractions.

The differences between the model predictions and experimental measurements for the major, minor, trace species are attributed to; the possible uncertainties in the experimental measurements, some missing reactions in the Master Mechanism, the uncertainties in the reaction rate parameters in the kinetic database and the uncertainties in the thermodynamic and transport properties database.
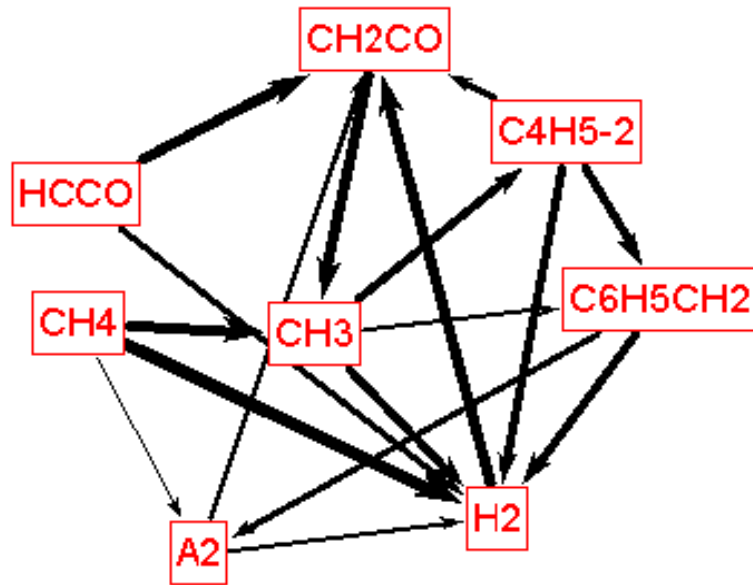
Figure 4. 57. A$_2$ formation pathways at HAB=4mm (both H and C flux) (n-heptane/ methanol flame)
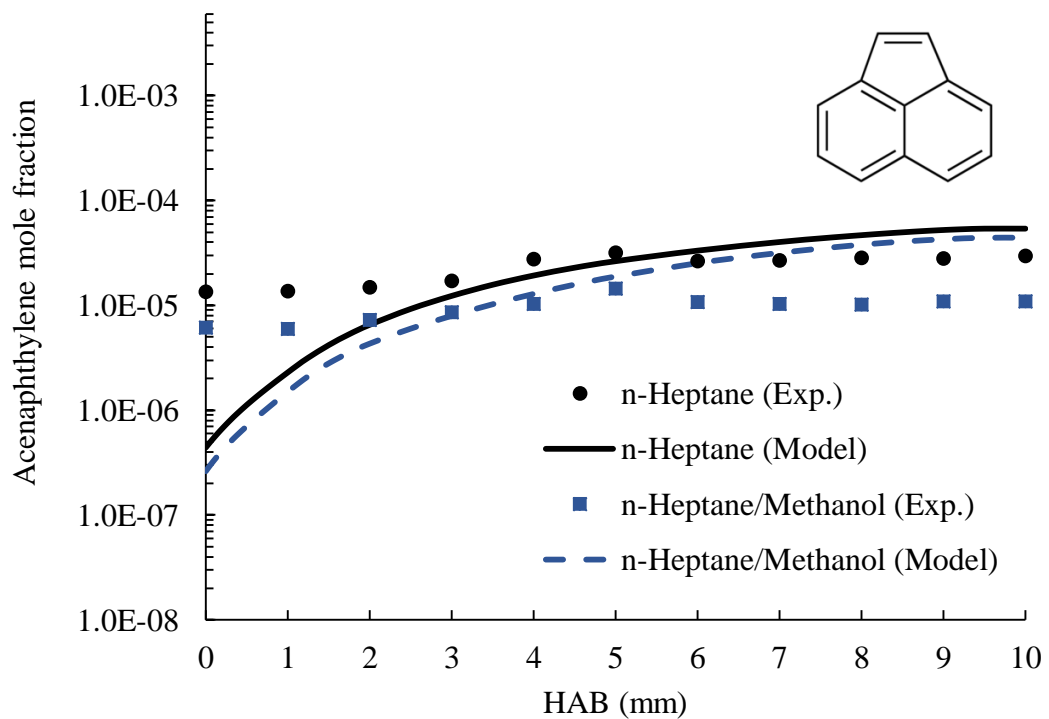
Figure 4. 58. Comparison of species profiles of acenaphthylene
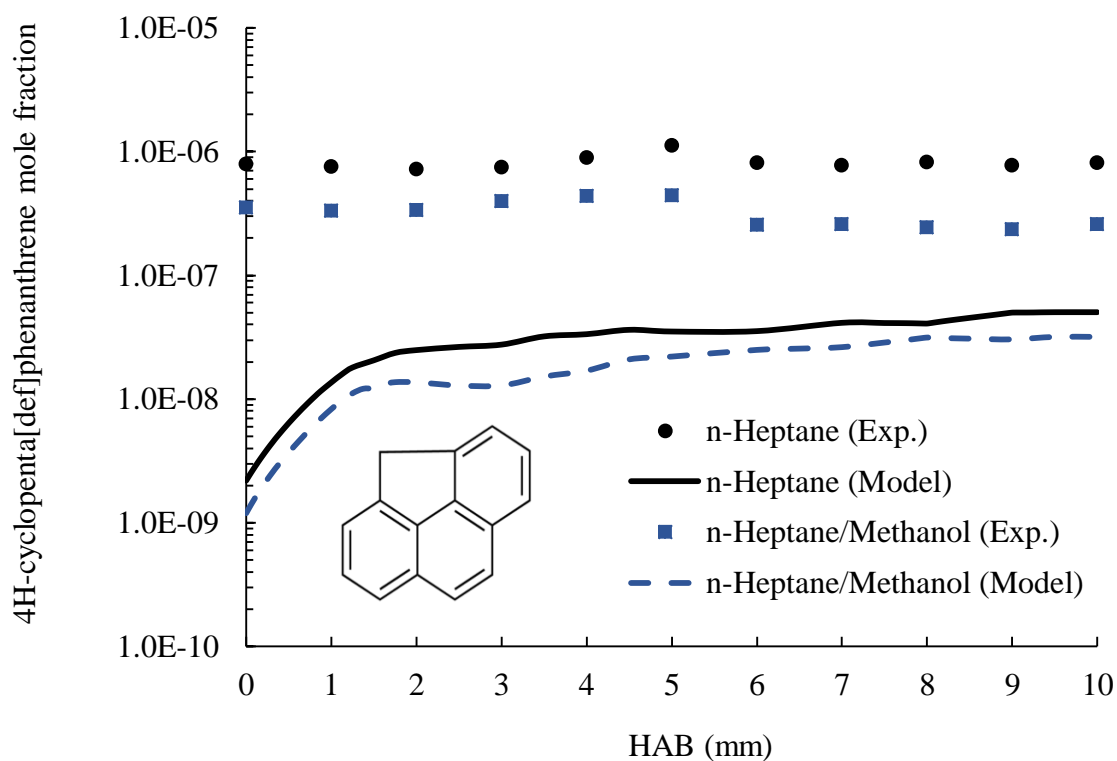
Figure 4. 59. Comparison of species profiles of 4H-cyclopenta[def]phenanthrene

4.4. Model reduction

The detailed chemical kinetic mechanisms generally consist of high number of species and reactions. This leads to enormous computation and makes the 3-D simulation processes difficult. Based on that, model reduction plays an important role to overcome these problems. Skeletal mechanism reduction is one of the mechanism reduction types. A skeletal mechanism is derived by omitting the unimportant reactions and species that can be carried out by particular analysis. There are several methods for skeletal reduction: principal component analysis (PCA) (Vajda, Valko, and Turányi 1985), directed relation graph (DRG) (Lu and Law 2005) and directed relation graph with error propagation (DRGEP) (Pepiot-Desjardins and Pitsch 2008), etc. The DRG and DRGEP methods are the most effective methods for the mechanism reduction since these methods are straightforward and effective methods that need less computation cost (An and Jiang 2013).

The theory of directed relation graph (DRG) can be identified by eliminating the unimportant species and the associated unimportant elementary reactions. Because of the

coupling of the species the removal of unimportant species from the master mechanism is done by the removal of a group of species strongly coupled to it. For instance, a species A can be strongly coupled to species B either directly if they appear together in a fast reaction or indirectly if each of them is strongly coupled to another species C, even if they themselves do not appear together in any reaction (Lu and Law 2005). The species B has to be kept in the mechanism if and only if their removal would directly bring out significant error to the production of species A. The rate of production of species A is considered as:

$$R_A = \sum_{i=1,I} v_{A,i}\, \omega_i \qquad (4.1)$$

where the subscripts i designate the ith elementary reaction, $v_{A,i}$ is the stoichiometric coefficient of species A, and ω_i the production rate.

The immediate error, (r_{AB}), is the removal of a species on the production rate of selected species and to quantify the direct influence of one species on another. The immediate error calculated by the equation below:

$$r_{AB} \equiv \frac{\sum_{i=1,j} |v_{A,i}\omega_i\delta_{Bi}|}{\sum_{i=1,j} |v_{A,i}\omega_i|} \qquad (4.2)$$

$$\delta_{Bi} = \left\{ \begin{array}{l} 1, \text{ if the } i^{th} \text{ reaction involves species B} \\ 0, \text{ otherwise} \end{array} \right\} \qquad (4.3)$$

where A is the selected species and B is the removed species.

The removal of species B from the reduced mechanism is expected to bring significant error on the production rate of species A. Accordingly, if A has to be kept, B should also be kept, which means species A strongly depends on species B.

To quantify the dependence of A on B, a small threshold value $\mathcal{E}$ should be defined. In case of $r_{AB} < \mathcal{E}$, the dependence can be considered to be negligible, and there is no edge from A to B (no direct dependence between A and B). A directed edge from A to B exists only if $r_{AB} \geq \mathcal{E}$. To run model reduction, the relative tolerance was defined as 500 % of the all major, minor, and trace species experimentally quantified. By defining the relative tolerance as a high value gives an opportunity to see different versions of reduced mechanisms. The differences between n-heptane mole fraction profiles in the

Master and Skeletal Mechanisms were calculated as an error percentage. The removal of the species/reactions is related with threshold values. Threshold value of 1 means the removal of all species/reactions. There was a sudden increase of the n-heptane mole fraction predictions percentage error with the increasing threshold value (Figure 4.60). The reduced mechanism that corresponds to that sudden increase point was selected as the optimal reduced mechanism. The Reduced Mechanism was obtained at threshold value of 0.1875. Figure 4.60 shows the effect of mechanism reduction on n-heptane mole fraction predictions.

The Master Mechanism of n-heptane/methanol flame contains 4480 reactions and 945 species, which is too large to be adopted by a 3-D simulation model. Therefore, a model reduction has been carried out using Chemkin software by DRG method to obtain a skeletal model which contains 1113 reactions and 156 species. Table 4.2 illustrates the number of reactions and species of Master and Reduced Mechanisms.
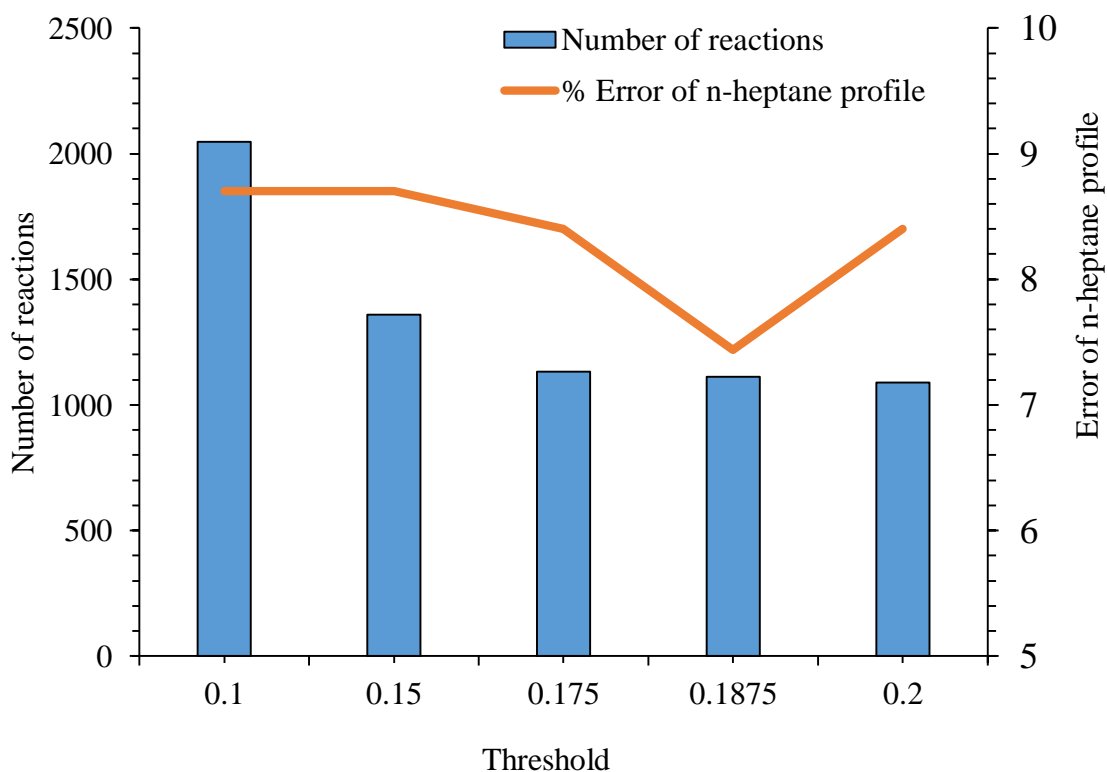
Figure 4. 60. Effect of mechanism reduction on n-heptane mole fraction predictions

Table 4. 2. The number of reactions and species of Reduced and Master Mechanisms

	Number of reactions	Number of species
Master Mechanism	4480	945
Reduced Mechanism	1113	156
Reduction %	75.15%	83.49%

4.9. Validation of Skeletal Mechanism

The Skeletal Mechanism was also validated against the same experimental data used for the detailed mechanism in order to investigate the prediction capability of the Skeletal Mechanism comparing with the Master Mechanism. The experimental conditions of ignition delay time experiment (Kumar and Sung 2011) and the premixed fuel-rich n-heptane/methanol flame experiment (Chen et al. 2012) are given in Table 4.1.

The hydrogen, carbon monoxide, and carbon dioxide mole fraction profiles of both experimental measurements and model predictions for the n-heptane/methanol flame study (Chen et al. 2012) are given in Figures 4.61-4.63. As seen in Figure 4.61, the Master Mechanism fits very well the experimental measurements of hydrogen mole fractions whereas the Reduced Mechanism slightly underpredicts them. The Reduced Mechanism predictions for the carbon monoxide mole fractions are almost the same as the Master Mechanism results, and both of them are in a good agreement with the experimental measurements (Figure 4.62). For carbon dioxide the Reduced Mechanism profile is slightly lower than Master Mechanism profile for HAB 3-9 mm (Figure 4.63). The average differences between the mole fraction predictions of the Reduced and Master Mechanisms of H_2, CO, and CO_2 are; 17%, 6% and 8%, respectively. Both mechanisms are in fair agreement with the experimental data.

The ignition delay time validations of the Reduced Mechanism were done for rapid compression machine RCM experimental data at 15 bar and an equivalence ratio of 1 (Figure 4.64). The Reduced Mechanism predictions of the ignition delay time were very close (almost the same) to the Master Mechanism predictions. Both the Master and Reduced Mechanisms gave closer predictions to the experimental measurements than the modeling results of Kumar and Sung (2011).
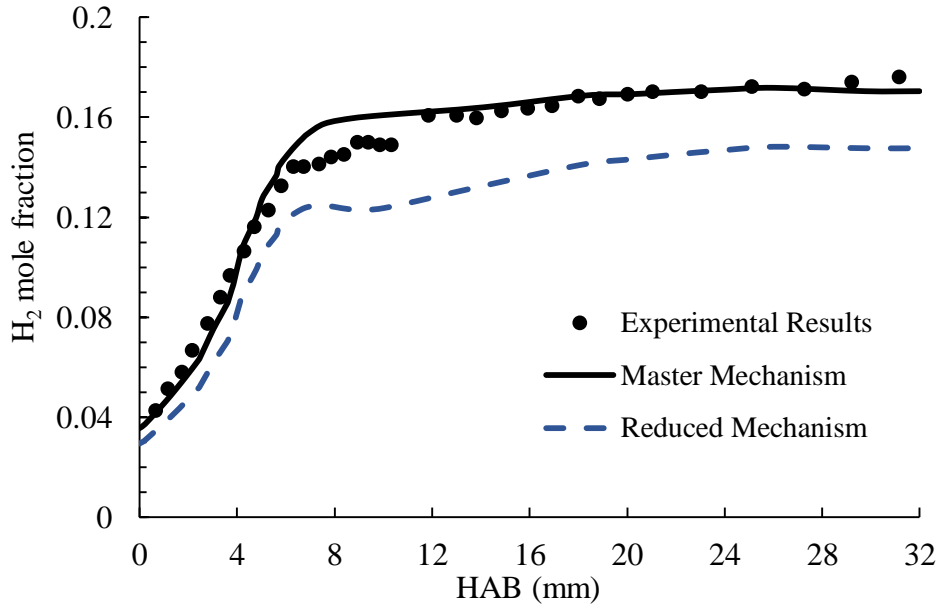
Figure 4. 61. Hydrogen mole fractions (Validation of the skeletal mechanism using premixed n-heptane/methanol flame) (Chen et al. 2012)
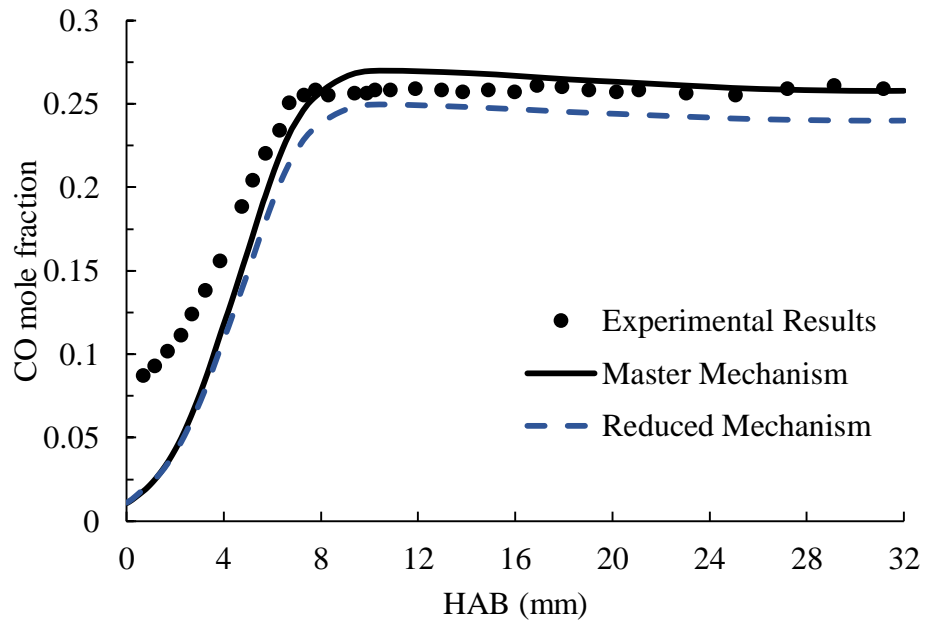
Figure 4. 62. Carbon monoxide mole fractions (Validation of the skeletal mechanism using premixed n-heptane/methanol flame) (Chen et al. 2012)
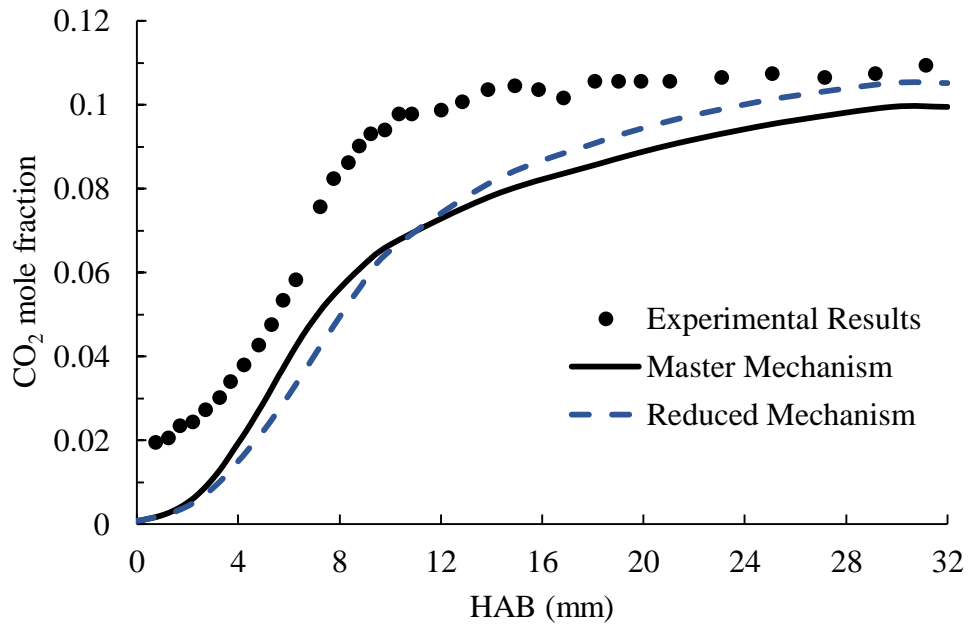
Figure 4. 63. Carbon dioxide mole fractions (Validation of the skeletal mechanism using premixed n-heptane/methanol flame) (Chen et al. 2012)
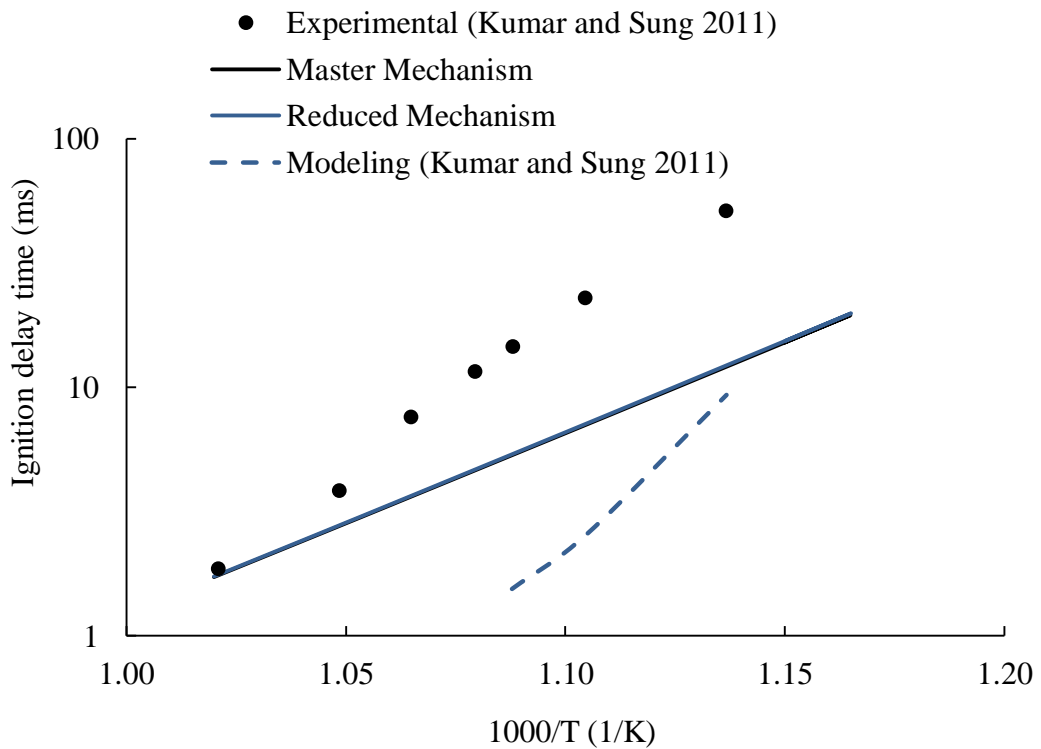
Figure 4. 64. Validations of the skeletal mechanism by ignition delay time (Kumar and Sung 2011)

According to the validation results of the Skeletal Mechanism, it can be used instead of the Master Mechanism when the computational power is limited.

4.10. Comparison Between the Master and Skeletal Mechanisms on the Target Flame

The experimental measurements of particular species of the target flame by Inal and Senkan (2002a) have been compared with the predictions of both Master and Skeletal Mechanisms for the n-heptane/methanol flame.

The comparisons between the predictions of the Master and Skeletal Mechanisms, and the experimental results for acetylene, propadiene, diacetylene and vinylacetylene for n-heptane/methanol flame are shown in Figure 4.65-4.68, respectively. Both mechanisms underpredict the experimental results for these species. Moreover, the Reduced Mechanism has given slightly better results than the Master Mechanism for these species (acetylene, propadiene, diacetylene and vinylacetylene) as seen in Figures 4.65-4.68. The average differences between the mole fraction predictions of the Reduced and Master Mechanisms of C_2H_2 and C_4H_4 are; 4% and 11%, respectively.

Figure 4. 65. Comparison between the Master and Skeletal Mechanisms of acetylene mole fraction predictions on the n-heptane/methanol flame

Figure 4. 66. Comparison between the Master and Skeletal Mechanisms of propadiene mole fraction predictions on the n-heptane/methanol flame

Figure 4. 67. Comparison between the Master and Skeletal Mechanisms of diacetylene mole fraction predictions on the n-heptane/methanol flame
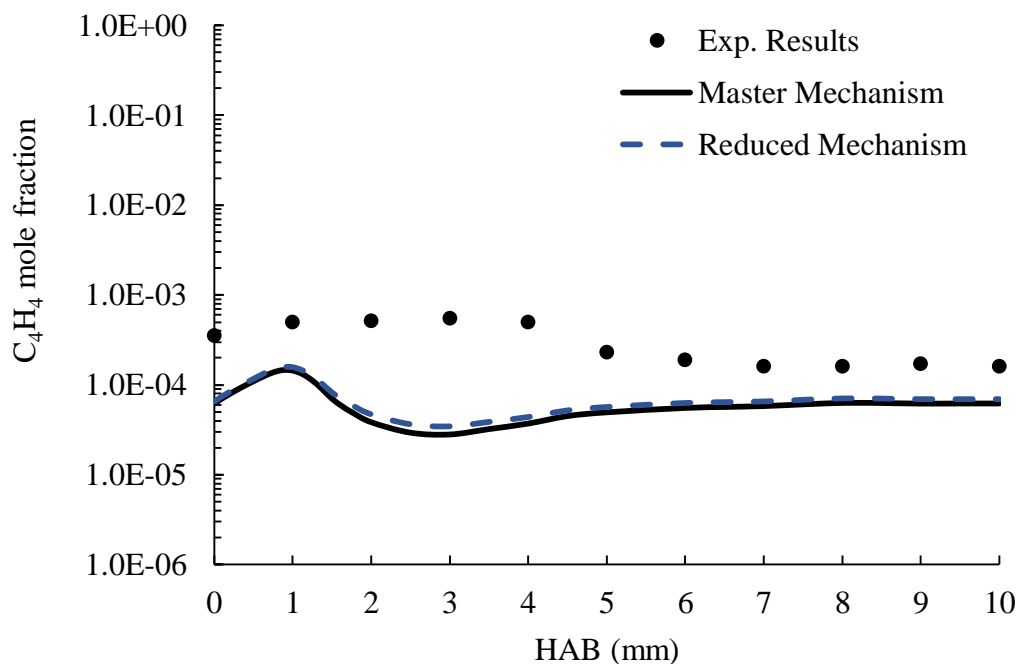
Figure 4. 68. Comparison between the Master and Skeletal Mechanisms of vinylacetylene mole fraction predictions on the n-heptane/methanol flame

For benzene and toluene, the difference between the Master and Skeletal Mechanisms predictions are relatively greater than the low-molecular-weight species as seen in Figures 4.69 and 4.70, respectively. For benzene, the Master Mechanism predictions are closer to the experimental results even though both mechanisms have overpredictions (Figure 4.69). The Reduced Mechanism performs better than the Master Mechanism at low HAB for toluene mole fractions predictions. However, at high HAB the Master Mechanism predictions are closer to the experimental data (Figure 4.70).

The average differences between the mole fraction predictions of the Reduced and Master Mechanisms of C_6H_6 and $C_6H_5CH_3$ are; 63% and 75%, respectively. The comparisons between the predictions of Master and Reduced Mechanisms, and experimental measurements for phenylacetylene, indene and naphthalene are shown in Figures 4.71-4.73, respectively. The model predictions of Master and Skeletal Mechanisms show overpredictions at HAB higher than 5mm for phenylacetylene, indene and naphthalene. Although there is a slight difference between the predictions of both mechanisms, they are in good agreements with experimental data.
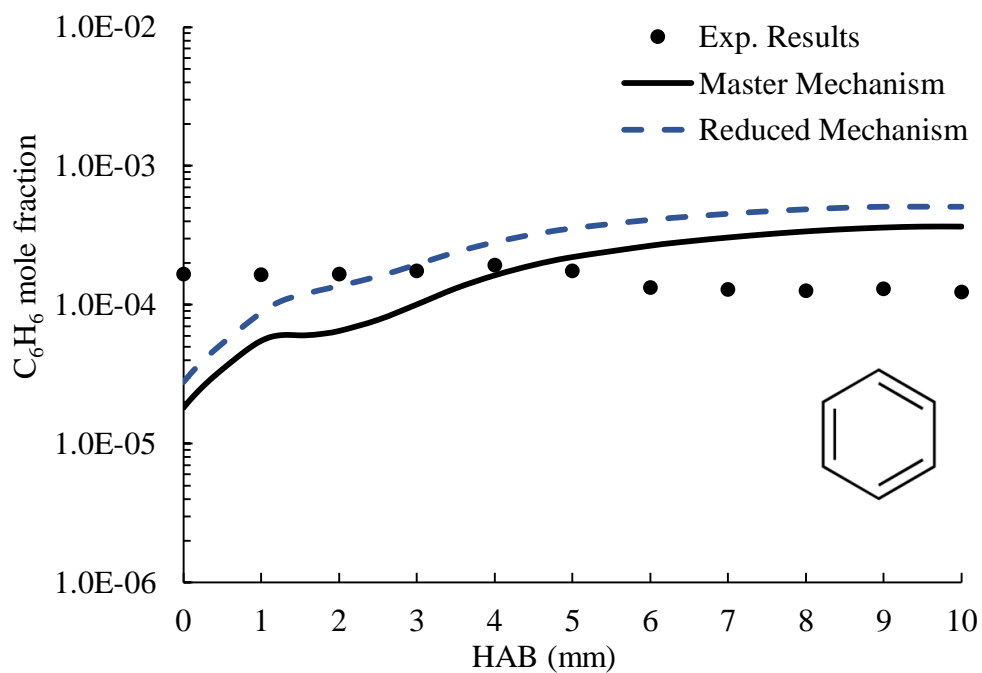
Figure 4. 69. Comparison between the Master and Skeletal Mechanisms of benzene mole fraction predictions on the n-heptane/methanol flame
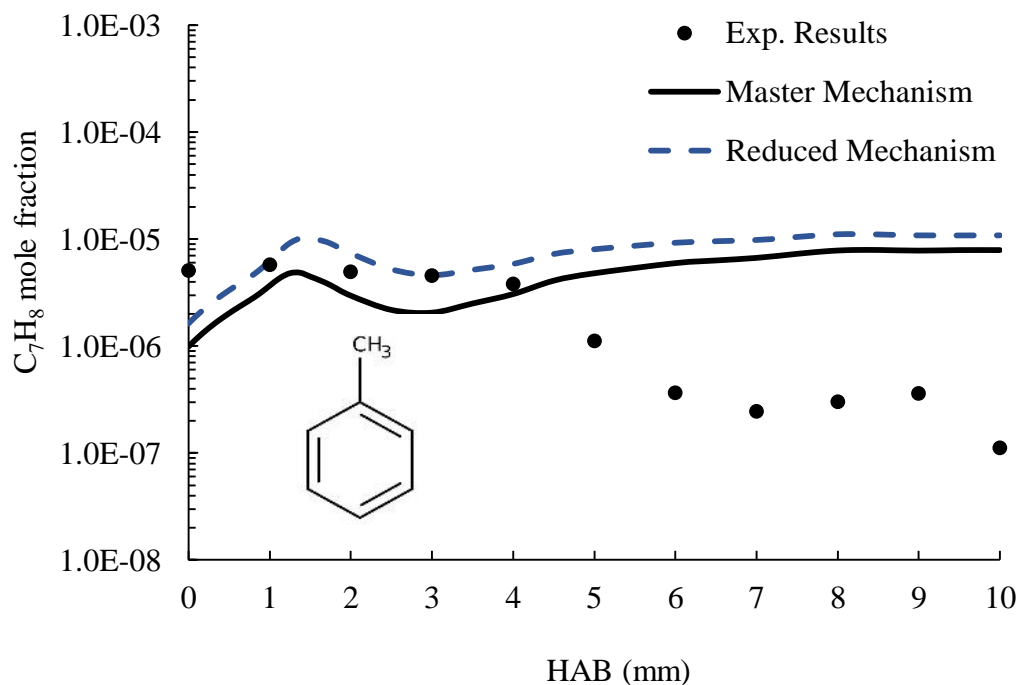
Figure 4. 70. Comparison between the Master and Skeletal Mechanisms of toluene mole fraction predictions on the n-heptane/methanol flame

As a result of the comparisons between the Skeletal and Master Mechanisms predictions, it can be deduced that the Skeletal Mechanism has given applicable results and it can be used for flame simulations instead of the Master Mechanism.
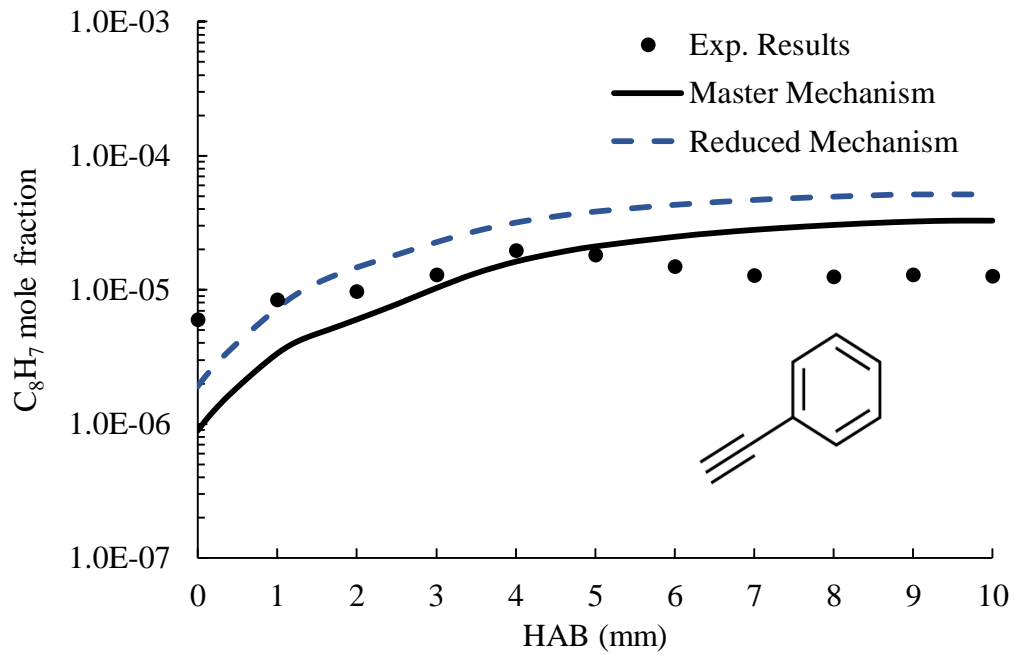
Figure 4. 71.   Comparison between the Master and Skeletal Mechanisms of phenylacetylene mole fraction predictions on the n-heptane/methanol flame
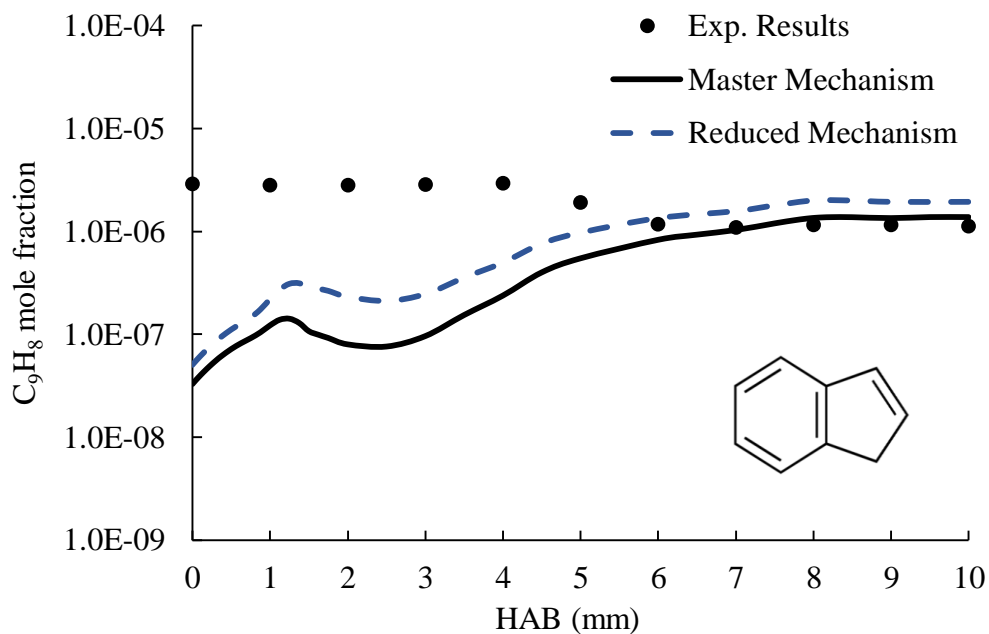
Figure 4. 72. Comparison between the Master and Skeletal Mechanisms of indene mole fraction predictions on the n-heptane/methanol flame
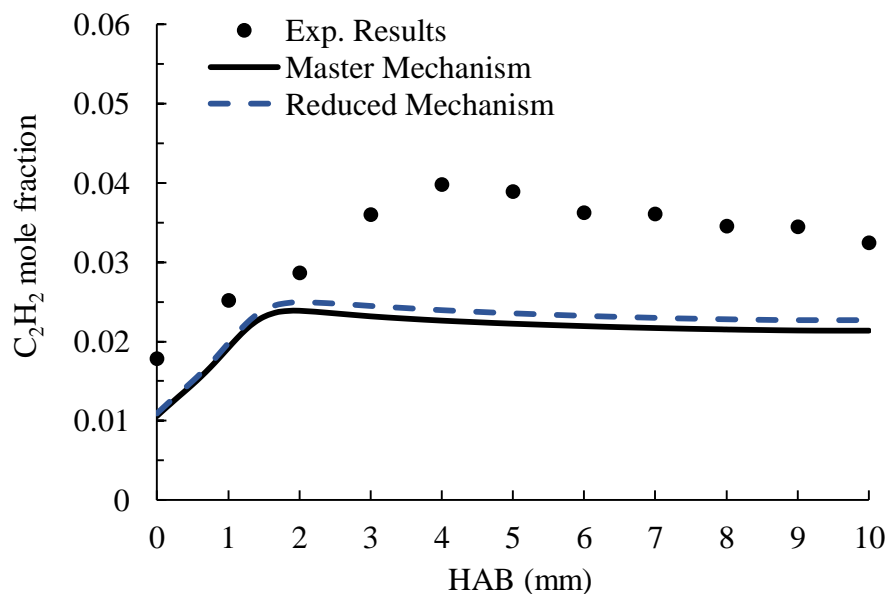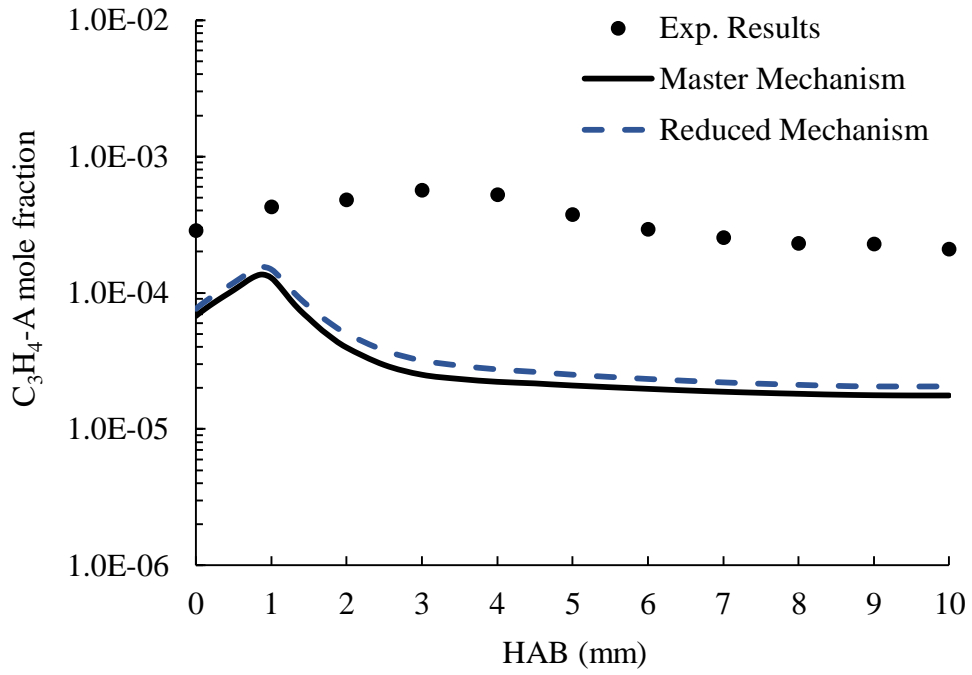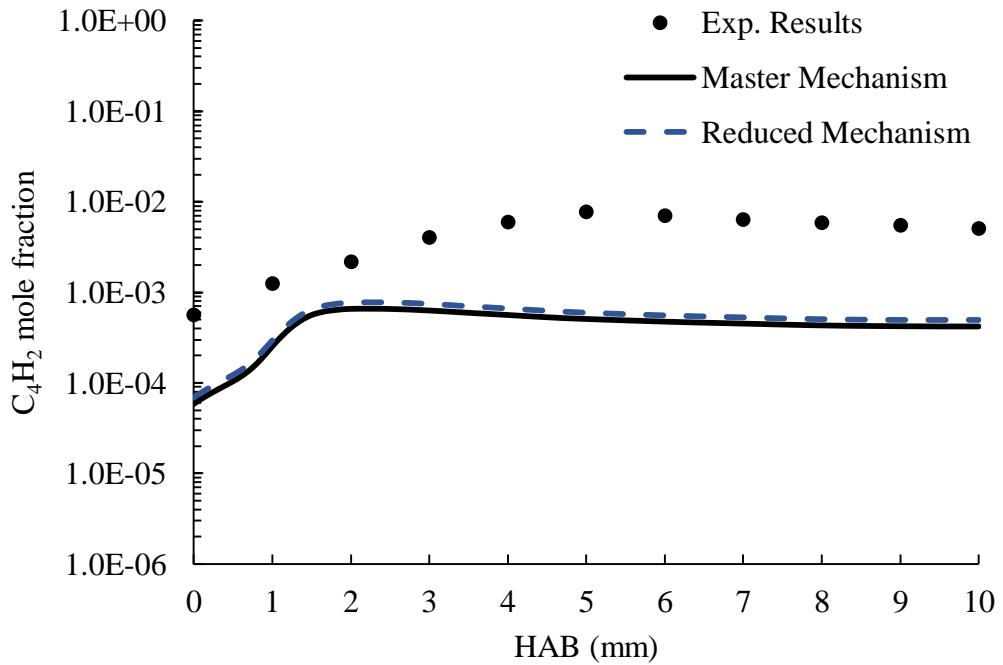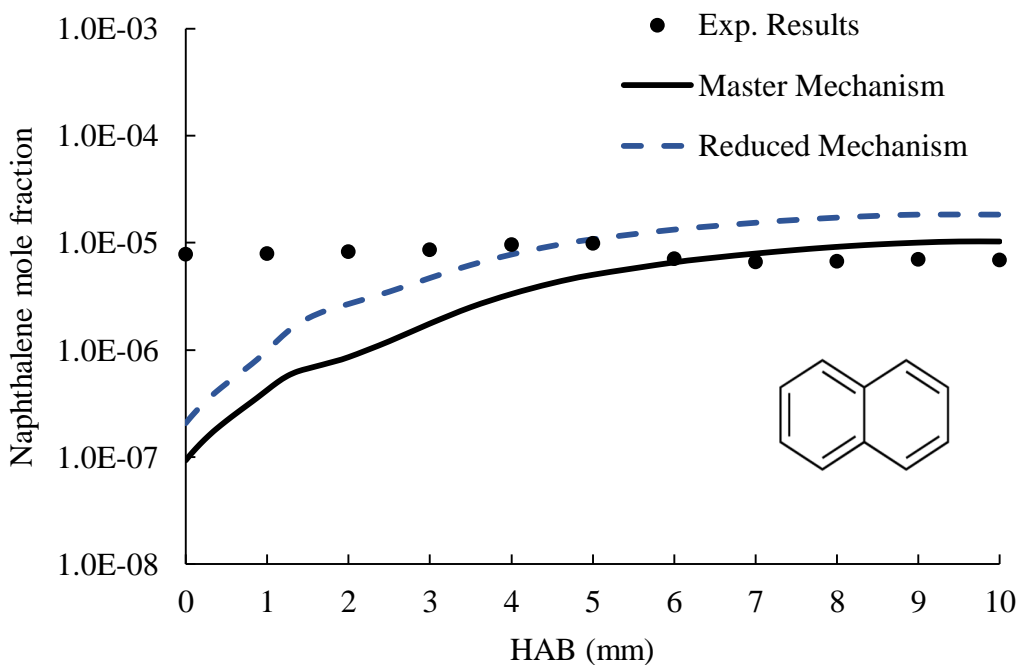

Figure 4. 73. Comparison between the Master and Skeletal Mechanisms of naphthalene mole fraction predictions on the n-heptane/methanol flame

CHAPTER 5

CONCLUSION

A detailed chemical kinetic model has been developed for the oxidation of n-heptane and n-heptane/methanol mixture to predict the effects of methanol addition on combustion chemistry. The Base Mechanism is about the detailed chemical kinetic model of n-heptane oxidation including the formation of polycyclic aromatic hydrocarbon species. The Donor Mechanism is methanol oxidation mechanism. The yielded Master Mechanism consists of 4480 reactions and 945 species. Sensitivity analysis for some species has been carried out to understand the most sensitive reactions across the flame that may improve the model predictions of species mole fractions. The Master Mechanism has been validated against experimental measurements of premixed flame species mole fractions and ignition delay time measurements in rapid compression machine. It has been applied to burner-stabilized, atmospheric pressure, laminar, premixed, fuel-rich n-heptane and n-heptane/methanol flames at an equivalence ratio of 2.10. The mechanism predicted most of the low-molecular weight stable products of the fuel-rich, premixed n-heptane and n-heptane/methanol flames. It has been found that methanol has reduced the mole fraction of these species. Based on the model predictions of aromatic and polycyclic aromatic hydrocarbon mole fractions, the addition of methanol to n-heptane fuel has reduced the mole fraction of these species. The reductions in the species mole fractions can be attributed to; the addition of methanol converts an active hydroxyl radical, OH, into inactive hydrogen peroxide, H_2O_2, that leads to reduction the system reactivity. The fuel oxygenates could be a reliable method for reducing toxic species mole fractions in hydrocarbon fuel combustion. Rate of production (ROP) and pathway analyses have been carried out for some species in both flames. The formation/decomposition of acetylene, propadiene, vinylacetylene, aromatics and polycyclic aromatic hydrocarbons were also investigated for the n- heptane and n-heptane/methanol flames. Acetylene, propargyl radical and vinylacetylene were found as important precursors for the formation of first and second aromatic ring species. The pathway analysis of benzene shows that benzene is mostly formed by a combination reaction of two propargyl radicals (C_3H_3) ($2C_3H_3=A_1$). In addition, benzene is formed by

the reaction between vinyl radical and vinylacetylene ($C_4H_4 + C_2H_3 = A_1 + H$). A model reduction has been conducted to investigate the combustion chemistry of n-heptane and n-heptane/methanol with less computational effort. By directed relation graph method (DRG), the Skeletal Mechanism has been generated with 1113 reactions and 156 species. The Skeletal Mechanism was in a good agreement with the Master Mechanism in terms of the species mole fraction predictions of the n-heptane/methanol flame. As future work, more sensitivity analysis for particular species should be carried out to improve the model predictions by the Master Mechanism. In addition, better model predictions can be achieved by including some missing reactions for the formation and decomposition of the major, minor, and trace species.

REFERENCES

Acarl, Shaun, Hue Nguyen, Rehab Elsamra, Minh Nguyen, and Jozef Peeters. 2005. "Pulsed laser photolysis and quantum chemical-statistical rate study of the reaction of the ethynyl radical with water vapor." *The Journal of chemical physics* 122:114-307.

Acrivos, Andreas, and Thomas Taylor. 1962. "Heat and mass transfer from single spheres in Stokes flow." *The Physics of Fluids* 5 (4):387-394.

An, Jiangtao, and Yong Jiang. 2013. "Differences between Direct Relation Graph and Error-propagation-based Reduction Methods for Large Hydrocarbons." *Procedia Engineering* 62:342-349.

An, Yan-zhao, Yi-qiang Pei, Jing Qin, Hua Zhao, and Xiang Li. 2015. "Kinetic modeling of polycyclic aromatic hydrocarbons formation process for gasoline surrogate fuels." *Energy Conversion and Management* 100:249-261.

Bakali, A. E., J. L. Delfau, and C. Vovelle. 1998. "Experimental Study of 1 Atmosphere, Rich, Premixed n-heptane and iso-octane Flames." *Combustion Science and Technology* 140 (1-6):69-91.

Bata, R. M., and V. P. Roan. 1989. "Effects of Ethanol and/or Methanol in Alcohol-Gasoline Blends on Exhaust Emissions." *Journal of Engineering for Gas Turbines and Power* 111 (3):432-438.

Baulch, D. L., C. J. Cobos, R. A. Cox, C. Esser, P. Frank, Th. Just, J. A. Kerr, M. J. Pilling, J. Troe, R. W. Walker, and J. Warnatz. 1992. "Evaluated Kinetic Data for Combustion Modelling." *Journal of Physical and Chemical Reference Data* 21 (3):411-734.

Braids, Olin C. 2001. "MTBE—Panacea or Problem." *Environmental Forensics* 2 (3):189-196.

Bugler, John, Brandon Marks, Olivier Mathieu, Rachel Archuleta, Alejandro Camou, Claire Grégoire, Karl A. Heufer, Eric L. Petersen, and Henry J. Curran. 2016. "An ignition delay time and chemical kinetic modeling study of the pentane isomers." *Combustion and Flame* 163:138-156.

Burke, Ultan, Wayne K. Metcalfe, Sinead M. Burke, K. Alexander Heufer, Philippe Dagaut, and Henry J. Curran. 2016. "A detailed chemical kinetic modeling, ignition delay time and jet-stirred reactor study of methanol oxidation." *Combustion and Flame* 165:125-136.

Canakci, Mustafa, Cenk Sayin, and Metin Gumus. 2008. "Exhaust Emissions and Combustion Characteristics of a Direct Injection (DI) Diesel Engine Fueled with Methanol−Diesel Fuel Blends at Different Injection Timings." *Energy and Fuels* 22 (6):3709-3723.

Chakir, A., M. Belliman, J. Boettner, and Cathonnet M. 1992. "Kinetic Study of N-Heptane Oxidation." *International Journal of Chemical Kinetics* 24:385-410.

Chan, Qing N. 2011. "Development of instantaneous temperature imaging in sooty flames."PhD Dissertation, School of Chemical Engineering, The University of Adelaide.

Chemkin-Pro®. 2018. ANSYS, Inc. Release 19.0.

Chen, Gen, Wu Yu, Jin Fu, Jun Mo, Zuohua Huang, Jiuzhong Yang, Zhandong Wang, Hanfeng Jin, and Fei Qi. 2012. "Experimental and modeling study of the effects of adding oxygenated fuels to premixed n-heptane flames." *Combustion and Flame* 159 (7):2324-2335.

Chen, Gen, Wu Yu, Xue Jiang, Zuohua Huang, Zhandong Wang, and Zhanjun Cheng. 2013. "Experimental and modeling study on the influences of methanol on premixed fuel-rich n-heptane flames." *Fuel* 103:467-472.

Cole, J. A., J. D. Bittner, J. P. Longwell, and J. B. Howard. 1984. "Formation mechanisms of aromatic compounds in aliphatic flames." *Combustion and Flame* 56 (1):51-70.

Collis, DC, and MJ Williams. 1959. "Two-dimensional convection from heated wires at low Reynolds numbers." *Journal of Fluid Mechanics* 6 (3):357-384.

Curran, H. J., P. Gaffuri, W. J. Pitz, and C. K. Westbrook. 1998. "A Comprehensive Modeling Study of n-Heptane Oxidation." *Combustion and Flame* 114 (1):149-177.

Dagaut, P., M. Reuillon, and M. Cathonnet. 1994. "High Pressure Oxidation of Liquid Fuels from Low to High Temperature. 2. Mixtures of n-Heptane and iso-Octane." *Combustion Science and Technology* 103 (1-6):315-336.

Dagaut, Philippe, Marcelline Reuillon, and Michel Cathonnet. 1995. "Experimental study of the oxidation of n-heptane in a jet stirred reactor from low to high temperature and pressures up to 40 atm." *Combustion and Flame* 101 (1):132-140.

Davis, S. G., and C. K. Law. 1998. "Laminar flame speeds and oxidation kinetics of iso-octane-air and n-heptane-air flames." *Symposium (International) on Combustion* 27 (1):521-527.

Degirmenci, Emre. 2018. "Detailed Chemical Kinetic Modeling of n-Heptane Flame." MSc Thesis, Chemical Engineering, Izmir Instutute of Technology (95).

Dooley, S., M. P. Burke, M. Chaos, Y. Stein, F. L. Dryer, V. P. Zhukov, O. Finch, J. M. Simmie, and H. J. Curran. 2010. "Methyl formate oxidation: Speciation data, laminar burning velocities, ignition delay times, and a validated chemical kinetic model." *International Journal of Chemical Kinetics* 42 (9):527-549.

Egolfopoulos, F. N., D. X. Du, and C. K. Law. 1992. "A Comprehensive Study of Methanol Kinetics in Freely-Propagating and Burner-Stabilized Flames, Flow and Static Reactors, and Shock Tubes." *Combustion Science and Technology* 83 (1-3):33-75.

EIA. 2019. "Annual Energy Outlook 2019." Washington, USA. Energy Information Administration. https://www.eia.gov/outlooks/aeo/.

Eisner, Alfred D., and Daniel E. Rosner. 1985. "Experimental studies of soot particle thermophoresis in nonisothermal combustion gases using thermocouple response techniques." *Combustion and Flame* 61 (2):153-166.

Eiteneer, Boris, and Michael Frenklach. 2003. "Experimental and modeling study of shock-tube oxidation of acetylene." 35 (9):391-414.

Energy-Information-Administration. 2003. "Status and Impact of State MTBE Bans." Washington, USA. http://www.eia.gov/oiaf/servicerpt/mtbeban/index.html.

Frenklach, Michael, David W. Clary, William C. Gardiner, and Stephen E. Stein. 1985. "Detailed kinetic modeling of soot formation in shock-tube pyrolysis of acetylene." *Symposium (International) on Combustion* 20 (1):887-901.

Frenklach, Michael, and Hai Wang. 1994. "Detailed Mechanism and Modeling of Soot Particle Formation." In *Soot Formation in Combustion: Mechanisms and Models*, edited by Henning Bockhorn, 165-192. Berlin, Heidelberg: Springer Berlin Heidelberg.

Frenklach, Michael, and JüRgen Warnatz. 1987. "Detailed Modeling of PAH Profiles in a Sooting Low-Pressure Acetylene Flame." *Combustion Science and Technology* 51 (4-6):265-283.

Green, W, and R West. 2019. "RMG-database." https://rmg.mit.edu/database/kinetics/.

Haas, Francis M., Marcos Chaos, and Frederick L. Dryer. 2009. "Low and intermediate temperature oxidation of ethanol and ethanol–PRF blends: An experimental and modeling study." *Combustion and Flame* 156 (12):2346-2350.

Hamdane, S, Y Rezgui, M J Kinetics Guemini, and Catalysis. 2012. "A detailed chemical kinetic mechanism for methanol combustion in laminar flames." *Kinetics and Catalysis* 53 (6):648-664.

Hansen, Nils, James A. Miller, Phillip R. Westmoreland, Tina Kasper, Katharina Kohse-Höinghaus, Juan Wang, and Terrill A. Cool. 2009. "Isomer-specific combustion chemistry in allene and propyne flames." *Combustion and Flame* 156 (11):2153-2164.

Hansen, Nils, Marina Schenk, Kai Moshammer, and Katharina Kohse-Höinghaus. 2017. "Investigating repetitive reaction pathways for the formation of polycyclic aromatic hydrocarbons in combustion processes." *Combustion and Flame* 180:250-261.

Held, T. J., A. J. Marchese, and F. L. Dryer. 1997. "A Semi-Empirical Reaction Mechanism for n-Heptane Oxidation and Pyrolysis." *Combustion Science and Technology* 123 (1-6):107-146.

Held, Timothy J., and Frederick L. Dryer. 1998. "A comprehensive mechanism for methanol oxidation." *International Journal of Chemical Kinetics* 30 (11):805-830.

Inal, Fikret. 1999. "Polycyclic aromatic hydrocarbons (PAH) and soot formation in premixed, laminar n-heptane flames: Effects of oxygenate additives."PhD Dissertation, Chemical Engineering, University of California Los Angeles.

Inal, Fikret, and Selim M. Senkan. 2002a. "Effects of equivalence ratio on species and soot concentrations in premixed n-heptane flames." *Combustion and Flame* 131 (1):16-28.

Inal, Fikret, and Selim M. Senkan. 2002b. "Effects of oxygenate additives on polycyclic aromatic hydrocarbons (PAHs) and soot formation." *Combustion Science and Technology* 174 (9):1-19.

Inal, Fikret, and Selim M. Senkan. 2005. "Effects of oxygenate concentration on species mole fractions in premixed n-heptane flames." *Fuel* 84 (5):495-503.

Ingemarsson, Asa T., Jorgen R. Pedersen, and Jim O. Olsson. 1999. "Oxidation of n-Heptane in a Premixed Laminar Flame." *The Journal of Physical Chemistry A* 103 (41):8222-8230.

Knyazev, Vadim D., Ákos Bencsura, Stanislav I. Stoliarov, and Irene R. Slagle. 1996. "Kinetics of the C2H3 + H2 ⇄ H + C2H4 and CH3 + H2 ⇄ H + CH4 Reactions." *The Journal of Physical Chemistry* 100 (27):11346-11354.

Kumar, Kamal, and Chih-Jen Sung. 2011. "Autoignition of methanol: Experiments and computations." *International Journal of Chemical Kinetics* 43 (4):175-184.

Lakshminarayanan, P. A., and Yogesh V. Aghav. 2010. "Ignition Delay in a Diesel Engine." In *Modelling Diesel Combustion*, edited by P. A. Lakshminarayanan and Yoghesh V. Aghav, 59-78. Dordrecht: Springer Netherlands.

Lopez, Jorge Gimenez, Christian Lund Rasmussen, Maria U. Alzueta, Yide Gao, Paul Marshall, and Peter Glarborg. 2009. "Experimental and kinetic modeling study of C2H4 oxidation at high pressure." *Proceedings of the Combustion Institute* 32 (1):367-375.

Lu, Tianfeng, and Chung K. Law. 2005. "A directed relation graph method for mechanism reduction." *Proceedings of the Combustion Institute* 30 (1):1333-1341.

Marinov, N. M., W. J. Pitz, C. K. Westbrook, M. J. Castaldi, and S. M. Senkan. 1996. "Modeling of Aromatic and Polycyclic Aromatic Hydrocarbon Formation in Premixed Methane and Ethane Flames." *Combustion Science and Technology* 116-117 (1-6):211-287.

Marinov, Nick M., William J. Pitz, Charles K. Westbrook, Antonio M. Vincitore, Marco J. Castaldi, Selim M. Senkan, and Carl F. Melius. 1998. "Aromatic and Polycyclic Aromatic Hydrocarbon Formation in a Laminar Premixed n-Butane Flame." *Combustion and Flame* 114 (1):192-213.

Mehl, Marco, William J. Pitz, Charles K. Westbrook, and Henry J. Curran. 2011. "Kinetic modeling of gasoline surrogate components and mixtures under engine conditions." *Proceedings of the Combustion Institute* 33 (1):193-200.

Melius, Carl F., James A. Miller, and Earl M. Evleth. 1992. "Unimolecular reaction mechanisms involving C3H4, C4H4, and C6H6 hydrocarbon species." *Symposium (International) on Combustion* 24 (1):621-628.

Methanol_Institute. 2016. "Methanol Blending Technical Product Bulletin." Singapore. Methanol Institute http://www.methanol.org/.

Park, Sungwoo, Yu Wang, Suk Ho Chung, and S. Mani Sarathy. 2017. "Compositional effects on PAH and soot formation in counterflow diffusion flames of gasoline surrogate fuels." *Combustion and Flame* 178:46-60.

Peeters, J., and G Mahnen. 1973. "Structure of Ethylene-Oxygen Flames. Reaction Mechanism and Rate Constants of Elementary Reactions." *Combust. Inst. European Symp* 1:53-58.

Pepiot-Desjardins, P., and H. Pitsch. 2008. "An efficient error-propagation-based reduction method for large chemical kinetic mechanisms." *Combustion and Flame* 154 (1):67-81.

Popa, Marcel Ginu, Niculae Negurescu, Constantin Pana, and Alexandru Racovitza. 2001. "Results Obtained by Methanol Fuelling Diesel Engine." *SAE International Technical Paper 2001-01-3748*.

Raj, Abhijeet, Iran David Charry Prada, Amer Ahmad Amer, and Suk Ho Chung. 2012. "A reaction mechanism for gasoline surrogate fuels for large polycyclic aromatic hydrocarbons." *Combustion and Flame* 159 (2):500-515.

Rasmussen, Christian Lund, Karin Hedebo Wassard, Kim Dam-Johansen, and Peter Glarborg. 2008. "Methanol oxidation in a flow reactor: Implications for the branching ratio of the CH3OH+OH reaction." *International journal of chemical kinetics* 40 (7):423-441.

Reuter, Robert M., Jack D. Benson, Vaughn R. Burns, Robert A. Gorse, Albert M. Hochhauser, William J. Koehl, Louis J. Painter, Brian H. Rippon, and James A. Rutherford. 1992. "Effects of Oxygenated Fuels and RVP on Automotive Emissions - Auto/Oil Air Quality Improvement Program." *SAE International Technical Paper 920326*.

Richter, H., and J. B. Howard. 2000. "Formation of polycyclic aromatic hydrocarbons and their growth to soot—a review of chemical reaction pathways." *Progress in Energy and Combustion Science* 26 (4):565-608.

Richter, Henning, and Jack B. Howard. 2002. "Formation and consumption of single-ring aromatic hydrocarbons and their precursors in premixed acetylene, ethylene and benzene flames." *Physical Chemistry Chemical Physics* 4 (11):2038-2055.

RMG-Group1. 2019. "RMG-database." https://rmg.mit.edu/database/kinetics/.

RMG-Group2. 2019. "RMG-database." https://rmg.mit.edu/database/kinetics/.

Samanta, Sudip K., Om V. Singh, and Rakesh K. Jain. 2002. "Polycyclic aromatic hydrocarbons: environmental pollution and bioremediation." *Trends in Biotechnology* 20 (6):243-248.

Saravanan, C. G., B. Saravanan, J. Sitharthaseelan, Sudhakar, A. Raja, and A. R. Sharavanan. 2002. "Fumigation of Methanol and Fuel Additives in a Diesel Engine Testing the Performance and Emission Characteristics." *SAE International Technical Paper 2002-01-2722*.

Seidel, Lars, Kai Moshammer, Xiaoxiao Wang, Thomas Zeuch, Katharina Kohse-Höinghaus, and Fabian Mauss. 2015. "Comprehensive kinetic modeling and experimental study of a fuel-rich, premixed n-heptane flame." *Combustion and Flame* 162 (5):2045-2058.

Shukla, Bikau, Akira Miyoshi, and Mitsuo Koshi. 2010. "Role of Methyl Radicals in the Growth of PAHs." *Journal of the American Society for Mass Spectrometry* 21 (4):534-544.

Skupinska, Katarzyna, Irena Misiewicz, and Teresa J Acta Pol Pharm Kasprzycka-Guttman. 2004. "Polycyclic aromatic hydrocarbons: physicochemical properties, environmental appearance and impact on living organisms." *Polish Pharmaceutical Society* 61 (3):233-240.

Stein, Stephen E., James A. Walker, Mahendra M. Suryan, and Askar Fahr. 1991. "A new path to benzene in flames." *Symposium (International) on Combustion* 23 (1):85-90.

Tsang, W., and R. F. Hampson. 1986. "Chemical Kinetic Data Base for Combustion Chemistry. Part I. Methane and Related Compounds." *Physical and Chemical Reference Data* 15 (3):1087-1279.

Vajda, S., P. Valko, and T. Turányi. 1985. "Principal component analysis of kinetic models." *International Journal of Chemical Kinetics* 17 (1):55-81.

Wang, Hai, and Michael Frenklach. 1997. "A detailed kinetic modeling study of aromatics formation in laminar premixed acetylene and ethylene flames." *Combustion and Flame* 110 (1):173-221.

Warnatz, Jürgen, Ulrich Maas, and Robert W. Dibble. 2006. *Combustion Physical and Chemical Fundamentals,Modeling and Simulation, Experiments,Pollutant Formation*. Berlin Heidelberg: Springer.

Weissman, Maja, and Sidney Benson. 1988. "Rate parameters for the reactions of vinyl and butadienyl radicals with hydrogen and acetylene." *The Journal of Physical Chemistry* 92 (14):4080-4084.

Westbrook, Charles K., William J. Pitz, and Henry J. Curran. 2006. "Chemical Kinetic Modeling Study of the Effects of Oxygenated Hydrocarbons on Soot Emissions

from Diesel Engines." *The Journal of Physical Chemistry A* 110 (21):6912-6922.

Xu, Hanjun, Chunde Yao, and Guanglan Xu. 2012. "Chemical kinetic mechanism and a skeletal model for oxidation of n-heptane/methanol fuel blends." *Fuel* 93:625-631.

Xu, Hanjun, Chunde Yao, Guanglan Xu, Zhandong Wang, and Hanfeng Jin. 2013. "Experimental and modelling studies of the effects of methanol and ethanol addition on the laminar premixed low-pressure n-heptane/toluene flames." *Combustion and Flame* 160 (8):1333-1344.

Yan, Fuwu, Lei Xu, Yu Wang, Sungwoo Park, S. Mani Sarathy, and Suk Ho Chung. 2019. "On the opposing effects of methanol and ethanol addition on PAH and soot formation in ethylene counterflow diffusion flames." *Combustion and Flame* 202:228-242.

Yanju, Wei, Liu Shenghua, Li Hongsong, Yang Rui, Liu Jie, and Wang Ying. 2008. "Effects of Methanol/Gasoline Blends on a Spark Ignition Engine Performance and Emissions." *Energy & Fuels* 22 (2):1254-1259.

Zhang, Fan, Shijin Shuai, Zhi Wang, Xia Zhang, and Jianxin Wang. 2011. "A detailed oxidation mechanism for the prediction of formaldehyde emission from methanol-gasoline SI engines." *Proceedings of the Combustion Institute* 33 (2):3151-3158.

Zhang, Kuiwen, Colin Banyon, John Bugler, Henry J. Curran, Anne Rodriguez, Olivier Herbinet, Frédérique Battin-Leclerc, Christine B'Chir, and Karl Alexander Heufer. 2016. "An updated experimental and kinetic modeling study of n-heptane oxidation." *Combustion and Flame* 172:116-135.